

**Design and Development of Ligand Conjugated
Biodegradable Nanoparticles Containing Paclitaxel to
Target Prostate Cancer Cells**

Thesis submitted by

IMAN EHSAN

DOCTOR OF PHILOSOPHY (PHARMACY)

**Department of Pharmaceutical Technology
Faculty Council of Engineering and Technology
Jadavpur University
Kolkata, India**

2022

**JADAVPUR UNIVERSITY
KOLKATA-700032, INDIA**

INDEX NO. 245/16/Ph

1. Title of the thesis: Design and Development of Ligand Conjugated Biodegradable Nanoparticles Containing Paclitaxel to Target Prostate Cancer Cells

2. Name, Designation and institution of supervisor:

Professor (Dr.) Biswajit Mukherjee

Professor,

Department of Pharmaceutical Technology,

Jadavpur University,

Kolkata-700032, India.

3. List of publications (related to thesis)

(i) Iman Ehsan, Leena Kumari, Ramkrishna Sen, Ashique Al Hoque, Biswajit Mukherjee, Alankar Mukherjee, Prasanta Ghosh, Sanchari Bhattacharya, J591 functionalized Paclitaxel loaded PLGA nanoparticles successfully inhibited PSMA overexpressing LNCaP cells, Journal of Drug Delivery Science and Technology, 75 (2022) 103689. <https://doi.org/10.1016/j.jddst.2022.103689>
(Impact Factor: 5.062)

Other Publications

(ii) Shreyasi Chakraborty, **Iman Ehsan**, Biswajit Mukherjee, Laboni Mondal, Saheli Roy, Krishna Das Saha, Brahamacharry Paul, Mita Chatterjee Debnath, Tanmoy Bera, Therapeutic potential of andrographolide-loaded nanoparticles on a murine asthma model, Nanomedicine 20 (2019) 102006. <https://doi.org/10.1016/j.nano.2019.04.009>. **(Impact Factor: 6.458)**

(iii) Sanchari Bhattacharya, Laboni Mondal, Biswajit Mukherjee, Lopamudra Dutta, **Iman Ehsan**, Mita Chatterjee Debnath, Raghuvir Gaonkar, Murari Mohan Pal, Subrata Majumdar, Apigenin loaded nanoparticle delayed development of hepatocellular carcinoma in rats, *Nanomedicine* 14 (2018) 1905-1917. <https://doi.org/10.1016/j.nano.2018.05.011>. (**Impact Factor: 6.458**)

(iv) Laboni Mondal, Biswajit Mukherjee, Shreyasi Chakraborty, Sanchari Bhattacharya, **Iman Ehsan**, Soma Sengupta, Murari Mohan Pal, Comparison of Enhanced Solubility Profile Analysis of Thermodynamic Parameters and Pharmacokinetic Profile Related to Tamoxifen Citrate Solubilisation, Novel Approaches in Drug Designing & Development, 3 (2018) 120-7.

Book Chapters

(i) Biswajit Mukherjee, Manasadeepa Rajagopalan, Samrat Chakraborty, Prasanta Ghosh, Manisheeta Ray, Ramkrishna Sen, **Iman Ehsan**, Hepatocellular Carcinoma: Diagnosis, Molecular Pathogenesis, Biomarkers, and Conventional Therapy, In: B. Mukherjee (Ed.), *Nanotherapeutics for the Treatment of Hepatocellular Carcinoma*. 2022 Mar 9:1.

(ii) Biswajit Mukherjee, Leena Kumari, **Iman Ehsan**, Prasanta Ghosh, Soumyabrata Banerjee, Samrat Chakraborty, Manisheeta Ray, Ashique Al Hoque, Ratan Sahoo, Guar gum-based nanomaterials in drug delivery and biomedical applications, In: H. Bera, C. M. Hossain, S. Saha (Eds.), *Biopolymer-Based Nanomaterials in Drug Delivery and Biomedical Applications*, Academic Press, 2021 pp. 143-164, <https://doi.org/10.1016/B978-0-12-820874-8.00016-6>

(iii) Biswajit Mukherjee, Samrat Chakraborty, **Iman Ehsan**, Apala Chakraborty, Leena Kumari, Alankar Mukherjee, Shounak Sarkhel, Conventional and nonconventional approaches to site-specific targeting of nanotherapeutics in some infectious diseases and metabolic disorders. In: S. Talegaonkar, M. Rai (Eds.) *Nanoformulations in human health*, Springer Nature Switzerland AG, 2020, pp. 111-132. https://doi.org/10.1007/978-3-030-41858-8_6

(iv) Biswajit Mukherjee , Soma Sengupta , Soumyabrata Banerjee, Moumita Dhara, Ashique Al Hoque, Leena Kumari, Ray, Manisheeta Ray, **Iman Ehsan**, Alankar Mukherjee, Transdermal Nanomedicines for Reduction of Dose and Site-Specific Drug Delivery, 2020. In: M. K. Das, Y. V. Pathak (Eds.), Nano Medicine and Nano Safety, Springer, Singapore, 2020, pp. 175-211. https://doi.org/10.1007/978-981-15-6255-6_8

(v) Biswajit Mukherjee, **Iman Ehsan**, Debasmita Dutta, Moumita Dhara, Lopamudra Dutta, Soma Sengupta, Nanomedicinal Genetic Manipulation: Promising Strategy to Treat Some Genetic Diseases, In: S. Beg, M. Rahman, M. A. Barkat, F.J. Ahmad (Eds.), Nanomedicine for the Treatment of Disease, Apple Academic Press, New York, 2019, pp. 103-140. <https://doi.org/10.1201/9780429425714>

4. List of patents: Nil

5. List of Presentations in National/ International/ Conferences/Workshops:

National

One Day National Symposium on Nanotechnology organized by Centre For Interdisciplinary Research and Education held on 25th March, 2017 at Birla Industrial and Technological Museum, Kolkata.

National Seminar on Clinical Research: Present Scenario in Pharmacovigilance and Clinical Trials held on 17th February, 2018 at Jadavpur University, Kolkata.

Indian Council of Medical Research (ICMR) Sponsored National Seminar on “Quality Control and Standardization of Ethnopharmaceuticals in the Present Era” held on 4th -5th March 2018 at Centurian University and Technology and Management Bhubaneswar, Odisha.

National Seminar on Pharmacy & Healthcare: Traditional Knowledge to Modern Techniques held on 14th September, 2018 at Jadavpur University, Kolkata.

International:

6th International Postgraduate Conference on Pharmaceutical Sciences 2018 held on 15th - 16th August, 2018 at International Medical University, Kuala Lumpur, Malaysia.

24th International Conference on Cancer Research and Pharmacology held on 5th - 6th August, 2019 in Singapore.

“STATEMENT OF ORIGINALITY”

I **Iman Ehsan** registered on 04/04/16 do hereby declare that this thesis entitled “**Design and Development of Ligand Conjugated Biodegradable Nanoparticles Containing Paclitaxel to Target Prostate Cancer Cells**” contains literature survey and original research work done by the undersigned candidate as part of Doctoral studies.

All information in this thesis have been obtained and presented in accordance with existing academic rules and ethical conduct. I declare that, as required by these rules and conduct, I have fully cited and referred all materials and results that are not original to this work.

I also declare that I have checked this thesis as per the “Policy on Anti Plagiarism, Jadavpur University, 2019”, and the level of similarity as checked by iThenticate software is 9%.

Signature of Candidate: *Iman Ehsan*

Date : *11.11.2022*



Certified by Supervisor: *Professor (Dr.) Biswajit Mukherjee*
(Signature with date, seal) *Department of Pharmaceutical Technology*
Jadavpur University
Kolkata-700032, India

CERTIFICATE FROM THE SUPERVISOR

This is to certify that the thesis entitled “**Design and Development of Ligand Conjugated Biodegradable Nanoparticles Containing Paclitaxel to Target Prostate Cancer Cells**” submitted by **Smt Iman Ehsan** , who got her name registered on 04.04.2016 for the award of Ph. D. (Pharmacy) degree of Jadavpur University is absolutely based upon her own work under the supervision of **Prof. (Dr.) Biswajit Mukherjee** and that neither her thesis nor any part of the thesis has been submitted for any degree/diploma or any other academic award anywhere before.



Signature of the Supervisor

and date with Office Seal

Professor (Dr.) Biswajit Mukherjee
Department of Pharmaceutical Technology
Jadavpur University
Kolkata-700032, India

ACKNOWLEDGEMENT

First and foremost, I would like to thank Almighty for the blessings and grace bestowed on me so that I am able to see this day. As I come to the end of this journey, I hope that my arduous efforts will be rewarded with success. It is a moment of fulfillment and delight to look back with a sense of content and thank an endless number of people who contributed in this journey.

I feel proud to acknowledge with great respect, a sense of regard, and gratitude my guide and mentor, Prof. (Dr.) Biswajit Mukherjee, Professor and Ex-Head, Department of Pharmaceutical Technology, Jadavpur University, Kolkata-700032. I am deeply indebted to him for providing endless support, his timely advice, meticulous scrutiny at each and every stage of my PhD, and his insistence on perfection. His erudite suggestions and encouragement gave me lots of confidence to proceed. It was the confidence he instilled in me that led me to broaden my horizons as a researcher. He patiently helped with his overwhelming attitude, proving moral support to proceed. It was a great honour to work under his guidance.

I convey my sincere thanks to Department of Science and Technology (DST PURSE II) for providing fellowship and financial assistance from 2016 to 2018. I would like to express my sincere gratitude to the Indian Council of Medical Research (ICMR), New Delhi, India, for providing financial assistance from 2018-2021 [Sanction No. 45/41/2018/Nano/BMS]. I wish to extend my thanks to all the teaching and non-teaching staff at the Department of Pharmaceutical Technology, Jadavpur University.

I extend my special thanks to Mrs. Dipa Mukherjee (Madam) for all her moral support, love, and encouragement. Alankar Mukherjee (Pinky) and Avinaba Mukerjee (Gullu) hold a very special place in this wonderful journey. Words are inadequate to express my sincere thanks to all my labmates, with whom I have shared some great moments Paromita di, Lopa di, Laboni di, Soma di, Debasmita di, Apala, Moumita di, Manisheeta, Bhabani da, Tapan da, Niladri da, Samrat da, Soumo da, Sahajit, Dipayan, Brahamacharry A very special thanks to Ashique, Leena, Ramkrishna, Prasanta da, Sandipan and Sanchari di for their help.

Lastly, I should admit that I owe my success to my Abbu, Mummy, my husband Shahab, my brothers Dr. Ehtesham and Osama, my lovely daughters Safaa and Irhaa, Ammi and all my family, who have always been a solid support and tried to keep me motivated and determined towards my objective so that I get the strength to push the boundaries and fight against all the odds. Last but not least, I should also express my gratitude to anyone else whom I should have mentioned here but missed out on unknowingly and unintentionally.

Date: 11.11.2022

Place: KOLKATA

Iman Ehsan

Iman Ehsan

*Dedicated to
My Parents,
My Sir (Prof. Biswajit Mukherjee),
My Husband, My daughters
and My brothers*

PREFACE

Prostate cancer has become one of the most common reasons for cancer-related deaths in males globally, is one of the most difficult cancers to cure. It is not invariably lethal; it is a heterogeneous disease that can vary from asymptomatic to a potentially fatal systemic cancer. As a result, such people may find it more acceptable to undergo early intervention to treat the problem with a less intrusive local treatment. Furthermore, patients who experience recurrence after radical prostatectomy may benefit from local therapy to reduce the risk of local and/or metastatic disease progression. The approach to prostate cancer treatment must specifically deliver formulations to the prostate while avoiding harm or toxicity to unaffected healthy tissues. Nanotechnology is rapidly expanding, and it is expected to have far-reaching consequences for the future of science and medicine. Active drug-targeted delivery methods like ligand attachment to the nanoformulations are widely employed as a significant effort to target cancer-specific cells more efficiently while minimizing negative effects on healthy tissues and simultaneously increasing biocompatibility, bioavailability, and active targeting at the cancer site with reduced doses of therapeutic agents and improved residence time in the body.

In this thesis, poly (D,L-lactide-co-glycolide) (PLGA) nanoparticles containing paclitaxel as a potent anticancer drug, conjugated with anti-PSMA antibody J591 for targeted delivery at the prostate cancer cells, were developed (Ab-PTX-NP). The work was carried out in vitro using prostate cancer cells that express the cell surface antigen PSMA. The antibody (anti-PSMA antibody J591) can recognize and bind to the PSMA on the surfaces of the prostate. PSMA is a transmembrane receptor whose expression is largely restricted to prostatic epithelium and prostate cancer cells, with its expression level increasing during the progression of malignancy. The pharmacokinetic parameters of the prepared formulations were studied in Balb/c male mice. Thus, Ab-PTX-NP exhibited the greatest potency in PSMA-expressing prostate cancer cells (LNCaP) and speed in eliciting apoptosis in PSMA-expressing prostate cancer cells. Herein, our formulation have shown a considerable potential to carry the prepared chemotherapeutic nanoparticles directly to the affected prostate cancer cells and proved to have greater efficacy than the free drug. Patients suffering from prostate cancer with a poor prognosis could receive exceptional care from it. To benefit society in the near future, we wish to further investigate our study extensively for translation from pre-clinical to clinical domain.

LIST OF ABBREVIATIONS

ANOVA	One way analysis of variance
°C	Celsius
Ab-PTX-NP	Antibody conjugated paclitaxel encapsulated nanoparticle
AEC	Animal Ethics Committee
AFM	Atomic Force Microscopy
AUC	Area Under the Curve
BNP	Blank nanoparticle
CL	Clearance
DCM	Dichloromethane
DDW	Double Distilled Water
DMSO	Dimethyl Sulfoxide
DNA	Deoxyribonucleic Acid
EDC	1- (3-dimethylaminopropyl)-3-ethylcarbodiimide hydrochloride
EDTA	Ethylene diamene tetra acetic acid
EPR	Enhanced permeability and retention
FACS	Fluorescence Activated Cell Sorter
FBS	Fetal Bovine Serum
FESEM	Field Emission Scanning Electron Microscope
FITC	Fluorescein Isothiocyanate
FTIR	Fourier Transform Infrared Spectroscopy
g	gram
I.V.	Intravenous

IC ₅₀	Inhibitory Concentration
ICH	International Council for Harmonization
ISO	International Organization for Standardization
J591 Ab	J591 monoclonal antibody
kDa	Kilo Dalton
LC/MS-MS	Liquid Chromatography and Mass Spectroscopy
mg	milligram
ml	milliliter
mm	millimeter
MMP	Mitochondrial Membrane Potential
MRT	Mean Residence Time
MTT	3-(4,5-Dimethylthiazol-2-Yl)-2,5-Diphenyltetrazolium Bromide
mV	Millivolt
ng	nanogram
NHS	N-hydroxysuccinimide
nm	nanometer
PBS	Phosphate Buffer Saline
PDI	Poly Dispersity Index
P-GP	P-glycoprotein
PLGA	Poly Lactic Co-Glycolic Acid
PSMA	Prostate specific membrane antigen
PTX	Paclitaxel
PTX-NP	Paclitaxel loaded PLGA nanoparticle
PVA	Poly (Vinyl Alcohol)

RH	Relative Humidity
RPM	Rotation per minute
RPMI	Roswell Park Memorial Institute Medium
SD	Standard deviation
SDS-PAGE	Sodium dodecyl sulfate-polyacrylamide gel electrophoresis
TEM	Transmission Electron Microscopy
TPGS	D- α -tocopherol polyethylene glycol succinate
USFDA	United States Food and Drug Administration
UV/vis	Ultraviolet-visible spectroscopy
v/v	Volume/volume
V _{ss}	Steady State Volume Distribution
w/v	Weight/volume
λ_{\max}	Maximum wavelength
μg	microgram
μl	microliter
μM	micromolar

CONTENTS

Chapter		Page No.
Chapter 1	Introduction	1-7
	1.1. Prostate cancer	1
	1.2. Nanoparticulate system-based drug delivery	2
	1.3. Biodegradable Poly(lactic-co-glycolic acid) nanoparticles	3
	1.4. Paclitaxel as potent anticancer drug	4
	1.5. Encapsulation of paclitaxel in PLGA nanoparticles	4
	1.6. Passive and active drug targeting of nanoparticles to prostate cancer	4
	1.7. PSMA as a target receptor for prostate cancer	6
	1.8. J591 as biomarker proteins for targeted therapy of prostate cancer	6
	1.9. Surface modification of paclitaxel-loaded PLGA nanoparticles for site specific delivery	7
	1.10. Present research envisaged	7
Chapter 2	Literature Review	8-13
	2.1. Information on prostate cancer	8
	2.2. Paclitaxel as an anticancer drug	9
	2.3. Nanotechnology and nanoparticles for cancer treatment	10
	2.4. Polymeric nanoparticles	11
	2.5. Poly-(D-L-lactide-co-glycolide) (PLGA) nanoparticles encapsulating anti-cancer drugs.	12
	2.6. Fabrication of the PLGA nanoparticles for site-specific delivery.	13
	2.7. Prostate specific membrane antigen (PSMA)	13
	2.8. J591 antibody site-specificity to PSMA	13
Chapter 3	Objectives and plan of study	15-16
	3.1. Objectives	15
	3.2. Plan of study	15
Chapter 4	Materials and equipments	17-21
	4.1. The chemicals used in the study have been listed below	17
	4.1.2. Animals and different cells used in the study	19
	4.2. Instruments	19

Chapter		Page No.
Chapter 5	Methodology	22-32
	5.1. Calibration curve of paclitaxel with the help of UV-visible spectroscopy	22
	5.2. Preparation of nanoparticles	23
	5.3. Fourier-transform infrared (FTIR) spectroscopy	23
	5.4 Physicochemical characterization of PTX-NP and Ab-PTX-NP	23-24
	5.4.1. Particle size and zeta potential	
	5.4.2 Drug loading and encapsulation efficiency	
	5.4.3 Scanning electron microscopy (SEM)	
	5.4.4 Transmission electron microscopy (TEM)	
	5.4.5 Atomic force microscopy (AFM)	
	5.5 Energy dispersive X-ray assay (EDX)	24
	5.6 Sodium dodecyl sulfate-polyacrylamide gel electrophoresis	25
	5.7 <i>In vitro</i> drug release analysis	25
	5.8 Accelerated stability study	26
	5.9. <i>In vitro</i> studies	26-30
	5.9.1. <i>In vitro</i> cytotoxicity (MTT) study	
	5.9.2. Western blot analysis of PSMA expression in prostate cancer cells	
	5.9.3. Cellular uptake study of PC3 and LNCaP cells <i>in vitro</i>	
	5.9.4. Induction of cell death by acridine orange/ethidium bromide dual staining	
	5.9.5. Mitochondrial membrane depolarization analysis using JC-1	
	5.9.6. Apoptosis assay	
	5.9.7. Nuclear morphology analysis by DAPI staining	
	5.10. Hemolysis evaluation	30
	5.11. <i>In-vivo</i> studies	30-31
	5.11.1. Pharmacokinetic study by LC-MS/MS method	
	5.11.2. LC-MS/MS analysis	
	5.12. Statistical analysis	32

Chapter		Page No.
Chapter 6	Results	33-59
	6.1. Preparation of standard curve of Paclitaxel	33
	6.2. Fourier-transform infrared (FTIR) spectroscopy	34
	6.3. Physicochemical characterization of prepared nanoparticles	36-42
	6.3.1. Drug loading and encapsulation efficiency	
	6.3.2. Particle size and zeta potential	
	6.3.3. Surface morphology of the prepared nanoparticles	
	6.4. Energy dispersive X-ray assay (EDX)	
	6.5. SDS-PAGE	
	6.6. <i>In vitro</i> drug release study	43
	6.7. Accelerated stability study	46
	6.7.1 Hydrolytic stability study	
	6.8. <i>In vitro</i> cellular studies	47-56
	6.8.1. Cell viability assay	
	6.8.2. Expression analysis of PSMA on LNCaP and PC3 cells by Western blot	
	6.8.3. Cellular uptake study on PC3 and LNCaP cells <i>in vitro</i>	
	6.8.4. Induction of cell death by acridine orange/ethidium bromide dual staining	
	6.8.5. Mitochondrial membrane depolarization analysis	
	6.8.6. Apoptosis study	
	6.8.7 Nuclear morphology analysis	
	6.9. Hemolysis study	56
	6.10. <i>In vivo</i> study	57
Chapter 7	Discussion	60-64
Chapter 8	Conclusion	65
Chapter 9	Summary	66
	Future Prospects	69a
Chapter 10	References	70-79
	Annexure	
	Publications	

LIST OF FIGURES

Figure No.	Legend	Page No
Figure 1.1.	Different types of nanoformulations used for drug delivery	3
Figure 1.2.	Active targeting by the nanoparticles	6
Figure 2.1.	Chemical structure of Paclitaxel	9
Figure 6.1.	Absorbance maxima of Paclitaxel	33
Figure 6.2.	Calibration curve Paclitaxel	34
Figure 6.3.	FTIR spectra of (A) Paclitaxel (drug), (B) PLGA, (C) PVA, (D) Physical mixture of PVA and PLGA, (E) Physical mixture of drug, PVA and PLGA, (F) Blank nanoparticles BNP, (G) Paclitaxel-loaded nanoparticles (PTX-NP), (H) TPGS, (I) Physical mixture of PVA, PLGA,TPGS, (J) Physical mixture of PLGA, PVA, drug, and TPGS	35
Figure 6.4.	Characterizations of PTX-NP and Ab-PTX-NP	
	A. Average particle size distribution of PTX-NP	38
	B. Average particle size distribution of Ab-PTX-NP	38
	C. Zeta potential of PTX-NP	39
	D. Zeta potential of Ab-PTX-NP	39
	E. Zeta potential, particle size of PTX-NP 1, PTX-NP 2 and PTX-NP 3	40
Figure 6.5.	Field emission scanning electron microscopy (A) PTX-NP at 16,000× magnification (B) Ab-PTX-NP at 13,000× magnification; Transmission electron microscopy (C) PTX-NP (D) Ab-PTX-NP; Atomic force microscopy (E) PTX-NP and (F) Ab-PTX-NP	41
Figure 6.6.	SDS-PAGE gel electrophoresis, Lane 1 in the SDS-PAGE gel showed the standard anti-PSMA monoclonal antibody Ab (J591), lane 2 represents for antibody conjugated PTX-NP, and lane 3 shows PAGE run of unconjugated NP followed by Blank in lane 4, and then the protein marker in lane 5.	43
Figure 6.7.	A. <i>In vitro</i> drug release profile of experimental formulations in phosphate buffer saline (pH 7.4) with 0.1% w/v tween 80	44
	B. <i>In vitro</i> drug release profile of Ab-PTX-NP in different pH (pH 3, 5, 7.4 and 10) media	44
Figure 6.8.	The pH-dependent hydrolytic degradation of the Ab-PTX-NP	47

Figure No.	Legend	Page No
Figure 6.9.	A. In vitro cytotoxicity of PTX, PTX-NP, Ab-PTX-NP and Ab-BNP was determined in LNCaP cells	48
	B. In vitro cytotoxicity of PTX, PTX-NP, Ab-PTX-NP and Ab-BNP was determined in PC3 cells.	48
Figure 6.10.	PSMA expression in LNCaP and PC3 cells detected by Western blot PSMA to GADPH ratio is shown graphically	49
Figure 6.11.	A. Flow cytometry analysis representing distribution of FITC PTX-NP and FITC Ab-PTX-NP in LNCaP cells after treating them for 0.5h, 2 h and 4 h respectively	50
	B. Flow cytometry analysis representing distribution of FITC PTX-NP and FITC Ab-PTX-NP in PC3 cells after treating them for 0.5h, 2 h and 4 h respectively	50
Figure 6.12.	A. Confocal microscopy images of LNCaP cells after treating with FITC PTX-NP and FITC Ab-PTX-NP for 4 h	51
	B. Confocal microscopy images of PC3 cells after treating with FITC PTX-NP and FITC Ab-PTX-NP for 4 h	52
Figure 6.13.	Confocal microscopy images of (A) LNCaP cells after treating with PTX , PTX-NP and Ab-PTX-NP (B) PC3 cells after treating PTX , PTX-NP and Ab-PTX-NP, for 24 h followed by staining with acridine orange (4 µg/ml) and ethidium bromide (4 µg/ml), by acridine orange/ethidium bromide (AO/EB) dual staining.	53
	C. Mean fluorescence intensity percentage obtained by acridine orange/ethidium bromide dual staining. Image J software was used.	54
Figure 6.14.	Loss of mitochondrial membrane potential as estimated by JC-1 staining analysis after treating the LNCaP (+ve PSMA) and PC3 (-ve PSMA) cells with PTX/ PTX-NP/Ab-PTX-NP for 24 h	55
Figure.6.15.	Quantification of apoptosis detected in LNCaP (+ve PSMA) and PC3 (-ve PSMA) cells treated with PTX/ PTX-NP/Ab-PTX-NP for 24 h	55
Figure 6.16.	Confocal microscopic image (100X) representating DNA degradation and apoptotic body formation upon treatment with PTX/ PTX-NP/Ab-PTX-NP for 24 in LNCaP (+ve PSMA) cells and in PC3 (-ve PSMA) cells	56
Figure 6.17.	Hemolytic activity of PTX/ PTX-NP/ Ab-PTX-NP	57

Figure No.	Legend	Page No
Figure 6.18.	Plasma concentration of paclitaxel upon i.v bolus injection (at a dose of 10mg/kg body weight) of PTX/ PTX-NP/ Ab-PTX-NP	59
Figure 9.1.	Summarization of the present study, which depicts that the optimized antibody conjugated formulation Ab-PTX-NP recognizes the positive PSMA prostate cancer cells, further internalization of Ab-PTX-NP results in apoptosis of cancerous cells. The hemolysis and pharmacokinetics study reveals the hemo-compatibility and efficiency of the formulation in the form of increased bioavailability and prolonged drug release from Ab-PTX-NP	67

LIST OF TABLES

Table No.	Legend	Page No.
Table 1.1.	Treatments for prostate cancer	1
Table 4.1.	List of materials/chemicals used in the study	17
Table 4.2.	The source of animals and different cell lines used in the study	19
Table 4.3.	List of instruments, equipments and devices used in the study	19
Table 6.1.	Composition of the experimental nanoparticles with PLGA: Drug at the ratio 10:1 along with drug loading and encapsulation efficiency.	37
Table 6.2.	Specific elemental composition (carbon, oxygen, nitrogen and sulphur) of nanoparticles	42
Table 6.3.	Equation of in vitro drug release kinetics tested on different release kinetic models, with corresponding R ² values and release exponent (n) (Korsmeyer–Peppas model).	45
Table 6.4.	Stability study of PTX-NP and Ab-PTX-NP after 90 days (3 months) stored at 4-8°C	46
Table 6.5.	IC ₅₀ values of PTX, PTX-NP and Ab-PTX-NP on different prostate cancer cells and normal cells.	49
Table 6.6.	Plasma pharmacokinetic parameters of paclitaxel released from PTX-NP/ Ab-PTX-NP/ PTX suspension after the intravenous bolus administration of PTX-NP/ Ab-PTX-NP/ PTX with an equivalent amount of drug in BALB/c mice.	58

1. Introduction

1.1. Prostate cancer

Prostate cancer is a common and recurrent cancer type in males globally, with a growing incidence of mortality. The risk of developing prostate cancer and associated mortality increases with age. Prostate cancer is often asymptomatic in the early stages. The most common complaint is problem with urination and other similar symptoms as observed in prostatic enlargement (Rawla, 2019). Patients may feel back pain and retention of urine in later or advanced stages of prostate cancer. In metastatic stage, prostate cancer cells might metastasize to axis skeleton causing uneasiness in normal activity. Prostate cancers can be easily detected in blood by increase concentration of prostate-specific antigen (PSA) above 4 ng/ml; PSA is a glycoprotein that is typically found in prostate. Prostate cancer can be further confirmed with the help of prostate tissue biopsy. Treatments for initial stage of prostate cancer includes surgical elimination of the prostate, radiation and androgen ablation but if the disease is at metastatic stage, none of the above approaches may offer significant benefit to the patients (Litwin et al., 2017). Androgen deprivation therapy is extensively accepted treatment, but over a period of clinical benefit, patients develop resistant to the therapy (Ertugen et al., 2020) which often results in Castration-Resistant Prostate Cancer (CRPC) (Karantanos et al., 2013).

Table 1.1: Treatments for prostate cancer

Treatment	Applications	Limitations
Surgical approach	Used for localized disease, often combined with chemotherapy and radiotherapy, which may be pre/postoperative	Cannot be used in when cancer metastasizes. Recurrence chances are high
Radiotherapy	With organ-specific tumours, it is effective. Restricts recurrence post-operation	It is linked to an increased incidence of collateral fatality.
Hormonal therapy	Effective against malignant tumors	High repetition and emergence rates
Chemotherapy	Effective along with hormonal therapy or monotherapy	Drug resistance, toxicity, damages healthy tissues
Genotherapy	Inhibits genes responsible for prostate cancer.	Often used in combination, along with chemotherapy

Over the years, many treatment strategies for prostate cancer have evolved. However, it has been demonstrated that combining chemotherapy with any of the therapeutic alternatives is considerably more effective than monotherapies (Galsky et al., 2010). As a result, the number of the United States food and drug administration (USFDA) approved drugs for the treatment of prostate cancer has increased remarkably (Omabe et al., 2021).

1.2. Nanoparticulate system based drug delivery

Numerous biological obstacles prevent cancer drugs from becoming effective. Some potent drugs approved or used for prostate cancer have some common limitations, such as non-specific distribution to other sites rather than the site of interest, resulting in a low amount of drug reaching the target and reducing its efficiency. Frequent dosing in higher doses increases the rate of collateral toxicity and the incidence of multidrug resistance (MDR) (Gillet et al., 2010). Many physio-chemical properties of drugs such as hydrophobicity, pharmacokinetic factors act as hindrance. To begin, there are numerous biological barriers that limit the efficacy of cancer therapeutics. Severe toxicity may often affect the healthy tissues of skin, hair, liver, spleen and many other tissues which have the tendency of dividing rapidly (Andreopoulou et al., 2015).

The nanoformulations are made up of materials such as a variety of polymers, inorganic vectors, and lipids etc, which are competent to be designed, developed to deliver cancer therapeutics. Polymeric nanoparticles consist of nanoparticles, dendrimers, nanocapsules, micelles, drug conjugates, protein nanoparticles, nanogels, while liposomes, exosomes, solid lipid nanoparticles are the examples of lipid nanoformulations. Carbon nanotubes, nano diamond, metallic nanoparticle, quantum dots, silica based nanoparticles, nanocrystalline are widely tried for treating prostate cancer (Yetisgin et al., 2020). The prime motive of the nanoformulations are to deliver the chemotherapeutic drugs either single or in combination in the optimum quantity to the desired cancerous tissues without causing toxicity to healthy tissues and non-specific distribution of potent anticancer drugs. Nanotechnology offers a platform with exceptional characteristics that ensure safe treatment, increased availability, and therapeutic worth in later stages of prostate cancer. Owing to the peculiar pathophysiological features of most solid tumors, such as deficient vasculature and limited lymphatic drainage, nanoparticle (NP) help in overcoming the hydrophobic nature and adverse outcomes such as nephrotoxicity and neurotoxicity, as well as other problems associated with chemotherapy, with a simultaneous enhancement of permeability and

retention (EPR) effect (Chakraborty et al., 2020; Chen et al., 2010). NP enable the drug to release in sustained pattern along with protection of the encased agent from enzymatic degradation. NP also prolong pharmacological action, thereby elevating the dose tolerance and minimizing nonspecific drug absorption-associated toxicity to improve safety and efficacy (Maleki et al, 2021; Huang et al., 2014)

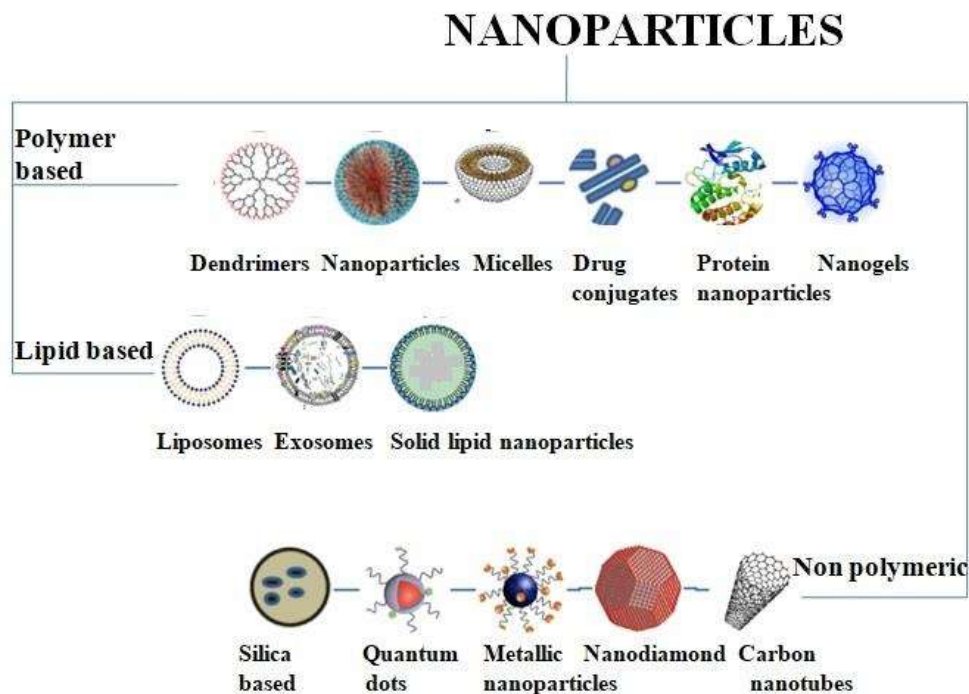


Figure 1.1. Different types of nanoformulations used for drug delivery

1.3. Biodegradable poly(lactic-co-glycolic acid) nanoparticles

Nanoparticles are the incredible part of novel drug delivery approach with advanced drug delivery abilities through the use of mechanism such as passive and active mechanisms. Nanoparticles concentrates drugs at disease sites, prolongs drug systemic circulation, improves elimination half life ($t_{1/2}$), releasing the drug in sustained manner while reducing the side effects and protecting drugs from humoral attacks (Sriraman et al., 2014).

Polymers serve as a boon for chemotherapeutics as it encapsulates the drug. Poly(lactic-co-glycolic acid) (PLGA) is one of the most extensively used biodegradable polymer for the preparation of nanoparticles. PLGA is approved by USFDA and can be used for humans by intravenous route. There is no systemic toxicity attributed with the use of PLGA as the hydrolysis of this polymer generates lactic acid and glycolic acid, both of which are rapidly

metabolised by the human body using cellular metabolic conversion to water and carbon dioxide via the Krebs cycle (Jain et al., 2000; Pagels et al., 2015). Numerous research have shown that PLGA nanoparticles enters into the cells efficiently mostly by specific and nonspecific endocytosis and releases the drug in a sustained manner (Panyam and Labhasetwar, 2004).

1.4. Paclitaxel as potent anti cancer drug

Paclitaxel was encapsulated in PLGA nanoparticles. Paclitaxel (PTX) is the best microtubule stabilized drug licensed by the USFDA for the therapeutic treatment of a range of malignancies such as breast, ovarian, and lung cancer. PTX inhibits mitosis and is effective in eradicating cancer cells during the interphase of the cell cycle (Afrooz et al., 2017). The physicochemical properties of PTX, in particular, severely limit its administration, due to its low solubility (0.0015 mg/mL) that has a negative impact on their polycyclic chemistry in aqueous solution and makes the potent PTX unsuitable for intravenous injections. In conventional standard-of-care chemotherapy, PTX is administered intravenously as Taxol, which is formulated with Cremophor EL and dehydrated ethanol, which result in hypersensitivity reactions and extreme toxicity, altering the in vivo pharmacokinetic drug profile and yielding unpredictable non-linear plasma pharmacokinetics (Gelderblom et al., 2001). Moreover, taxol therapy resulted in drug resistance due to the presence of P-glycoprotein (P-GP) in PTX, which is actively involved in pumping PTX out of the cancerous cells (Gallo et al., 2003). To avoid the drug resistance caused by taxol, several P-GP inhibitors, including verapamil were co-administered, which further resulted in side effects (Stage et al., 2020).

1.5. Encapsulation of Paclitaxel in a PLGA nanoparticle

Encapsulation of PTX leads to increased aqueous solubility of PTX delivery. Due to the increased permeability and retention (EPR) effect, nano size promotes the selective transport of PTX into the tumour location. As a consequence, higher maximum tolerated doses (MTD) of NP are recognised. The pharmacokinetic characteristics of the medication from NP are also enhanced, for example, by lengthening the half-life and accumulating PTX in tumours.

1.6. Passive and active targeting as drug targeting of nanoparticles to prostate cancer

Nanoparticles can be administered either directly in the blood circulation or the surface of the nanoparticles can be engineered for site specific delivery. When the NP are available in the

cancer tissue through circulation, due to characteristic feature of leaky vasculature or dysfunctional lymphatic drainage of the cancerous tissue, the NP enter in the tumor sites due to enhanced permeability and retention of the tumor tissues (EPR) and it is known as passive targeting. The presence of tight junctions in the normal healthy tissues does not facilitate the entry of drug loaded NP. The malformation of endothelial cells initiates rapid angiogenesis in cancer tissues to nurture for further proliferation. Angiogenesis results in formation of gaps with pore size 100-800 nm to allow the accumulation of nanoparticles to release drug via passive targeting (Haley and Frenkel 2008). Due to the significant variation found in various types of tumor, and within the same tumour, the passive targeting phenomenon is highly diverse. There have been cases where patients' therapy responses have varied dramatically. NP systems can be engineered with suitable ligands to target the cancer cells, which will promote tumour absorption and minimize drug adverse effects.

Active targeting aims at delivering the drug directly to the affected cancerous tissues. For this, the NP are fabricated with ligands that could bind to its respective receptor exclusively overexpressed on cancer cells. Prostate specific membrane antigen (PSMA) receptor is overexpressed on cancerous prostate, PSMA can be targeted using various ligands such as J591 antibody or other anti-PSMA antibody to bind with it. Asialoglycoprotein receptor (ASGPR) which is present largely on the surface of hepatic cells can be targeted by galactosamine respectively (Mukherjee. et al., 2022). This would facilitate drug-loaded nanoparticles to enter the cancer cells with the help of receptor-mediated endocytosis. The affinity and density of the ligand, the level of ligand-receptor interaction, the stability, and the non-toxicity of the targeting ligand are some crucial factors that determine how effective active targeting approaches are. The putative ligand conjugation prevents nanoparticles to cross the blood brain-barrier, consequently, averting any nonselective actions on the central nervous system that results in increased targeting and bioavailability to the affected cells (Huang et al., 2014). Thus, active targeting initiates selective delivery of chemotherapeutics, eliminating unintended toxicity, delivering the therapeutic payload within the therapeutic window for an extended period of time in a sustained manner.

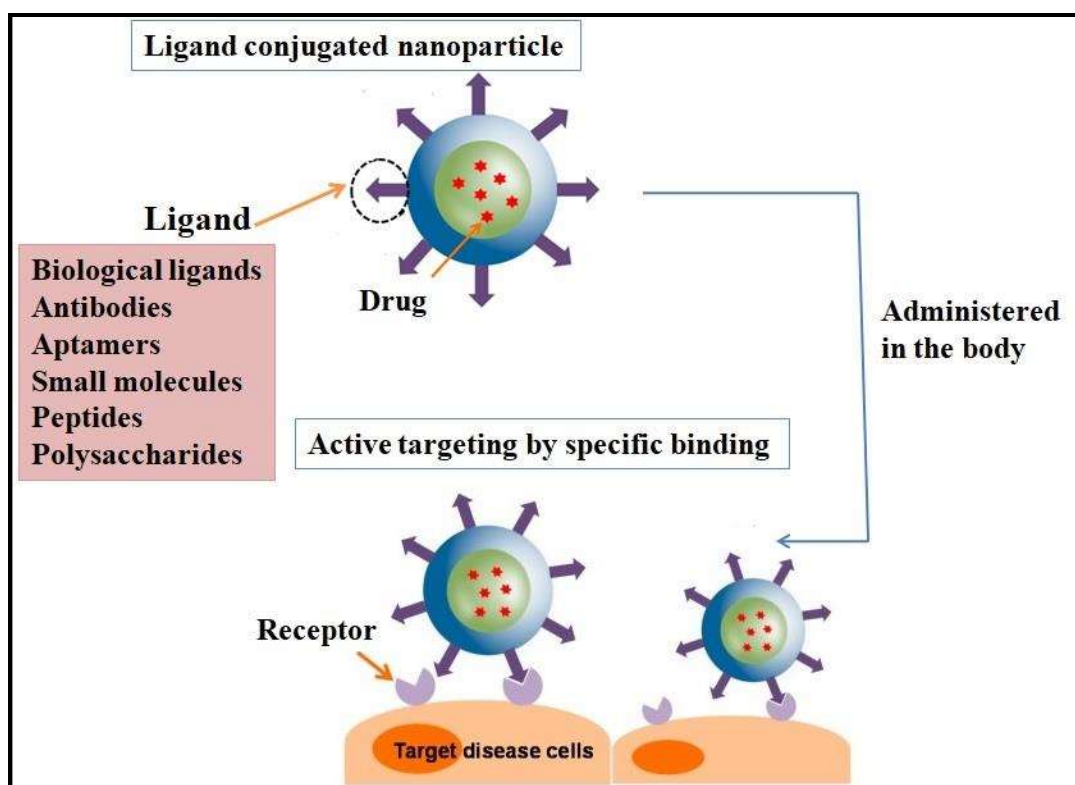


Figure 1.2. Active targeting by the nanoparticles

1.7. PSMA as target receptor for prostate cancer

Our study will utilize the ubiquitous overexpression of the prostate-specific membrane-antigen (PSMA) on cancerous prostate cells. PSMA plays an imperative role in diagnosis, managing as well as treating prostate cancer. The aggrandized PSMA glutamate carboxypeptidase II, having a molecular weight of about 100kDa, is enhanced and progressively elevated in prostate adenocarcinoma and in the neovasculature of solid tumors. It positively correlates with tumor progression or metastasis in prostate cancer tissue, thus, differentiating benign tumors from malignant disease (Gaertner et al., 2017; Maghsoudi et al., 2019). More crucially, the presence of internalization motif in the cytoplasmic tail of PSMA might suggest that the ligand nanotherapeutics may get internalised into the cell (Mangadlao et al., 2018).

1.8. J591 as biomarker proteins in for targeted therapy of prostate cancer

J591, an anti-PSMA monoclonal antibody (Ab), has already been developed to target PSMA and has demonstrated cellular internalization (Moffatt et al., 2006; Chang et al., 2004). The absence of the majority of extra-prostatic expression of PSMA on normal vasculature endothelium makes feasible for J591 ab to target the prostate cancer cells.

1.9. Surface modification of Paclitaxel loaded PLGA nanoparticles for site specific delivery

Various ligands such as antibodies, aptamers, peptides are used for site specific delivery of chemotherapeutics. In our present work, surface of Paclitaxel loaded PLGA nanoparticles was fabricated with J591 antibody. The surface modification was done with the help of 1-(3-dimethylaminopropyl)-3-ethylcarbodiimide hydrochloride (EDC) and N-hydroxysuccinimide (NHS), which forms peptide bonds between the amine groups of the J591 Ab and the carboxyl groups of the PLGA (Lee et al., 2021). The attachment of antibody is done through the amine group present on the surface of nanoparticle conserves the activity of the antibodies while simultaneously preventing nonspecific protein absorption (Tan et al., 2015). Ligand conjugated nanoparticles in prostate cancer therapy in the field of nanomedicine may lead promising future.

1.10. Ab-PTX-NP research envisaged

In our present study, focus on delivering paclitaxel as a chemotherapeutic payload by encapsulating it in a designed PLGA nanoparticle (PTX-NP), and further conjugating it with J591 Ab (Ab-PTX-NP), aids in the higher cellular internalization of Paclitaxel to PSMA expressed prostate cancer cells. Elevated cellular uptake of Paclitaxel by the prostate cancer cells was possible by using the extracellular apical domain of PSMA, which contains binding site for humanized J591 Ab, enabling it as a plausible target, and it may hold potential promise for tumor targeting. The current goal of the investigation was to target PSMA positive (+ve) LNCaP cells with J591 conjugated nanoparticles containing paclitaxel. It appraised the selectivity of Ab-PTX-NP to PSMA (+ve) prostate cancer cells, its cellular internalization, and drug related apoptotic activity in those cells. Further, pharmacokinetic assessment of the formulation was conducted in Balb/c mice. J591 has been widely used for imaging (Taylor et al., 2012). However, in our study, it has been utilized as a ligand, which when conjugated to the drug loaded nanoparticle can be utilized for advanced prostate chemotherapy.

2. Literature review

2.1. Information on prostate cancer

Today, the leading cause of cancer-related mortality among males is prostate cancer. Age, ethnicity, and inheritance are all significant contributors to the onset and progression of prostate cancer, while the precise reason is unknown. Age is thought to be the biggest risk factor, with most instances being identified in males between the ages of 60 and 70 (Sharma et al., 2017).

Early-stage prostate cancer generally has no symptoms and progresses slowly, necessitating only active observation. Worldwide variations in incidence rates are a result of diverse approaches to diagnostic testing. Age has a significant impact as mentioned earlier, on both the incidence and fatality rates of prostate cancer, with older men experiencing the greatest incidence. Early stage diagnosis is difficult due to non-prominent symptoms, and in late stages of metastasis, treatment becomes very difficult (Rawla, 2019).

Prostate cancer patients can now receive more accurate prognostic information due to enhanced risk categorization tools, imaging technologies, and biomarkers. For some men, local therapy followed by monitoring for disease development is an acceptable treatment plan for prostate cancer. As treatment-related side effects are better identified, surgical and radiation procedures are continually evolving. Due to the early administration of novel medications, the median survival for men with metastatic illness has also increased. With recent developments, prostate cancer may now be correctly diagnosed and controlled more effectively in accordance with tumour biology, patient preferences, and other factors (Litwin et al., 2017).

2.2. Paclitaxel as an anticancer drug

Cancer is a condition with a high mortality rate. Despite substantial research, not all attempts in the field of medicine have been successful. Chemotherapy is administered to more than half of all cancer patients. One such successful discovery is the Paclitaxel isolated from the Pacific Yew tree (Priyadarshini and Keerthi, 2012). Paclitaxel is a crystalline powder that ranges in colour from white to off-white. Its empirical formula is $C_{47}H_{51}NO_{14}$, and its molecular weight is thought to be 853.9 units. It has strong hydrophobicity and is particularly insoluble in water. It melts at a temperature of 216-217 °C. Paclitaxel targets tubulin,

stabilises and prevents microtubule disintegration. The beta-tubulin subunit has been identified as the site of drug binding.

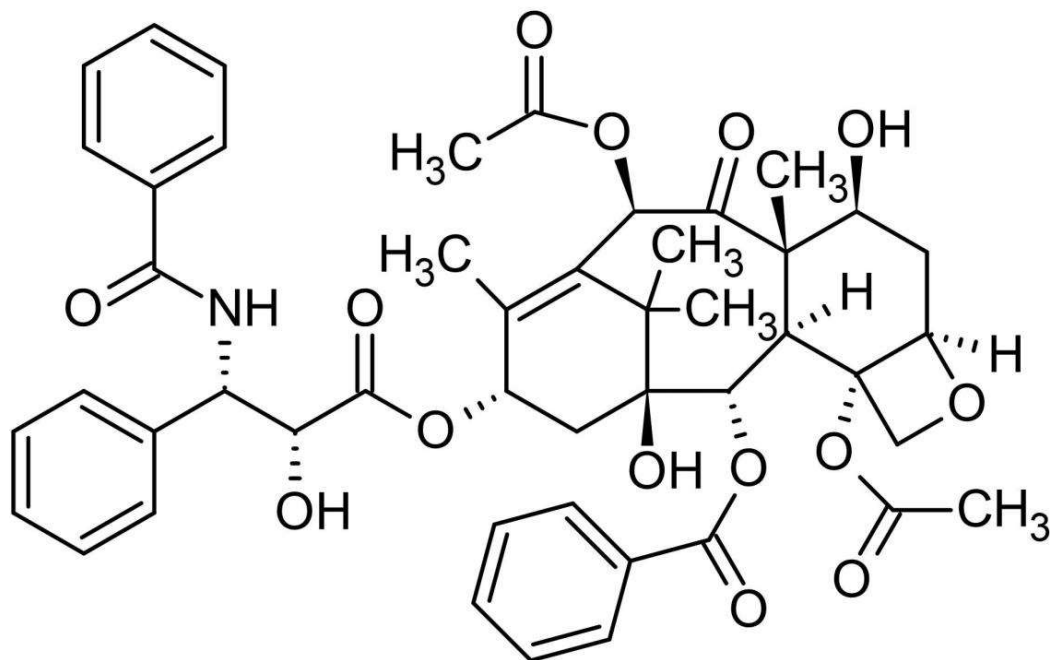


Figure 2.1. Chemical structure of Paclitaxel

2.3. Nanotechnology and nanoparticles for cancer treatment

Rizvi and Saleh (2018) in his review, mentioned that the invention of pharmaceutical novel drug delivery such as nanoparticles has created new opportunities for the treatment of complicated diseases. Nanoparticles usually used for cancer treatments are in the size range between 100 and 500 nm. The nanoparticles may be developed into smart systems, encasing therapeutic and imaging chemicals. He further adds that nanoparticles can be manipulated in their size, surface properties, and material composition. The prolonged drug release from the formulation reduces medication-related toxicity while also improving patient compliance with less frequent dosage. Treatment for AIDS, cancer, and other diseases has benefited from nanotechnology, which has also improved diagnostic procedures.

The introduction of nanoparticles in the area of cancer has given scientists the knowledge they need to investigate brand-new approaches to the detection, prevention, and therapy of cancer. Utilizing nanotechnology has made it possible to create nano-sized formulations that may be used to encapsulate anti-cancer drugs that have proven good benefits but are often toxic owing to the high number of doses required for prolonged usage (Siddiqui et al., 2012).

They also presented an innovative idea in which nanotechnology was used to improve the effectiveness of chemoprevention and described recent uses of nanotechnology in the diagnosis, imaging, therapy, and prevention of cancer. Cho et al., (2008), describes that cancer nanotherapeutics is increasing and that these formulations are being used to overcome the shortcomings of conventional drug delivery techniques, such as non-specific biodistribution and targeting, a lack of water solubility, insufficient oral bioavailability, and low therapeutic indices. In order to extend the biodistribution of cancer therapies for a longer period of time in the circulation, nanoparticles have been designed for the ideal size and surface qualities. Additionally, they have the capacity to deliver their loaded active medications to cancer cells by selectively using the unique pathophysiology of tumours, such as their increased permeability and retention impact on the tumour microenvironment.

There is a substantial interest in developing therapeutic options for the treatment of prostate cancer based on the use of nanoformulations to overcome the lack of specificity of conventional chemotherapeutic agents as well as for the early detection of precancerous and malignant lesions. Sanna et al., (2012) highlighted on the recent development of nanotechnology strategies adopted for the management of prostate cancer, in particular, the combination of targeted and controlled-release polymer nanotechnologies. However, several limitations facing nanoparticle delivery to solid tumours, such as heterogeneity of intratumoural barriers and vasculature, cytotoxicity and/or hypersensitivity reactions to currently available cancer nanomedicines, and the difficulty in developing targeted nanoparticles with optimal biophysicochemical properties, have been addressed for successful tumour eradication (Sanna et al., 2012).

2.4. Polymeric nanoparticles

Biodegradable polymeric nanoparticles are being exploited as cutting-edge medication delivery devices because of their adaptability and diverse set of qualities. This kind of carrier has a lot of potential for controlled delivery of vaccines and treatments for cancer (Hans et al., 2002). Rezvantab et al., (2018) also mentioned that PLGA nanoparticles have demonstrated their promise as drug delivery vehicles for several therapeutic agents (such as proteins, chemotherapy, antibiotics, antiseptics, anti-inflammatory, and anti-oxidant medicines), and they can be advantageous for tumor-and/or DNA-targeting. Biodegradable nanoparticles have the potential to deliver cancer therapeutics within the body. Biodegradable nanoparticles are attracting more attention. For a variety of drugs, vaccines, and biomolecules

to be used in a variety of medical applications, they offer improved biocompatibility, superior drug encapsulation, and practical release profiles (Mahapatro et al., 2011). Numerous studies have been conducted on biodegradable nanoparticles made of poly (D,L-lactide-co-glycolide) (PLGA) for the sustained and targeted/localized administration of various agents, such as plasmid DNA, proteins, peptides, and low molecular weight chemicals (Panyam et al., 2002). Poly (lactic-co-glycolic acid) is one of the most efficient biodegradable polymeric nanoparticles. Because of its controlled and sustained release capabilities, minimal toxicity, and biocompatibility with tissue and cells, it has received USFDA approval for use in drug delivery systems. With excellent efficacy and low side effects, the use of PLGA nanoparticles in cancer treatment has a bright future, thanks to growing experience in this field, (Mirakabad et al., 2014), Numerous cancer treatments, such as photodynamic therapy, hyperthermia, and tumor-targeted medication delivery, can be carried out using materials based on poly (lactic-co-glycolic acid) (PLGA), which are often employed in such configurations (Danhier et al., 2012).

Various surface modifications of nanoparticles to enhance in-vivo circulation, distribution, and multimodal functionalities, along with specific applications such as tumour targeting, oral delivery, and delivery of these particles to the central nervous system, have been reviewed in this manuscript. Also, different factors that affect optimal drug encapsulation, factors that affect drug release rates, and surface modifications of nanoparticles to improve in-vivo circulation, distribution, and multimodal functions have all been looked at.

2.5. Poly-(D-L-lactide-co-glycolide (PLGA) nanoparticles encapsulating anti-cancer drugs.

There have been numbers of studies in which anti-cancer drugs are encapsulated in PLGA nanoparticles. Mandal et al., (2018) developed PLGA nanoparticles with chemotherapeutic agents to treat hepatocellular carcinoma, which increased the drug water solubility, a decrease in chemotherapy related adverse effects and toxicity, an enhancement in the pharmacokinetic characteristics and tissue distribution through the faulty lymphatic system and leaky neovasculature of tumour cells, and an enhancement in the anti-tumor efficacy of anticancer agents. PLGA has been particularly useful in the development of drug nanocarriers for cancer therapy due to its excellent biocompatibility, biodegradability, high stability, and low immunogenicity. The prepared formulation can also passively target new drug delivery systems and has an improved permeability and retention effect (EPR).

Bhattacharya et al., (2018) developed apigenin-loaded PLGA nanoparticles and looked into the effectiveness of the anticancer drug apigenin both in vitro and in vivo, in order to suppress the growth of liver cancer. The PLGA nanoparticles were ideal for the purpose due to their non-toxic and biodegradable qualities.

Sahoo et al., (2004) in their work, evaluated the effectiveness of biodegradable nanoparticles made of PLGA loaded with paclitaxel in inhibiting tumour growth. Chemotherapy is still the treatment of choice for prostate cancer, although its efficacy is limited by conventional routes of administration, low drug response, and severe toxicity. In a murine model of prostate cancer, the antiproliferative activity of PLGA NP was assessed in a human prostate cancer cell line (PC3) and its impact on tumour inhibition. The nanoparticles were 220 nm in diameter with 5.4% w/w drug loading and demonstrated sustained release of the encapsulated medication (60% release in 60 days).

2.6. Fabrication of the PLGA nanoparticles for site-specific delivery.

Active targeting of PLGA nanoparticles to cancer cells

Drug delivery technologies that are conventional and that have a variety of limitations are being replaced by multifunctional nanoparticles. Nanoparticles that have been specially designed to target cancer cells have the potential to lessen the collateral harm that medicines' overall toxic effects cause to healthy tissue. Since the recently discovered methodologies demonstrate superior targeted anticancer therapeutic delivery with better treatment results, practical ways are being considered to advance cancer therapy. Effective cancer therapy necessitates both types of targeting including passive and active, as well as a comprehensive awareness of numerous physiologic impediments to targeted delivery (Ahmad et al., 2019). Bazak et al., (2015) also writes about targeting of nanoparticles that may be accomplished in two ways: passive targeting and active targeting. The effective localisation of nanoparticles into the tumour microenvironment is made possible by passive targeting. Active targeting makes it easier for tumour cells to specifically take up nanoparticles.

To successfully deploy nanoparticle carriers as medication delivery systems, it is essential to target them to disease areas. Researchers have concentrated on surface modification of nanoparticles using biological ligands in addition to optimization of their physicochemical features. Such ligands have the ability to bind certain receptors on the surface of target cells. Additionally, biological ligands can promote the absorption of modified nanoparticles, and the process is known as "active targeting" of nanoparticles. In this review work, the

researcher highlighted the recent developments in the area of biological ligands for nanoparticle-mediated drug delivery. Such ligands include proteins, antibodies, polysaccharides, aptamers, peptides, and small molecules. The review seems to be useful to biomedical researchers who use NP for imaging and medicine delivery (Yoo et al., 2019).

Mondal et al., (2019) in their work fabricated the surface of PLGA nanoparticles containing doxorubicin (DOX) by conjugating it with CD-340 antibody to target breast cancer cells. When compared to the treatments with the unconjugated and conjugated nanoparticles, the CD-340 surface modified nanoparticle formulation revealed preferentially more of the formulation accumulation in the tumour region. The ligand linked nanoparticles shown significant promise in reducing the cardiac toxicity of DOX in mice, a notable adverse effect of the medication, as well as tumour development

2.7. Prostate specific membrane antigen (PSMA)

The use of cell surface antigens as biomarkers has the capability to significantly improve early diagnosis, prognosis, and therapeutic response in a wide range of disorders, including malignancies (Sanjeev et al., 2021). In prostate cancer, the transmembrane glycoprotein known as PSMA, which is found on the cell membrane, is particularly and prominently expressed. Additionally, tumour invasiveness is correlated with its expression level. Over the past 20 years, a great deal of research has been done on PSMA as a molecular target of prostate cancer. Evidence examined by Wang et al., (2022) indicates that considerable advancements in PSMA-targeted prostate cancer treatment have been made. Here, it was mentioned about the various PSMA-targeted treatments for prostate cancer, such as using attaching ligand with radiotherapy, examples ^{177}Lu -PSMA-RLT and ^{225}Ac -PSMA-RLT, conjugating the antibody with respective drugs to form conjugates such as MLN2704, PSMA-MMAE, MEDI3726. Also therapeutic efficacy of cellular immunotherapy, photodynamic therapy and imaging-guided surgery were discussed.

2.8. J591 antibody site-specificity to PSMA

J591 is widely used in diagnostic purposes, it is engineered with several formulations to target PSMA. Russell et al., (2013), in the study prepared prostate cancer-targeted magnetic nanoparticles (MNPs) and conjugated them with J591, an antibody particularly attaches to the prostate specific membrane antigen (PSMA). PSMA is present above 90% on the surface of the prostate cancer cells, which also includes castration-resistant prostate cancer cells. This conjugation causes internalization of the prostate cancer-targeted MNPs. Tailored MNPs

should improve the site- specificity along with sensitiveness of magnetic resonance imaging (MRI) to allow for more accurate staging patients and eventual targeted medication administration. It is further mentioned that the conjugation did not affect the cell binding of J591Ab to the PSMA positive prostate cancer cells. The prepared formulation was taken up more readily which was confirmed by Prussian blue staining for iron and plasma optical emission spectroscopy for attachment of antibody. In vivo experiments were carried out on immunosuppressed mice with subcutaneous LNCaP-LN3 (PSMA-positive) xenografts using a 16.4T MRI imaging system. The results of administration of J591-MNP conjugates showed similar augmentation of MRI as obtained by NMR. Mice administered systemic J591-MNPs underwent live imaging, which revealed prostate tumour uptake.

Tse et al., (2015) prepared and evaluated J591antibody conjugated iron oxide magnetic nanoparticles. The results showed enhanced magnetic resonance imaging (MRI) on investigation, when targeted with conjugated nanoparticles as compared to unconjugated nanoparticles. The reason for enhanced MRI would be specific to binding of PSMA by J591 fabricated iron oxide magnetic nanoparticles. The results were depicted in SCID mice at predetermined time, when the above nanoparticles were injected intravenously. It was also noted that the antibody conjugation did not hinder its specificity. Hence, it is proved that PSMA-targeting nanoparticles fabricated with J591 antibody have the caliber to localize in prostate cancer.

A PSMA antibody functionalized formulation may be very helpful for targeted prostate cancer treatment. Nagesh et al., (2016), developed a tailored nanoparticle system encapsulating docetaxel to enhance its distribution and action at the tumour location by functionalizing it with J591 for prostate cancer. In his findings, conjugated formulations demonstrated strong anti-cancer activity, when compared to PSMA-negative PC3 cells and PSMA-positive C4-2 cells. The J591-conjugated formulation was profoundly taken up by C4-2 (PSMA+) cells. While PC-3 tumours did not exhibit a similar targeting capability in ex-vivo experiments, C4-2 tumours did, which suggests tumor-specific targeting. It was concluded from the study that a PSMA antibody functionalized SPION-DXT formulation may be very helpful for targeted prostate cancer treatment.

3. Objectives and plan of study

3.1. Objectives

To develop and optimize Paclitaxel (as a therapeutic agent) loaded poly lactic co-glycolic acid (PLGA) nanoparticles and further conjugating it with J591 antibody (anti-PSMA) and investigate them as a targeted therapy against prostate cancer cells.

This study is divided in following sections:

- Paclitaxel loaded nanoparticles (PTX-NP) will be prepared and conjugated with an anti-PSMA antibody J591 for site specific delivery. Physicochemical properties of the prepared formulation will be studied
- Further, investigation to target PSMA overexpressed on LNCaP cells with J591 conjugated nanoparticles containing paclitaxel will be done
- Appraised selectivity of Ab-PTX-NP to PSMA (+ve) prostate cancer cells, its cellular internalization, and drug related apoptotic activity in prostate cancer cells will be studied
- Pharmacokinetic assessment of the optimized formulation will be was conducted in Balb/c mice.

3.2. Plan of study

The study is planned as delineated below

❖ Preformulation studies

- Detection of interaction between drug and excipients by Fourier-transform infrared spectroscopy (FTIR)
- Development of Standard Calibration Curve of Paclitaxel by UV Spectroscopy.

❖ Preparation and optimization of PLGA nanoparticles encapsulating Paclitaxel

- Preparation of Paclitaxel loaded polymeric nanoparticles (PTX-NP) by multiple emulsion and solvent evaporation.
- Conjugation of the prepared nanoparticle with J591 antibody to ensure site specific delivery to the prostate cancer cells (Ab-PTX-NP).
- Confirmation of the successful antibody conjugation.

- Evaluation of morphological characterizations of the prepared experimental nanoparticles will be done by using field emission scanning electron microscopy (FESEM), transmission electron microscopy (TEM), atomic force microscopy (AFM), DLS for the determination of the size and zeta potential.
- Assessment of stability of prepared optimized nanoparticles by accelerated stability study and hydrolytic stability study.

❖ ***In-vitro* drug release studies**

- *In-vitro* drug release various experimental formulations will be performed in PBS (pH 7.4) with 0.1%w/v tween 80. The drug release of Ab-PTX-NP in citric acid buffer (pH 3), acetic acid buffer (pH 5), PBS (pH 7.4) with 0.1%w/v tween 80 and bicarbonate buffer (pH 10) using cumulative drug release method.
- Assessment of various drug release kinetics and regression coefficients of the prepared formulation in different buffers.

❖ ***In- vitro* cellular experiments in LNCaP and PC3 cells**

- Examination of the expression of PSMA on LNCaP cells
- Cytotoxicity study by MTT assay
- *In vitro* cellular uptake both qualitative and quantitative study, cellular apoptosis, apoptosis-induced morphological alterations by dual staining with acridine orange/ethidium bromide (AO/EB), determination of the loss and alteration of mitochondrial membrane potential (MMP), Quantification of apoptotic/necrotic cells by flow cytometry.

❖ **Hemolysis study**

❖ ***In-vivo* experiments**

- Pharmacokinetic studies of drug-loaded experimental nanoparticles and free paclitaxel in male Balb/c mice and evaluation of pharmacokinetic parameters.

❖ **Statistical Analysis**

- One way analysis of variance (ANOVA) will be used, followed by Tukey's test conducted for comparison between the experimental groups.

4. Materials and equipments

4.1. The chemicals used in the study have been listed below

Table 4.1. List of materials/chemicals used in the study

Serial No	Name	Source
1.	Acetone	Merck Life Science Pvt. Ltd, Bengaluru
2.	Acetonitrile	Merck Life Science Pvt. Ltd, Bengaluru
3.	Bicinchoninic acid (BCA)	Sigma-Aldrich Co, St Louis, MO, USA.
4.	Cell lysis buffer	Abcam
5.	Chloroform	Merck Life Science Pvt. Ltd, Bengaluru
6.	Citric acid	Merck Life Science Pvt. Ltd, Bengaluru
7.	4',6'Diamidino-2-phenylindole (DAPI)	Thermo Fisher Scientific, Mumbai, India
8.	Dichloromethane (DCM)	Merck Life Science Pvt. Ltd, Bengaluru
9.	Disodium hydrogen phosphate	Merck Life Science Pvt. Ltd, Bengaluru
10.	Dimethylsulfoxide (DMSO)	Merck Life Science Pvt. Ltd, Bengaluru
11.	Ethylene diamene tetra acetic acid (EDTA)	Merck Life Science Pvt. Ltd, Bengaluru
12.	1-(3-dimethylaminopropyl)-3-ethylcarbodiimide hydrochloride (EDC)	Himedia Laboratories Pvt. Ltd., Maharashtra, Mumbai, India.
13.	Ethyl Acetate	Merck Life Science Pvt. Ltd, Bengaluru,
14.	FBS	HiMedia Laboratories, Mumbai, India
15.	Fluorescein isothiocyanate (FITC)	HiMedia Laboratories, Mumbai, India
16.	FITC annexin V/dead cell apoptosis kit	Thermo Fisher Scientific, Waltham, MA, USA
17.	Glacial acetic acid	Merck Life Science Pvt. Ltd, Bengaluru,
18.	J591 monoclonal antibody (J591 Ab)	Dr Neil Bhandar, Cornell University, San Diego, California, United States.
19.	5,5',6,6'-Tetrachloro-	Invitrogen (Carlsbad, CA, USA).

Serial No	Name	Source
	1,1',3,3'-tetraethyl benzimidazolylcarbocyanine iodide (JC-1)	
20.	Methanol	Merck Life Science Pvt. Ltd, Bengaluru,
21.	MTT 3-(4,5-dimethylthiazol- 2-yl)-2,5- diphenyltetrazolium bromide	HiMedia Laboratories, Mumbai, India
22.	N-hydroxysuccinimide (NHS)	Himedia Laboratories Pvt. Ltd., Maharashtra, Mumbai, India.
23.	Paclitaxel (PTX)	A gift samples provided by Fresenius Kabi Oncology, Kolkata, West Bengal, India with 99.95% purity
24.	Penicillin-Streptomycin	HiMedia Laboratories, Mumbai, India
25.	PLGA Acid-terminated PLGA (ratio, 75:25; molecular weight, 4,000– 15,000 Da)	Sigma-Aldrich Co, St Louis, MO, USA.
26.	Pluronic F-68	HiMedia Laboratories, Mumbai, India
27.	Pluronic F127	Sigma-Aldrich Co, St Louis, MO, USA.
28.	Potassium dihydrogen phosphate	Merck Life Science Pvt. Ltd, Bengaluru,
29.	Polyvinyl alcohol (PVA) (M.W. 85,000- 1,24,000) (MW 150,000)	S D Fine-Chemicals limited, Mumbai, India
30.	Roswell Park Memorial Institute Medium (RPMI 1640)	HiMedia Laboratories, Mumbai, India
31.	Sodium acetate	Merck Life Science Pvt. Ltd, Bengaluru,
32.	Sodium bicarbonate	Merck Life Science Pvt. Ltd, Bengaluru,
33.	Sodium carbonate	Merck Life Science Pvt. Ltd, Bengaluru,
34.	Sodium citrate	Merck Life Science Pvt. Ltd, Bengaluru,
35.	Sodium hydroxide	Merck Life Science Pvt. Ltd, Bengaluru,

Serial No	Name	Source
36.	Trypsine	HiMedia Laboratories, Mumbai, India
37.	Tween 80	SD Fine Chemicals limited, Mumbai, India
38.	D- α -tocopherol polyethylene glycol succinate (TPGS)	Sigma-Aldrich Co, St Louis, MO, USA.
39.	Water for HPLC 41. Millex-GP Syringe Filter Unit, 0.22 μ m, polyethersulfone, 33 mm, gamma sterilized Millipore Corp. Billerica, MA, USA	Merck Life Sc. Pvt. Ltd., Mumbai, Maharashtra, India
40.	Milli-Q water Millipore	Corp. Billerica, MA, USA

4.1.2 Animals and different cells used in the study

Table 4.2 The source of animals and different cells used in the study

Animals	Source
Balb/C male mice	National Institute of Nutrition (NIN), Hyderabad, Telangana, India.154/GO/RBiBt- S/RL/99/CPCSEA
Human Cells	Source
LNCaP cells, PC3 and HEK 293 cells	National Centre for Cell Sciences, Pune, India

4.2. Instruments

Table 4.3 List of Instruments and equipments used in the study are mentioned

Serial No	Name	Source
1.	Atomic force microscope	Dimension icon, Bruker, Billerica, Massachusetts, USA
2.	Bath sonicator	Trans-O-Sonic, Mumbai, India
3.	FAC Scan Flow Cytometer	BD biosciences, San Jose, CA,USA

Serial No	Name	Source
4.	CO ₂ incubator	Thermo Fisher Scientific, Waltham, MA USA
5.	Cold centrifuge	HERMLE Labortechnik GmbH, Wehingen, Germany
6.	Confocal microscope	TCS-SP8 confocal microscope, Leica, Germany
7.	Digital pH meter (EUTECH)	Thermo Fisher Scientific India Pvt. Ltd., Hiranandani Business Park, Mumbai India
8.	Digital weigh balance	Sartorius Corporate Administration, Otto-Brenner-Straße 20, Goettingen, Germany
9.	Disposable syringe (Dispo Van)	Hindustan Syringes and Medical Devices Limited, Ballabgarh, Faridabad, Haryana, India
10.	FTIR instrument	Magna-IR 750, Series II, Nicolet Instruments Inc, Madison, Wisconsin, USA
11.	Normal freezer	LG double door, Yeouido-dong, Seoul, South Korea
12.	-80° C Freezer (Model no U410-86)	New Brunswick Scientific, Eppendorf House, Arlington Business Park, Stevenage, UK
13.	High speed homogenizer	IKA Laboratory Equipment, Model T10B Ultra-Turrax, Staufen, Germany
14.	Incubator shaker	BOD-INC-1S, Incon, India
15.	Laminar airflow bio-safety hood	Thermo Fisher Scientific, Waltham, MA USA
16.	LC-MS/MS	LC: Shimadzu Model 20AC, MS: AB-SCIEX, Model: API4000, Software: Analyst 1.6
17.	Laboratory Freeze Dryer (lyophilizer)	Instrumentation India, Kolkata, India
18.	Magnetic stirrer	Remi Sales & Engineering Ltd, Ganesh Chandra Avenue, Bando House, Dharmatala, Kolkata, India
19.	0.22 membrane filter	Merck Life Science Pvt. Ltd, Mumbai, India
20.	Microplate reader	Spectromax ,Japan
21.	Particle size and zetasizer	Zetasizer nano ZS 90, Malvern Zetasizer Limited, Malvern, UK

Serial No	Name	Source
22.	Scanning Electron microscope	SEM Joel JSM-7600 F, Tokyo, Japan
23.	Transmission electron microscope	TEM, JEOL JEM-2010, JEOL, USA
24.	UV-VIS spectrophotometer	LI-295 UV VIS Single Beam, Lasany International, India
25.	Vortex mixture	Remi Sales & Engineering Ltd, Ganesh Chandra Avenue, Bando House, Dharmatala, Kolkata, India
26.	Zeiss Light microscope.	Carl Zeiss: Axiostar plus, Jena, Germany

5. Methodology

5.1. Calibration curve of Paclitaxel with the help of UV-visible spectroscopy

The maximum wavelength (λ_{\max}) of PTX is reported to be 227 nm (Chakraborty et al., 2020) in different solvents. We ran an absorbance spectrum between 200 and 600 nm to find the exact absorption maximum of the drug procured for our research. In order to conduct this study, a small amount of PTX was dissolved in acetonitrile-water (60:40 v/v). The software was used to establish a baseline for the research (LI-295 UV VIS Single Beam Spectrophotometer).

To begin, 1 mg/ml Paclitaxel stock solution was made with acetonitrile water. The paclitaxel stock solution was then diluted to produce a range of solutions with known concentrations, and the absorbance was recorded in a LI-295 Ultra Violet Visible single beam spectrophotometer against blank solution (without drug). Both the slope and regression coefficient were obtained from the graph made by plotting absorbance versus concentration.

5.2. Preparation of nanoparticles

Paclitaxel loaded biodegradable PLGA nanoparticles (PTX-NP), and FITC labeled PTX-NP were prepared by multiple emulsion solvent evaporation method (Mandal et al. 2018; Bhattacharya et al. 2018) mentioned below. Interim alterations of solubilizers such addition of TPGS (0.03%w/v), Tween 80 (14% v/v), Pluronic- F 68 (0.5% w/v) and Pluronic F-127 (0.5% w/v) along with PVA (2.5% w/v) in the organic phase to detect the drug loading and stability for the optimization of nanoparticles were done. The formulation PTX-NP with solubilizer TPGS (0.03%w/v) was selected as an optimized formulation.

To prepare PTX-NP, 5 mg of the drug (PTX), 50 mg biodegradable polymer PLGA with the addition of TPGS (0.03% w/v), were dissolved in 3 ml solvent comprising of 1 part of dichloromethane and 1 part of acetone [1:1 (v/v)]. The primary emulsion was made by adding polyvinyl alcohol (PVA) drop by drop from the stock solution (2.5 percent v/v aqueous PVA solution) to the organic phase while homogenising at 16000 rpm with a high-speed homogenizer. Subsequently, water/oil/water (w/o/w) type multiple emulsion was made in 75 ml of 1.5% PVA solution by adding the formed primary w/o emulsion gradually and homogenized (16000 rpm) (IKA laboratory equipment, model 10B Ultra-Turrax, Staufen, Germany) for 8 min. After homogenization, the emulsion was kept on bath type sonicator (TRANS-O-SONIC, Mumbai, India, 30±3 kHz, in cold water) for 30 min, and then left

overnight to stir on a magnetic stirrer to evaporate the organic solvent. The next day, it was centrifuged for 10 min (3000 rpm at 4°C) which helps to separate the nanoparticles from larger size particles. Thereafter, the supernatant was centrifuged for 45 min (16000 rpm at 4°C). The pellet obtained was washed twice using water and stored at -20°C. A freeze dryer (Laboratory Freeze Dryer, Instrumentation India, Kolkata, India) was used to lyophilize the final product. Blank nanoparticles (BNP) were also prepared following similar method without the encapsulation of the drug (PTX) in the organic phase.

Conjugation of prepared nanoparticles with antibody (Ab-PTX-NP)

The conjugation of J591 Ab to the surface of the prepared nanoparticles was done using EDC and NHS as mentioned in the literature (Mondal et al., 2019). In brief, a weighed quantity of lyophilized optimized nanoparticles (PTX-NP) were suspended in PBS (1 mg/1 mL). 1 μ L J591 Ab (from the primary stock) was added to the prepared solution. Subsequently, the solution was incubated at 25°C for 1 h, and then centrifuged at 16,000 rpm for 10 min to redundant antibodies. The precipitate thus obtained after centrifugation was resuspended in PBS and followed by washing thrice to get rid of any residual antibody that may be present on the surface of the conjugated nanoparticles. The final product was then lyophilized and stored stored at 4°C (Mukherjee et al., 2014).

5.3. Fourier-transform infrared (FTIR) spectroscopy

Fourier-transform infrared (FTIR) spectroscopy was utilized to look for any possible interactions between the drug and the selected excipients used for the preparation of PTX-NP as reported (Chakraborty et al., 2019). Paclitaxel, PVA, PLGA, physical mixture of PLGA and PVA, physical mixture of PLGA, PVA and PTX, BNP, PTX-NP, TPGS, physical mixture of PLGA, PVA, TPGS and physical mixture of PLGA, PVA, drug, and TPGS were mixed with infrared grade potassium bromide (1:100 ratio) and compressed in a hydraulic press to form pellets. The above pellets were scanned from the range of 4000 cm^{-1} and 400 cm^{-1} using FTIR spectroscopy (IRAffinity 1, Shimadzu, Japan).

5.4. Physicochemical characterization of PTX-NP and Ab-PTX-NP

5.4.1. Particle size and zeta potential

The lyophilized nanoformulations were resuspended (Milli-Q® water), sonicated for 15min and were examined for particle size of the nanoformulations, its distribution, PDI value along with zeta potential, in the Zetasizer Nano ZS 90 (Malvern Instruments, Malvern, UK) at 25C.

Data Transfer Assistance (DTA) software (Malvern Zetasizer Limited, Malvern, UK) was used for the analyses of the data.

5.4.2. Drug loading and encapsulation efficiency

To evaluate the drug loading and its encapsulation efficiency of PTX- NP and Ab-PTX-NP, 2mg of each formulation was dissolved in 2ml of acetonitrile water (6:1 v/v) followed by sonication for 30 min. it was then centrifuged for 10 min at 16000 rpm. The absorbance was recorded with the help of Ultra Violet Visible single beam spectrophotometer against blank solution (acetonitrile water (6:1 v/v) without drug). The percentage of Drug loading and encapsulation efficiency was calculated (Das et al., 2015).

Actual drug loading (weight %) = (Amount of drug present in nanoparticles/Total weight of nanoparticles sample analyzed) X 100 (%)

Drug loading efficiency (%) = (Actual drug loading/Theoretical drug loading) X 100 (%)

5.4.3. Scanning electron microscopy (SEM)

The surface morphology of lyophilized PTX-NP and Ab-PTX-NP were studied by SEM (Joel JSM-7600 F, Tokyo, Japan). The samples were taken on adhesive carbon tapes which were placed on metallic stubs followed by platinum coating using sputter coater (QUORUM Q 150T ES) and observed in the SEM instrument as per the published protocol. (Bhattacharria et al., 2018; Mandal et al., 2018).

5.4.4. Transmission electron microscopy (TEM)

The lyophilized samples were resuspended in Milli-Q water and a drop of it was placed on a carbon-coated copper grid (300#; Ted Pella Inc., CA, USA). The excess solution was removed using blotting paper and dried overnight. It was then visualized in the TEM instrument (JEM 2100; JEOL, Tokyo, Japan).

5.4.5. Atomic force microscopy (AFM)

A small quantity of lyophilized PTX-NP and Ab-PTX-NP was resuspended in Milli-Q water and a drop of each sample was placed on respective fresh cover slips and dried overnight. Further investigation for three-dimensional morphology of the particles using a Pico view 5500 (Agilent Technologies, Santa Clara, CA, USA) was done.

5.5. Energy dispersive X-ray assay (EDX)

Energy dispersive X-ray (EDX) analysis determined the elemental composition and encapsulation of the drug in PTX-NP and Ab-PTX-NP. EDX was conducted in a SEM instrument (JSM 60, JEOL, Tokyo, Japan). The experimental formulations were lyophilized followed by spreading it on the metal stub and coating it with platinum (Maji et al., 2014).

5.6. Sodium dodecyl sulfate-polyacrylamide gel electrophoresis SDS-PAGE

To confirm the conjugation of the antibodies on the surface of PTX-NP, the resuspended PTX-NP, Ab-PTX-NP, and BNP in PBS buffer in 0.2 mg/ml concentration and standard anti-PSMA J591 monoclonal antibody (1 μ L) was mixed with 2XLaemmli gel loading buffer (each 5 μ L) separately. Along with the marker, PTX-NP, Ab-PTX-NP, and BNP were loaded to a 10% SDS-PAGE gel. Gel electrophoresis was done by running the gel (80 V up to stacking and 100V up to resolving) (Hu et al., 2010; Aggarwal et al., 2013)

5.7. *In vitro* drug release analysis

The evaluation pattern of drug release from the commercial formulation (CF), PTX, PTX-NP and Ab-PTX-NP *in vitro* in phosphate buffer saline (PBS, pH 7.4) with 0.1% tween 80 was studied. *In vitro* drug release study was evaluated for each of the experimental samples which were weighed (2 mg each) individually and resuspended in 2ml of the respective buffers. (The amount of PTX present in 2mg of PTX-NP and Ab-PTX-NP was 138.8 μ g and 128 μ g, respectively). It was followed by the incubation maintained at 37°C with agitation 60 rpm in BOD incubator shaker. At different time intervals 0.5, 1, 2, 4, 6, 10, 12, 24, 48, 72 till 2200 h, 1ml (supernatant) from each sample was collected after 10 min of cold centrifugation (16,000 rpm in Hermile Labortechnik GmbH, Wehingen, Germany). The volume (1ml) was replaced with the respective buffers. The samples were resuspended with the help of vortex and were placed in the incubator and maintained in the same mentioned condition till the next sampling. The drug was determined by reading the absorbance measured in the UV-VIS spectrophotometer at 227 nm against fresh respective media/buffer. The calibration curve obtained facilitates calculating the drug's concentration. To ensure reproducibility, the operation was done three times (Mandal et al., 2018; Mondal et al., 2019). Further, the release pattern of PTX from Ab-PTX-NP in citrate buffer (pH 3), acetate buffer (pH 5) and bicarbonate buffer (pH 10) for duration of 90 days according to the method described above and calculated in the cumulative drug release method (Mondal et al., 2019).

Different release kinetics models with their equations are listed below:

Zero-Order: $Q_t = Q_0 + K_0t$ (% CDR vs. time)

First-Order: $\text{Log } Q_t = \text{Log } Q_0 - Kt / 2.303$ (log % ADR vs. time)

Higuchi model: $Q_t = k_H (t)^{0.5}$ (% CDR vs. root of time)

Hixson-Crowell model: $Q_0^{1/3} - Q_t^{1/3} = K_{HC} t$ (Cube root of % ADR vs. time)

Korsmeyer-Peppas model: $M_t/M_\infty = Kt^n$ (log % CDR vs. log t)

Where, CDR is cumulative drug release, ADR is amount of drug to be released, Q_t is amount of drug release in time t, Q_0 is initial amount of drug, K is release rate constant, k_H is the release rate constant for the Higuchi model, K_{HC} is the rate constant for Hixson-Crowell rate equation, M_t/M_∞ is fraction of drug released at time t, and n is the release exponent in Korsmeyer-Peppas model.

5.8. Accelerated stability study:

To assess the impact of temperature and relative humidity (RH) on the stability of PTX-NP and Ab-PTX-NP, weighed amounts of PTX-NP and Ab-PTX-NP were stored in a refrigerator (zone III) at 4-8 °C, and at 30 °C, 75% RH and 40 °C, 75% RH for 30, 60 and 90 days, according to the International Conference on Harmonization (ICH) guidelines (ICH, 2003). Experimental samples at the mentioned time points were analyzed for the drug loading and morphology.

The hydrolytic stability of PTX-NP and Ab-PTX-NP was ascertained in various pH buffers (citrate buffer pH 3, acetate buffer pH 5, phosphate buffer pH 7.4) for 30 days. (Details are given in the Supplementary file).

Weight variations were measured for each sample over time according to the formula,

$$\text{Weight change (\%)} = (W_0 - W_t)/W_0 \times 100$$

Where, W_0 and W_t represents as the initial weight and weight at time t, respectively.

5.9. *In vitro* studies

5.9.1. *In vitro* cytotoxicity (MTT) study

Two different human prostate carcinoma cells, LNCaP and PC3, were purchased from National Centre for Cell Science (NCCS), Pune, India. Cells were maintained in Roswell

Park Memorial Institute Medium (RPMI 1640) (Hi-Media) supplemented with 10% fetal bovine serum (FBS, Thermo Fisher Scientific, Waltham, USA.), 100 U/ml penicillin, 100 U/ml streptomycin and kept in 5% CO₂ incubator (MCO-15AC; Sanyo, Tokyo, Japan) at 37°C.

The experiments were performed to investigate the cytotoxicity of PTX, PTX-NP, Ab-PTX-NP and the antibody conjugated blank nanoparticles (Ab-BNP) using 3-(4,5-dimethylthiazol-2-thiazolyl)-2,5-diphenyl-2H-tetrazolium bromide (MTT) analysis to obtain the IC₅₀ values of our various experimental formulations in positive PSMA (LNCaP), negative PSMA cells (PC3) and normal kidney cells (HEK 293). All the above mentioned cells were seeded in 96 well plates. The number of cells was 5000 per well. Different concentrations of the experimental formulations were used to treat the cells for 24 h followed by the addition of MTT. The treated cells are incubated at 37°C for 4 h. the addition of DMSO leads to the solubilization of intracellular formazan crystals. Thus, in a microplate reader (Spectromax, Japan) at 540 nm, the color intensity was measured and the cytotoxic effects of PTX, PTX-NP, Ab-PTX-NP and Ab-BNP were calculated (Shi et al., 2018; Sen et al., 2021). Cell viability assay was done on normal human kidney cells HEK 293, since the human normal prostate cell line such as RWPE-1 was not available. The study was conducted on human normal embryonic kidney cell line (HEK 293) just to evaluate the effect of the experimental formulation treatment on any normal cell line. HEK 293 cell type is one most common cell line used for research purposes due to their easy maintenance, robustness and reliable growth (Yao-Cheng et al., Yifan et al., 2020). Besides, the HEK 293 cells are also frequently used as a control in many studies to investigate the effects of treatments on cancer-specific cell lines (Summart et al., 2020). The cell viability assay on normal human kidney cells HER 293 was done in a similar way.

5.9.2. Western blot analysis of PSMA expression in prostate cancer cells

LNCaP and PC3 were cultured until the cell count reached to logarithmic phase, followed by rinsing with phosphate buffer saline (PBS), cooled with the help of ice, radioimmunoprecipitation assay (RIPA) protein lysis buffer was utilized for suspension to make up to 400 µl. The resulting supernatant of centrifuged (15000 rpm/ 4°C for 15 min) cell lysates was transferred to a 1.5 mL centrifuge tube. A bicinchoninic acid (BCA) kit was used for the assay of protein concentration. The lysate samples were supplemented with 5X sodium dodecyl sulfate-polyacrylamide gel electrophoresis (SDS-PAGE) loading buffer, the

protein was denatured by mixing and boiling for 5 min. After separation of protein using SDS-PAGE and transferring to a polyvinylidene fluoride (PVDF) membrane through semi-dry blotting method. After blocking the membrane with a 5% skim milk buffer at room temperature and probing it with diluted anti-PSMA monoclonal antibody at 4°C overnight and probing it with the secondary antibody at room temperature for 2 h. After each antibody incubation, the membranes were washed thrice with PBS (Fan et al., 2015). After the development of immunoreactive bands by chemiluminescent HRP detection agent (Luminata™ Forte Western HRP substrate was used for the assay), the images were captured in BioRad Gel Documentation System using Image Lab Software (Ghosh et al., 2017).

5.9.3. Cellular uptake study of PC3 and LNCaP cells *in vitro*

In vitro cellular uptake of FITC- labeled conjugated and unconjugated PTX-NP was investigated in LNCaP and PC3 human prostate carcinoma cells. The uptake was quantified at 0.5, 2 and 4 h with a flow-cytometer (Becton Dickinson LSR New Jersey, USA). The data were acquired through FACS Diva software (BD Bioscience), New Jersey, USA). Cells were seeded at a concentration of 1×10^5 cells/ml on a cover slip placed on a Petri dish (60 mm) for 24 h to allow the cells to proliferate, adhere and confluent. Complete medium for cell growth was replaced with incomplete medium (culture medium without FBS) in each dish. The next day, cells had reached ~80% confluence, and the cells were treated with FITC labelled PTX-NP and Ab-PTX-NP for 0.5, 2 and 4 h. Plates were removed from the incubator at a predetermined interval and washed three times with sterile cold PBS. Once this was done, the cells were suspended in phosphate-buffer saline. Using a flow cytometer (Becton Dickinson, LSR Fortessa, New Jersey, USA) using FACS Diva software (BD Biosciences, New Jersey, USA), we compared the fluorescent intensities of cells in the control group (cells without treatment) to those treated with the experimental nanoparticles.

Further, the qualitative uptake of the experimental formulations in LNCaP and PC3 cells was investigated by confocal laser microscopy using FluoView FV10i, Olympus microscope using channels FITC (excitation/emission 495nm/519nm) and DAPI (excitation/emission 359nm/461nm) with an objective magnification of 60X. In this study, the cells were seeded in a 6-well plate for cellular uptake study at 1×10^5 cells per well. The following day, complete media was replaced with incomplete media, and cells were treated for 4 hours with FITC-conjugated PTX-NP and Ab-PTX-NP. After the treatment, the coverslips were rinsed three times with sterile cold PBS. The cells were then treated with paraformaldehyde at a

concentration of 4% (w/v). Before imaging, fixed cells were rinsed in PBS, labelled with DAPI, and covered with DPX (dibutylphthalate polystyrene xylene) (Sainee et al., 2021).

5.9.4. Induction of cell death by acridine orange/ethidium bromide dual staining

The induction of cell death by PTX/ PTX-NP/ Ab-PTX-NP was observed in confocal laser microscopy by acridine orange/ethidium bromide (AO/EB) dual staining as observed by Olympus Fluoview 10i confocal microscope. Filters used were of acridine orange DNA (green) (Excitation (Ex)/Emission (Em) 502/526 nm) and propidium iodide red (Ex/Em 537/619 nm). Cell suspensions were poured on cover slips placed in 12- well plate kept in CO₂ incubator for 24 h to allow the cells to grow. After 24 h, complete medium in each well was replaced with incomplete medium followed by treatment with the IC₅₀ concentration of PTX/ PTX-NP/ Ab-PTX-NP. Post treatment, the cover slips were washed thrice with sterile PBS followed by dual staining with AO/EB. Morphological changes due to apoptosis were observed under confocal microscope. Dead cells that had undergone apoptosis were distinguished in both the cell lines by manually counting from the images for each treatment. The total fluorescence intensity of each treatment was calculated using ImageJ software, and plotted (Dutta et al., 2019 Tawfeeq et al., 2018).

5.9.5. Mitochondrial membrane depolarization analysis using JC-1

Variation in transmembrane potential difference occurs when mitochondrial membrane becomes depolarized. LNCaP and PC3 cells were harvested in 60mm dishes followed by overnight humidified incubation. The cells were treated with PTX, PTX-NP and Ab-PTX-NP for 24h. Further cells were taken off from the dishes to be incubated with 10µl of 200µM 5,5',6,6'-tetrachloro-1,1',3,3'-tetraethylbenzimidazolyl-carbocyanine iodide (JC-1) in 1ml complete media for 10min at 37°C in dark. After centrifugation the cells were suspended in buffer and analyzed by a flow cytometer.

5.9.6. Apoptosis assay

Annexin V-FITC/PI dual staining using a FITC annexin V/dead cell apoptosis kit (Thermo Fisher Scientific, Waltham, MA, USA) was used to perform and quantify cancer cells, upon various treatments to quantitatively measure the ability of free drug, PTX-NP and Ab-PTX-NP to trigger apoptosis or necrosis in LNCaP (PSMA +ve) and PC3 (PSMA -ve) cells, respectively. The procedures were followed as mentioned in the kit. Data were obtained using a FACS Aria flow cytometer (Becton Dickinson, Holdrege, Nebraska, USA) using channels

of FITC (Ex/Em 488 nm/530 nm) and PE-Texas red (Ex/Em 561 nm/616 nm) and post capturing analysis was done with BD FACS Diva software (Becton Dickinson, Holdrege Nebraska, USA) (Tousi et al.,2021; Sen et al., 2021).

5.9.7. Nuclear morphology analysis by DAPI staining

DAPI was used to visualize the apoptotic outcome on the cell morphology of LNCaP and PC3 after treating them with PTX, PTX-NP and Ab-PTX-NP with their respective IC₅₀ dose for 24 h (Pillai et al., 2015). For the analysis, on the cover slips, LNCaP and PC3 cells were grown separately. It was placed in 35 mm dish for 24 h in humidified air containing 5% CO₂ followed by the treatment with PTX, PTX-NP and Ab-PTX-NP for another 24 h at 37 °C. It was then washed with PBS followed by fixation in 70% ethanol at -20 °C for 15 min. Again followed by washing thrice with PBS at room temperature, LNCaP and PC3 cells were treated with DAPI solution (4 µg/ml) for 5min. After following the protocol, the cells were imaged to identify the changes in a confocal laser scanning microscope (Leica, DFC 420C, Germany) and further processed in the software named Leica application suite (Gaonkar et al., 2017; Mandelkow et al., 2017)

5.10. Hemolysis evaluation

Freshly drawn blood samples from male balb/c mice were placed in heparinised tubes and centrifuged (5 min at 4 °C). After discarding the supernatant, PBS (pH 7.4) was used to wash the erythrocytes, which was utilized for hemolysis study. To each well of a 96-well plate, 190 µl of the obtained erythrocyte suspension was added and further, it was treated with 10 µl of PTX-NP and Ab-PTX-NP (in order of increasing concentration of PTX, e.g. 0.5, 1, 2.5, 10, 15, 30, 50, 75, 100µM), respectively. 10 µl of PBS to 190 µl of erythrocyte suspension served as a negative control, while 10 µl of TritonX-100 (10%) to 190 µl the erythrocyte suspension was taken as a positive control. The samples were further incubated (37 °C for 1 h) with occasional stirring. Centrifugation for 5 min leads to separation of the unlysed erythrocytes. Hence, on completion of the experiment, the optical density (OD) of the supernatant was measured at 570 nm. The % lysis was calculated from the values obtained from the experimental samples accordingly. All the experiments were performed thrice (Gaonkar et al., 2017; Fornaguera et al., 2015; Liu et al.,2017).

5.11. *In-vivo* studies

5.11.1 Pharmacokinetic study by LC-MS/MS method

The animals (male balb/c mice body weight: 25-30 g) were obtained from National Institute of Nutrition, Hyderabad, India. All animals were kept in polypropylene cages and were housed and maintained under standard laboratory conditions to conduct pharmacokinetic experiments. The standard protocol for housing of animals (12 h light/ dark cycle) was maintained with optimum temperature 25 ± 2 °C and relative humidity (RH) $55 \pm 5\%$, respectively. Animals were given a standard basal feed and drinking water ad libitum. Before being sacrificed, the animals were fasted for 12 hours with unrestricted water. All animal experiments were conducted after getting approved from the Animal Ethics Committee (AEC), Jadavpur University, Kolkata, India (Ref: AEC/PHARM/1702/24/2017, Dated: 01.06.2017).

Four groups of animals were formed, 36 mice in each group (n=3), Balb/c male mice. The first group of animals received (PTX), the second group received PTX-NP, and the third group of animals received Ab-PTX-NP. The fourth group of animals served as a control group and did not receive any treatment. The experimental formulations (equivalent to paclitaxel, dose 10mg/kg body weight) were administered through tail vein in mice. The animals were anaesthetized before sacrifice. At predetermined time points (at 0.25, 0.5, 1, 2, 4, 6, 8, 10, 24, 48, 72 and 96 h) after drug administration, the blood was collected after animal sacrifice. Terminal heart puncture was done to collect blood into a microcentrifuge tube containing an EDTA solution. Plasma was separated immediately with the help of centrifugation at 5000 rpm for 6 minutes at 4 °C. Until analysis, the plasma was kept at -80°C. The drug content in the blood serum was analyzed by tandem liquid chromatography and mass spectrophotometry (LC-MS/MS). (Mondal et al., 2019; Ma et al., 2015; Karra et al., 2013). Docetaxel was used as an internal standard.

5.11.2. LC-MS/MS analysis

100 µl of the sample to be analysed by (LC-MS/MS) was precipitated along with 300 µl of (1:1) acetonitrile-methanol mixture, along with docetaxel (200 ng/ml) as internal reference. The prepared mix of the sample was mixed for 10 minutes followed by centrifugation (10,000 rpm for 5 minutes at 4 °C). 100 µl of collected supernatant collected was mixed with water (100 µl) before being injected in the LC-MS/MS system (LC: Shimadzu Model 20AC, MS: AB-SCIEX, Model: API4000, Software: Analyst 1.6). YMC Triat C18158 column (30

x 2.1 mm, YMC Corp Japan) was used for elution of analytes followed by a gradient elution technique of injecting volume of 20 μ l, consisting of mobile phase A consisting of 0.1% formic acid in water and mobile phase B consisting of 0.1% formic acid in methanol-acetonitrile-water (45:45:10) at a flow rate of 0.8 ml/min for a total run time of 3.0 minutes (Mandal et al., 2018; Alves et al., 2018).

5.12. Statistical analysis

All the data of the experiments are demonstrated as mean \pm standard deviation (SD). One way analysis of variance (ANOVA) was used, followed by Tukey's test conducted for comparison between the experimental groups. A statistical level of significance of $P < 0.05$ was used.

6. Results

6.1. Preparation of standard curve of Paclitaxel

The maximum wavelength (λ_{\max}) of Paclitaxel was determined by dissolving it in acetonitrile water, which was found to be 227 nm utilizing UV-VIS Spectrophotometer with LI-295 Scanning Software. The depiction of the absorbance spectrum of Paclitaxel is shown in **Figure 6.1**. The spectra indicates purity of Paclitaxel, which correlates with reported literature (Chakraborty et al., 2020). The calibration curve was made with different concentrations of Paclitaxel, the data was taken in triplicate and calibration curve was plotted **Figure 6.2**. The equation obtained from calibration curve was applied to determine the drug-loading and encapsulation efficiency of experimental Paclitaxel loaded nanoparticles. The calibration curve was also used to assess the quantity of paclitaxel released in vitro from different experimental nanoparticles in various release media at different time intervals.

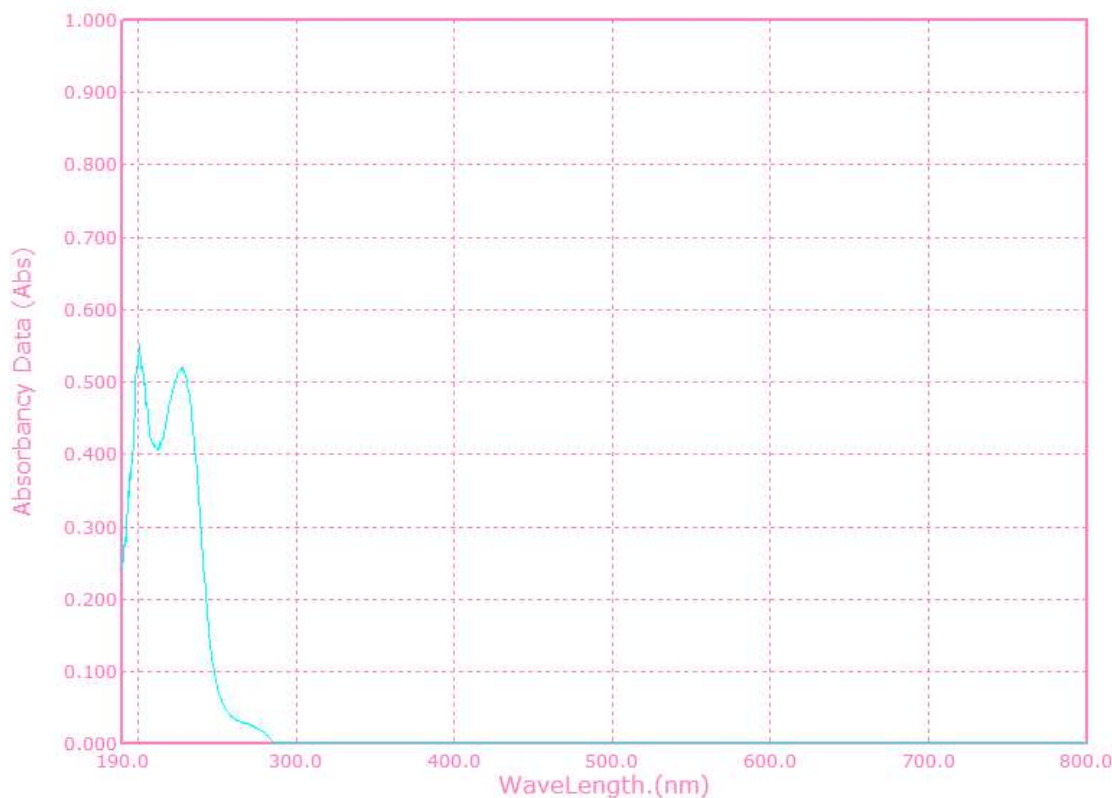


Figure 6.1 Absorbance maxima of Paclitaxel

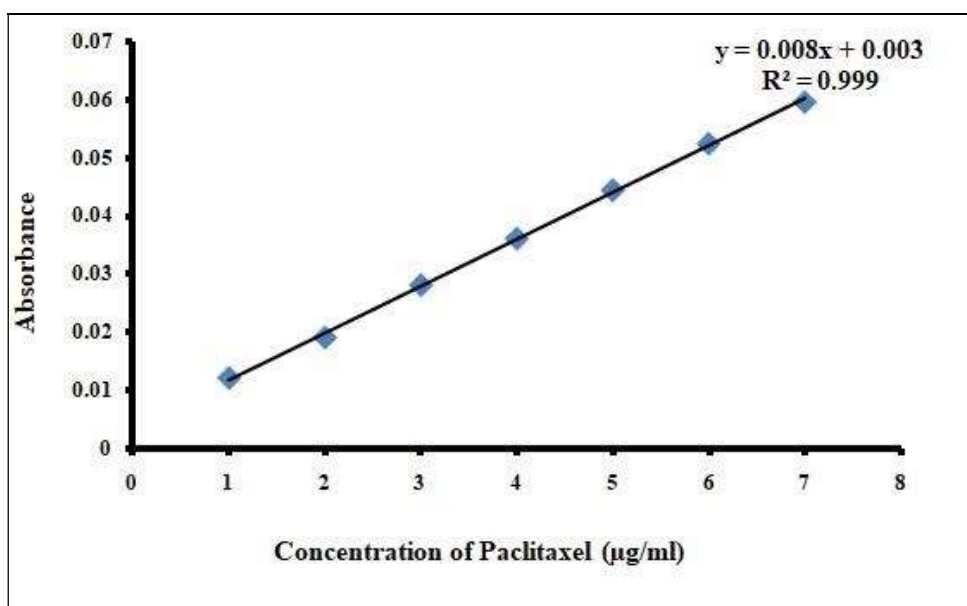


Figure 6.2. Calibration curve of Paclitaxel

6.2. Fourier-transform infrared (FTIR) spectroscopy

The FTIR spectrophotometric investigation revealed the characteristic peaks of Paclitaxel and the excipients used for the preparation of Paclitaxel loaded nanoparticles and exhibited no chemical interactions between them as shown in **Figure 6.3**. Pure PTX shows peaks of N-H stretching at 3440 cm^{-1} and asymmetric and symmetric vibrations at 2944 cm^{-1} for CH_2 . The peaks at 1720 cm^{-1} , 1246 cm^{-1} , 1072 cm^{-1} were observed due to C=O stretching vibrations of the ester group, C=N stretching and C=O stretching vibrations, respectively. For C-H in-plane and C-H out-of-plane C-C=O, the peaks were seen at 980 cm^{-1} and 710 cm^{-1} , respectively. PLGA portrayed peaks characteristic of O-H at 3508 cm^{-1} ; C-H at 2998 cm^{-1} and C=O at 1754 cm^{-1} , respectively. The characteristic PVA peaks were noticed at 3450 cm^{-1} with O-H, 2930 cm^{-1} with C-H, 1738 cm^{-1} , and 1096 cm^{-1} with C=O stretching vibrations. The PTX-NP and blank formulation shows the signature bands of PVA and PLGA and the absence of PTX, indicating no free drug molecule on the nanoparticles. The spherical shape of the nanoparticles might be attributed to physical interactions resulting in minimal peak shifts due to the influence of some weak physicochemical interactions, such as the formation of weak H-bonds, van der Waals attraction force, and dipole-dipole interactions.

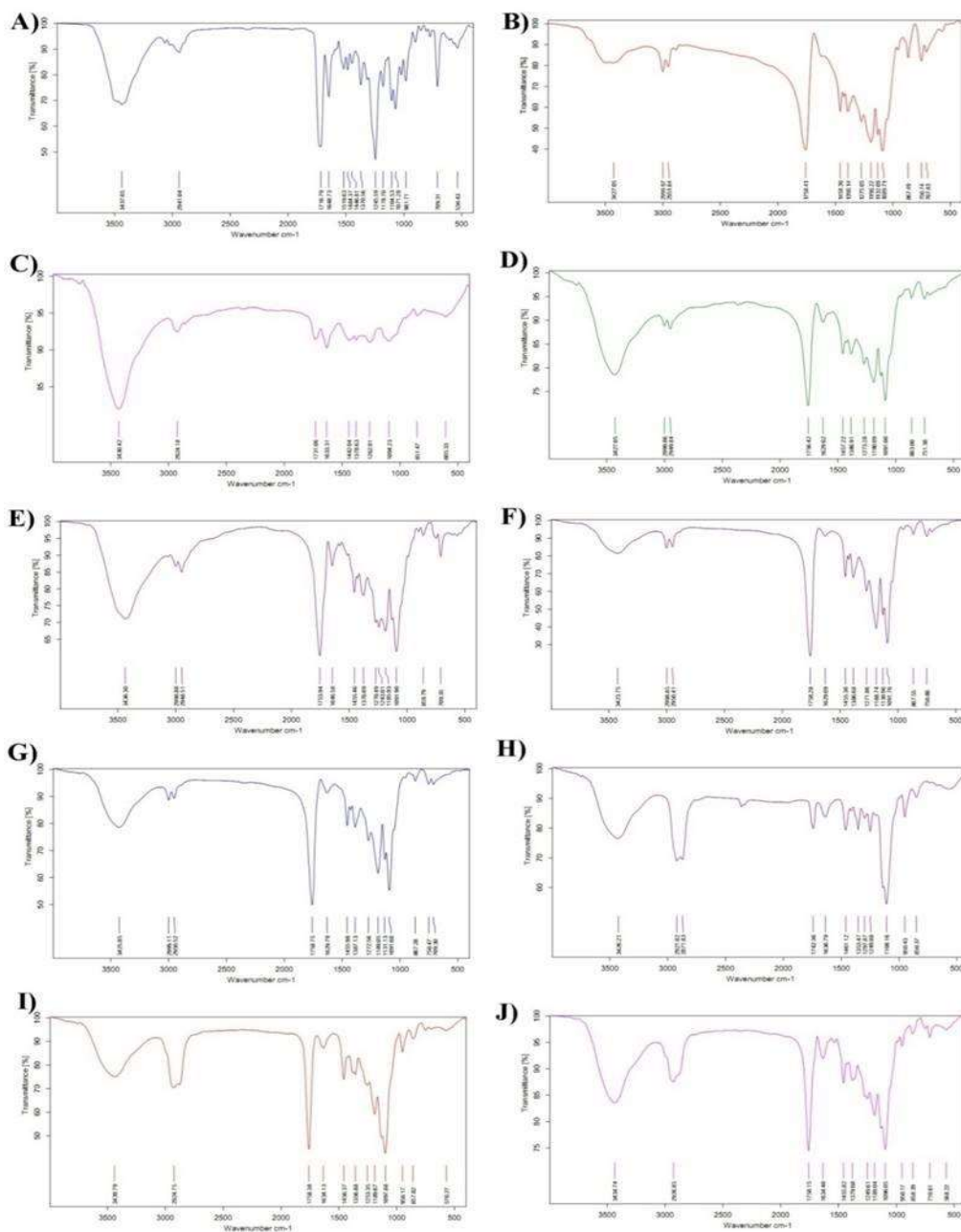


Figure 6.3. FTIR spectra of (A) Paclitaxel (drug), (B) PLGA, (C) PVA, (D) Physical mixture of PVA and PLGA, (E) Physical mixture of drug, PVA and PLGA, (F) Blank nanoparticles BNP, (G) Paclitaxel-loaded nanoparticles (PTX-NP), (H) TPGS, (I) Physical mixture of PVA, PLGA, TPGS, (J) Physical mixture of PLGA, PVA, drug, and TPGS

6.3. Physicochemical characterization of prepared nanoparticles

Various nanoparticulate formulations with and without the drug were developed. The formulation (PTX-NP) was optimized after varying different solubilizers such as TPGS, Tween 80, Pluronic-127 and Pluronic-68 with PVA (2.5% w/v) to increase the sustained action and stability of the formulation for the desired duration (Mondal et al., 2019) as mentioned in **Table 6.1**. The optimized formulation PTX-NP enhanced the solubility of the PTX, ensued by conjugating with J591 Ab as the ligand attached on the surface of the optimized PTX-NP to obtain Ab-PTX-NP.

6.3.1. Drug loading and encapsulation efficiency

Therapeutic efficiency such as drug loading is a prerequisite that dictates the amount of formulation to be administered in the body. The drug loading of prepared nanoparticles was calculated as mentioned in **Table 6.1**. The optimized formulation without antibody conjugation, designated here as PTX-NP, was found to be $6.96\% \pm 0.19\%$ and the encapsulation efficiency as $76.61\% \pm 2.09\%$, respectively. In the case of Ab-PTX-NP, drug loading was found to be $6.44\% \pm 0.75\%$ and its encapsulation efficiency as $70.85\% \pm 0.83\%$. The above obtained values of drug loading and encapsulation efficiency were used for further investigation.

Table 6.1 Composition of the experimental nanoparticles with PLGA: Drug at the ratio 10:1 along with drug loading and encapsulation efficiency.

Formulation	Stabilizer/ Solubilizer used	Particle size (Z-average) (nm) ^a	Zeta potential (mV) ^a	Polydispersity index ^a	Drug loading (%) ^a	Encapsulation efficiency (%) ^a
PTX-NP (optimized formulation)	PVA (2.5% w/v) & TPGS (0.03%w/v)	221 ±1.2	-20±1.6	0.554±0.06	6.96%±0.19%	76.71%±2.09%
Ab-PTX-NP (optimized formulation with antibody conjugation)	PVA (2.5% w/v) & TPGS (0.03%w/v)	295±0.18	-13.5± 3.3	0.512±1.4	6.44%±0.75%	70.85%±0.83%.
PTX-NP1	PVA (2.5% w/v) & Tween80 (14%v/v)	349.2±26	-8.39±2.9	0.120±1.1	5.19%±0.11%	57.09% ±1.22%
PTX-NP2	PVA (2.5% w/v) & Pluronic-127 (0.05%w/v)	409.1±18	-5.46±2.3	0.181±0.03	5.06%±0.05%	55.73± 0.50%
PTX-NP3	PVA (2.5% w/v) & Pluronic-68 (0.05%w/v)	418.4±33	-4.97±0.07	0.305±3.9	4.72%±0.07%	51.92%±0.78%.

NB: PTX-NP, PLGA nanoparticle encapsulating paclitaxel; Ab-PTX-NP, Antibody conjugated PLGA nanoparticle encapsulating paclitaxel; PLGA, poly (lactide-co-glycolide); PVA, poly vinyl alcohol; TPGS, D - α -tocopherol polyethylene glycol succinate.

^a Each value represents mean \pm SD (n = 3).

6.3.2. Particle size and zeta potential

The average particle size found with Zetasizer for PTX-NP was 221 nm, while the size increased slightly after antibody conjugation, unveiling the particle size as 295 nm for Ab-PTX-NP (**Figure 6.4A and B**). Its polydispersity index (PI) of 0.554 ± 0.6 and 0.512 ± 1.4 was obtained for PTX-NP and Ab-PTX-NP (**Table 6.1**). The zeta potentials of PTX-NP and Ab-PTX-NP were -20 mV and -13.5 mV respectively (**Figure 6.4C and D**). The particle size and zeta potential of PTX-NP 1, PTX-NP 2 and PTX-NP 3 are shown in (**Figure 6.4 E**).

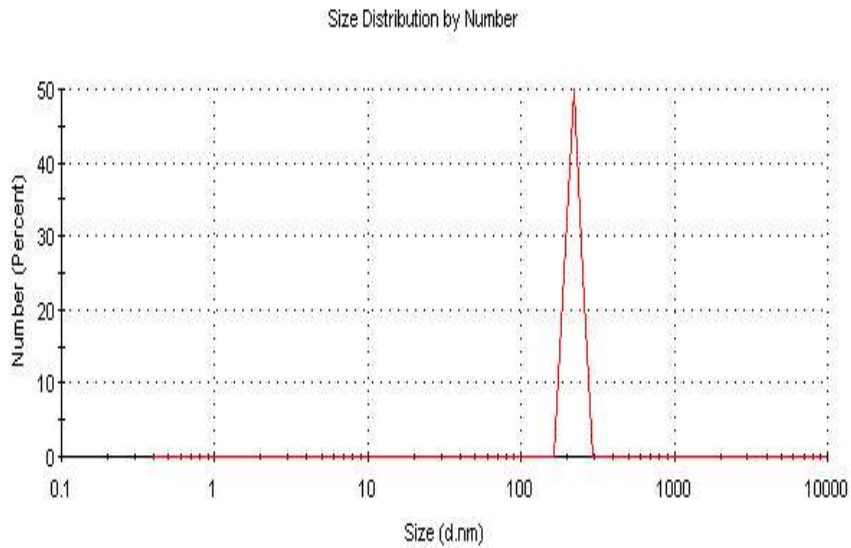


Figure 6.4 A. Average particle size distribution of PTX-NP

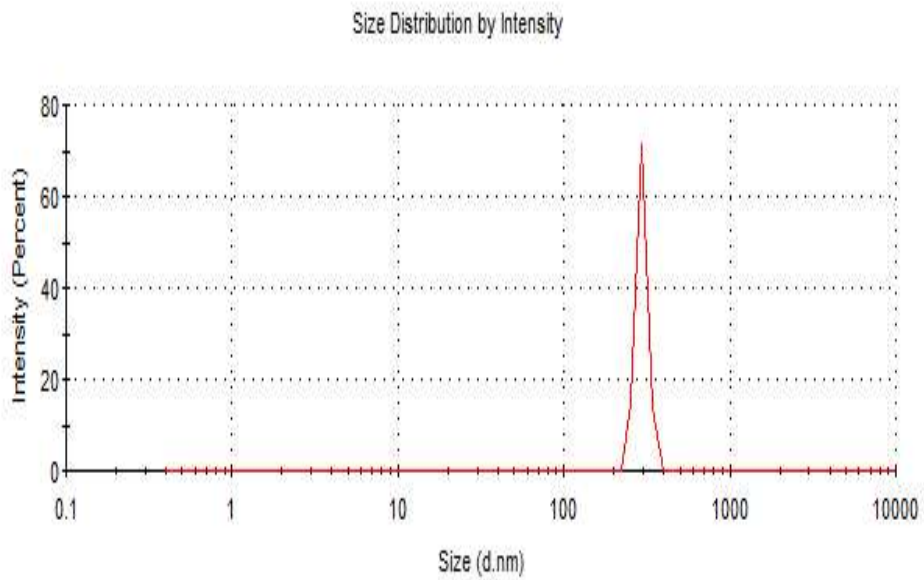


Figure 6.4 B. Average particle size distribution of Ab-PTX-NP

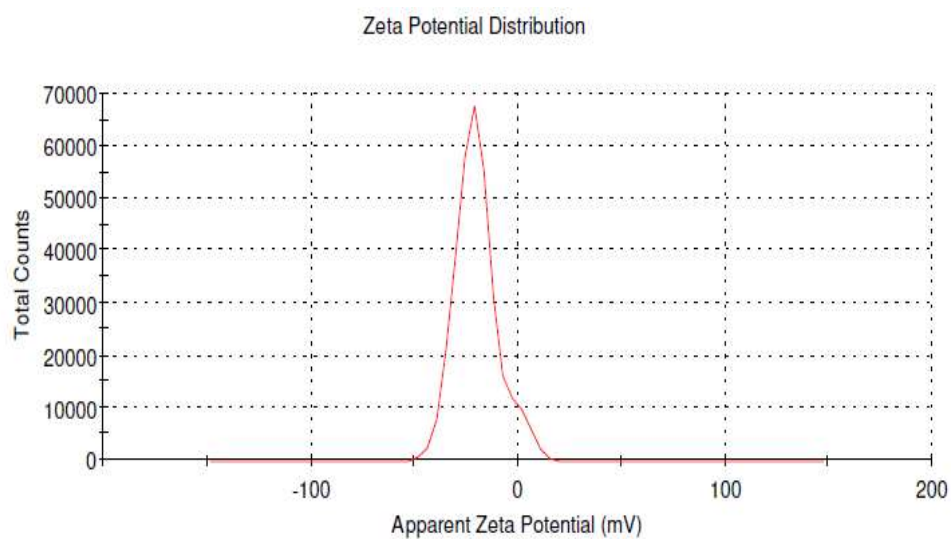


Figure 6.4C. Zeta potential of PTX-NP

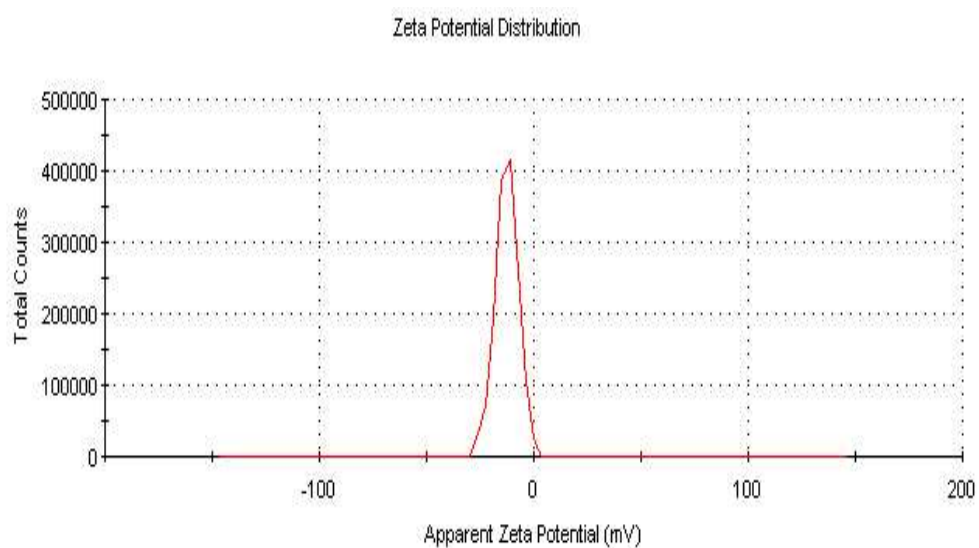


Figure 6.4D. Zeta potential of Ab-PTX-NP

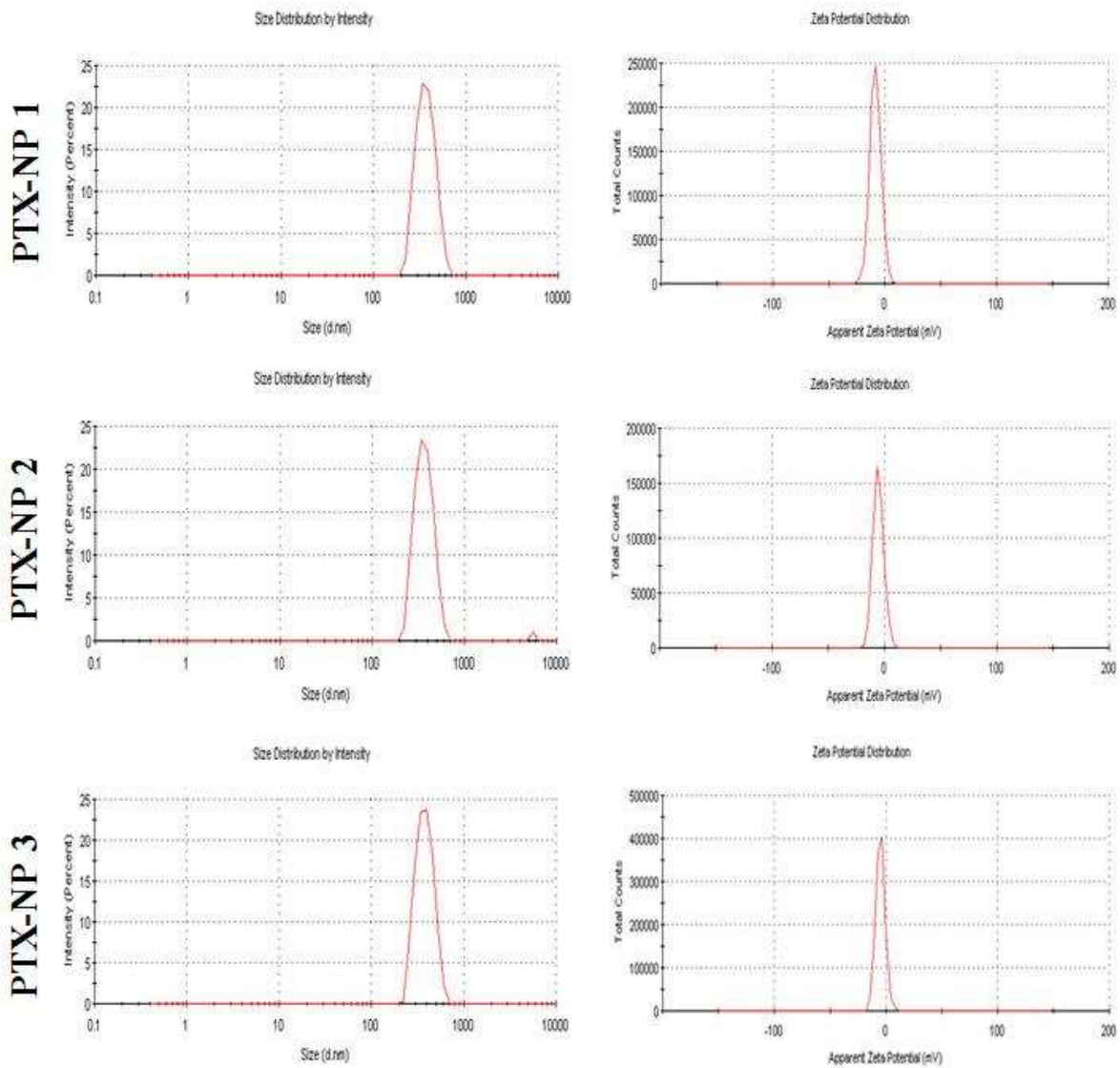


Figure 6.4 E. Zeta potential and particle size of (A) PTX-NP 1 (B) PTX-NP 2 and (C) PTX-NP 3

6.3.3. Surface morphology of the prepared nanoparticles

The surface morphology of PTX-NP and Ab-PTX-NP analysed via FESEM images (**Figure 6.5A and B**) confirmed the particles were in the nano range as well as thickly distributed. The drug was homogeneously distributed within the nanoparticle, which was confirmed by TEM analysis (**Figure 6.5C and D**) for both PTX-NP and Ab-PTX-NP without any notable difference. The three dimensional AFM images of PTX-NP and Ab-PTX-NP (**Figure 6.5E and F**) assured the smooth surface of the spherical nanoparticles in a close packed array, distinguished, narrow size distribution with structural rigidity without any significant difference between the two formulations.

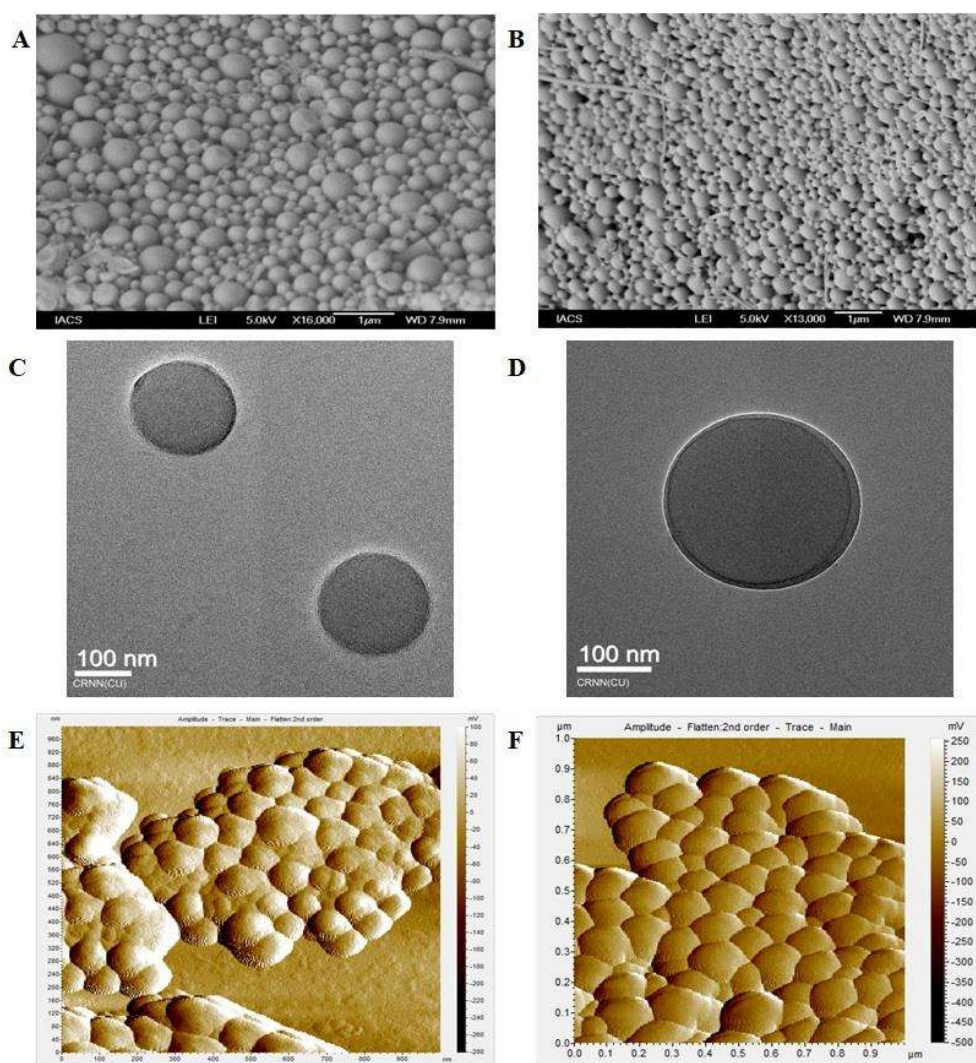


Figure 6.5. Field emission scanning electron microscopy (A) PTX-NP at 16,000× magnification (B) Ab-PTX-NP at 13,000× magnification; Transmission electron microscopy (C) PTX-NP (D) Ab-PTX-NP; Atomic force microscopy (E) PTX-NP and (F) Ab-PTX-NP.

6.4. Energy dispersive X-ray assay (EDX)

The elemental composition of the PTX-NP and Ab-PTX-NP was determined by EDX, which confirms the weight as well as the atomic percentage of carbon, oxygen, nitrogen, and sulphur as mentioned in **Table 6.2**. The presence of nitrogen in PTX is seen in PTX-NP and Ab-PTX-NP, thus it can be presumed that the Paclitaxel is encapsulated in the nanoparticles, and the lack of nitrogen in blank nanoparticles advocates the absence of paclitaxel in them respectively.

Table 6.2. Specific elemental composition (carbon, oxygen, nitrogen and sulphur) of nanoparticles

Sample	Carbon count		Oxygen count		Nitrogen count		Sulphur count	
	Weight	Atomic	Weight	Atomic	Weight	Atomic	Weight	Atomic
	%	%	%	%	%	%	%	%
Blank NP	43.14	50.64	56.86	49.36	-	-	-	-
PTX-NP	48.72	54.20	35.19	30.19	16.09	15.61	-	-
Ab-PTX-NP	52.19	53.91	21.25	20.77	24.89	23.89	1.67	1.43

Note: Weight % and atomic % of elements in Blank NP, PTX-NP and Ab-PTX-NP

Abbreviations: BNP, blank nanoparticles; PTX-NP, PLGA nanoparticle encapsulating paclitaxel; Ab-PTX-NP, Antibody conjugated PLGA nanoparticle encapsulating paclitaxel.

6.5. SDS-PAGE

To determine the conjugation of J591 antibody to the prepared nanoparticles, SDS-PAGE was conducted. The PTX-NP and Ab-PTX-NP were compared with J591 antibody which demonstrated that the integrity of J591 Ab was ensured in Ab-PTX-NP after conjugation (**Figure 6.6**). Furthermore nanoparticles were conjugated well with the antibody, and the antibody-conjugated particles ran slightly slowly.

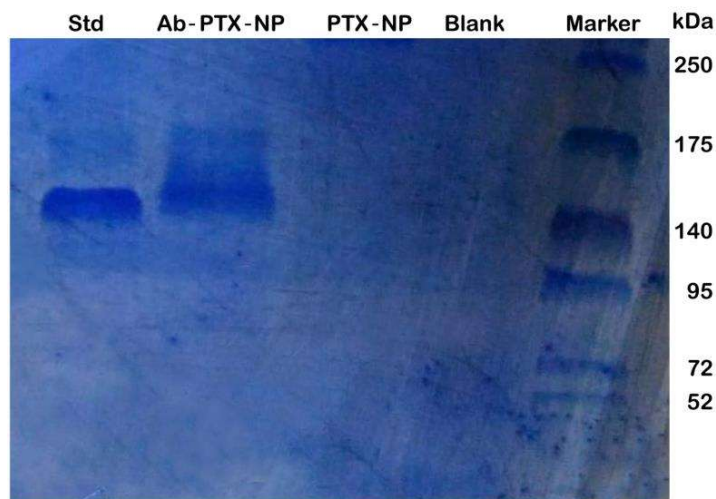


Figure 6.6. SDS-PAGE gel electrophoresis, Lane 1 in the SDS-PAGE gel showed the standard anti-PSMA monoclonal antibody Ab (J591), lane 2 represents for antibody conjugated PTX-NP, and lane 3 shows PAGE run of unconjugated NP followed by Blank in lane 4, and then the protein marker in lane 5.

6.6. *In vitro* drug release analysis

The *in vitro* PTX release profiles from paclitaxel suspension (PS), commercial formulation of PTX (CF), Ab-PTX-NP, and PTX-NP were studied for 90 days (**Figure 6.7A**). The release profile of PTX from unconjugated PTX-NP followed a similar middling pattern to its release from Ab-PTX-NP. An invariable and optimum drug release of $74.56\% \pm 2.35\%$ and $68.83\% \pm 3.07\%$ was depicted in phosphate (pH 7.4) buffer saline with 0.1% w/v of tween 80, which imitates the minimally alkaline environment of the blood.

Further, drug release from our decider nanoparticles Ab-PTX-NP for 90 days in various buffers of varying pH was studied cumulatively (**Figure 6.7 B**). The *in vitro* drug release in different pH media revealed that the release of PTX from Ab-PTX-NP was increased in lower pH media, i.e. PTX release in citrate buffer (pH 3) was rapid $96.56\% \pm 1.02\%$. The release of PTX in acetate buffer (pH 5) was $92.43\% \pm 1.81\%$, which might assert steady, prolonged drug distribution in the acidic environment of tumor cells (pH around 4.5–5.5). The release was lower in the bicarbonate buffer $29.30\% \pm 1.43\%$ medium (pH 10). It was noted that in different buffers utilized to examine the release of Ab-PTX-NP, an initial burst release for 24 h was manifested, subsequently releasing the drug in sustained manner for 90 days. PTX-NP delineated stability in mouse serum for at least 24 h in our previous studies [38]. PLGA nanoparticles stability in serum condition (100% FBS) was seen in the present study. It can

be summarized that in various pH media, the stability of PLGA nanoparticles was maintained during the study period.

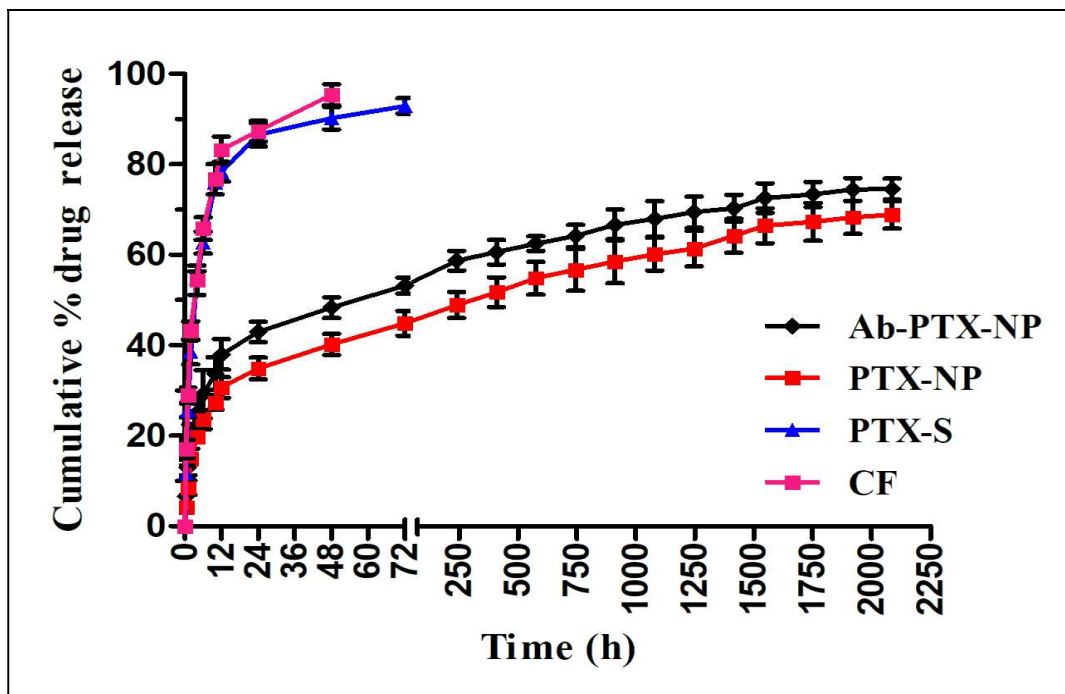


Figure 6.7A. *In vitro* drug release profile of experimental formulations in phosphate buffer saline (pH 7.4) with 0.1% w/v tween 80

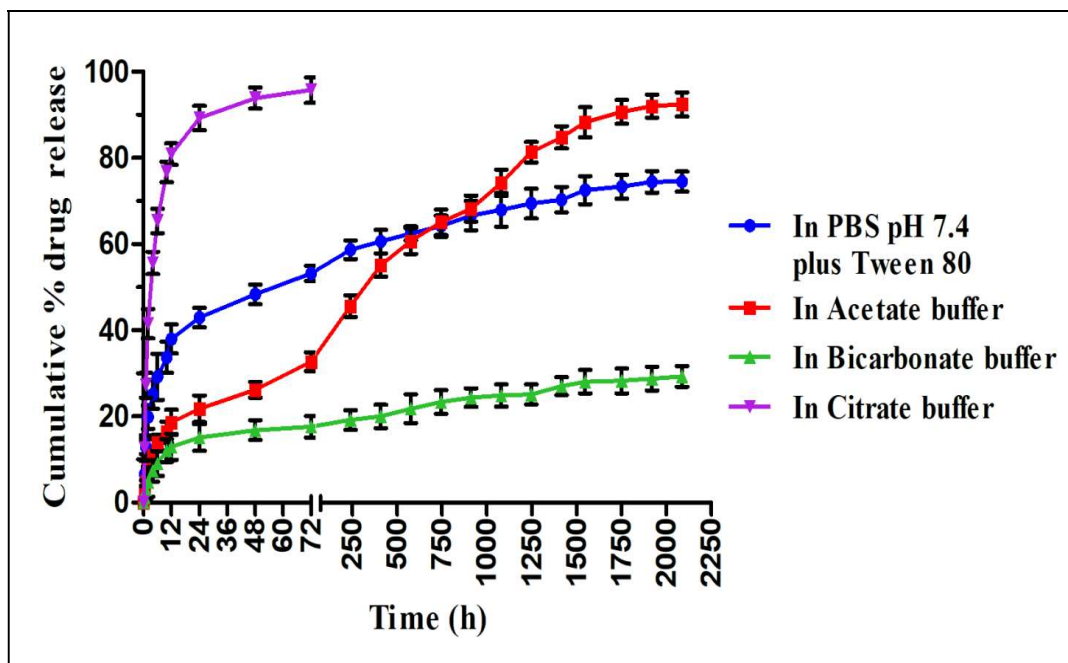


Figure 6.7B. *In vitro* drug release profile of Ab-PTX-NP in different pH (pH 3, 5, 7.4 and 10) media

Different kinetic models were used to assess drug release kinetic data. Various regression coefficient (R^2) data showed that the PTX release for both PTX- NP and Ab-PTX-NP in PBS (pH 7.4) with 0.1% w/v tween 80 complied with Korsmeyer-Peppas kinetics. It depicted good linearity ($R^2= 0.9179$) and the release exponent (n) value of the drug was 0.21 for PTX-NP, while for Ab-PTX-NP R^2 was 0.9185 and “n” value 0.18, suggesting release by Fickian diffusion (Jahromi et al., 2020). PTX release from Ab-PTX-NP in acetate buffer, bicarbonate buffer, and citrate buffer also followed Korsmeyer–Peppas kinetic model, suggesting diffusion release pattern of paclitaxel from Ab-PTX-NP (Table 6.3).

Table 6.3 Equation of in vitro drug release kinetics tested on different release kinetic models, with corresponding R^2 values and release exponent (n) (Korsmeyer–Peppas model).

Kinetic models	Ab-PTX-NP			PTX-NP in	
	in Phosphate buffer saline pH 7.4 (with 0.1% tween 80)	Ab-PTX-NP in Citrate buffer	Ab-PTX-NP in Acetate buffer	Ab-PTX-NP in Bicarbonate buffer	Phosphate buffer saline pH 7.4 (with 0.1% tween80)
Zero order	$y = 0.026x + 32.946$ $R^2 = 0.6334$	$y = 0.2626x + 52.126$ $R^2 = 0.2804$	$y = 0.0436x + 19.109$ $R^2 = 0.8823$	$y = 0.0111x + 10.601$ $R^2 = 0.7194$	$y = 0.0257x + 26.689$ $R^2 = 0.6951$
First order	$y = 0.0002x + 1.8123$ $R^2 = 0.78$	$y = 0.0056x + 1.5595$ $R^2 = 0.5395$	$y = 0.0005x + 1.9309$ $R^2 = 0.9878$	$y = 6E-05x + 1.9504$ $R^2 = 0.7588$	$y = 0.0002x + 1.8576$ $R^2 = 0.8182$
Higuchi model	$y = 1.2664x + 25.344$ $R^2 = 0.7976$	$y = 5.7801x + 37.223$ $R^2 = 0.5591$	$y = 1.8066x + 15.394$ $R^2 = 0.9442$	$y = 0.5249x + 7.6348$ $R^2 = 0.8572$	$y = 1.2283x + 19.569$ $R^2 = 0.8473$
Korsmeyer Peppas model	$y = 0.1831x + 1.2968$ $R^2 = 0.9185$ n=0.18	$y = 0.2216x + 1.5847$ $R^2 = 0.7956$ n=0.22	$y = 0.3499x + 0.825$ $R^2 = 0.99$ n=0.34	$y = 0.228x + 0.7338$ $R^2 = 0.8943$ n=0.22	$y = 0.2122x + 1.1616$ $R^2 = 0.9179$ n=0.21
Hixson-Crowell model	$y = 0.0007x + 0.6091$ $R^2 = 0.7326$	$y = 0.0108x + 1.2137$ $R^2 = 0.4403$	$y = 0.0013x + 0.2878$ $R^2 = 0.9691$	$y = 0.0002x + 0.1723$ $R^2 = 0.7458$	$y = 0.0006x + 0.4734$ $R^2 = 0.779$

6.7. Accelerated stability study

Physicochemical and morphological characteristics of PTX-NP and Ab-PTX-NP along with the maintaining of drug content stored at 4–8 °C, refrigerator (zone III) remained unchanged, while at 30 °C, 75% RH and 40 °C, 75% RH, PTX-NP and Ab-PTX -NP retained its PTX content but spherical morphology was distorted, when kept for 90 days (3 months). Studies on the stability requirements of these samples were performed and drug assay (drug content analysis) where drug content remained nearly unchanged (6.3-6.8%)

Table 6.4. Stability study of PTX-NP and Ab-PTX-NP after 90 days (3 months) stored at 4-8°C

Formulation	Stability after 90days at 4-8°C	
	Drug loading (%)	Encapsulation (%) Efficiency
PTX-NP (optimized formulation)	6.72% ±0.10%	74.04%± 1.17%
Ab-PTX-NP (optimized formulation)	6.23%±0.13%	68.65%± 1.44%

6.7.1 Hydrolytic stability study

The hydrolytic stability study for 4 weeks revealed an increment of weight loss with the lowering of pH as shown in **Figure 6.8**. The amount of loss of mass from Ab-PTX-NP in pH 10, pH 7.4, pH 5 and pH 3 was 14.53%±1.33%, 25.73%±1.55%, 35.83%±1.61% and 56.97%±1.55%, respectively. The Ab-PTX-NP displayed a weight loss of 3.1%±0.15% after 24 h in mouse serum (pH 7.3) at 24h.

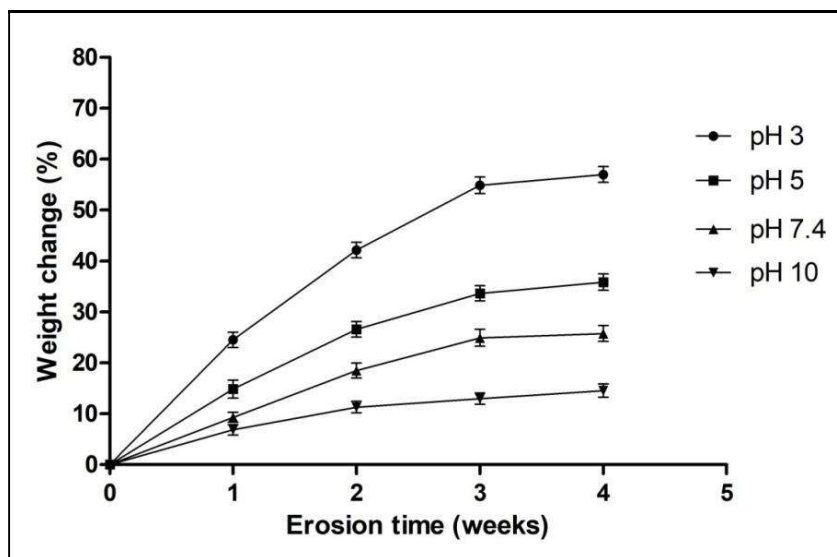


Figure 6.8. The pH-dependent hydrolytic degradation of the Ab-PTX-NP

Data show mean \pm SD (n = 3).

6.8. *In vitro* cellular studies

6.8.1. Cell viability assay

In vitro cytotoxic potential was evaluated with the help of 3-(4,5-dimethylthiazol-2-thiazolyl)-2,5-diphenyl-2H-tetrazolium bromide (MTT) analysis to obtain the IC_{50} values of our various experimental formulations, i.e., Ab-BNP, PTX, PTX-NP and Ab-PTX-NP in positive PSMA cells (LNCaP), negative PSMA cells (PC3) and normal kidney cells.

Cell growth inhibitory effect of PTX, PTX-NP, and Ab-PTX-NP determined by the assay displayed that Ab-PTX-NP had lowest IC_{50} doses, exhibited the highest cytotoxicity toward LNCaP cells (+PSMA) than in PC3(-PSMA), as portrayed in **Figure 6.9A and B**. At different concentrations (0–60 μ M) for 24 h, the IC_{50} value of PTX-NP and Ab-PTX-NP reveals as 20.6 μ M and 7.8 μ M which were evidently much lesser than the IC_{50} value of PTX that was 27.2 μ M in LNCaP cells. In PC3 cells, a narrow difference of IC_{50} value of PTX-NP and Ab-PTX-NP (22.9 μ M and 21.3 μ M) was observed. That may be due to the lack of PSMA. The antibody conjugated blank nanoformulation Ab-BNP on investigation yielded the antibody concentration as non toxic to prostate cancer cells. The formulations, PTX-NP and Ab-PTX-NP, showed negligible antiproliferative activity in normal kidney cells, HEK 293. Since it showed no toxic manifestation in HEK 293, possibly it had less or negligible toxicity toward other normal cells (**Table 6.5**). *In vitro* cytotoxicity of PTX, PTX-NP, Ab-PTX-NP and Ab-BNP was determined in LNCaP and PC3 cells.

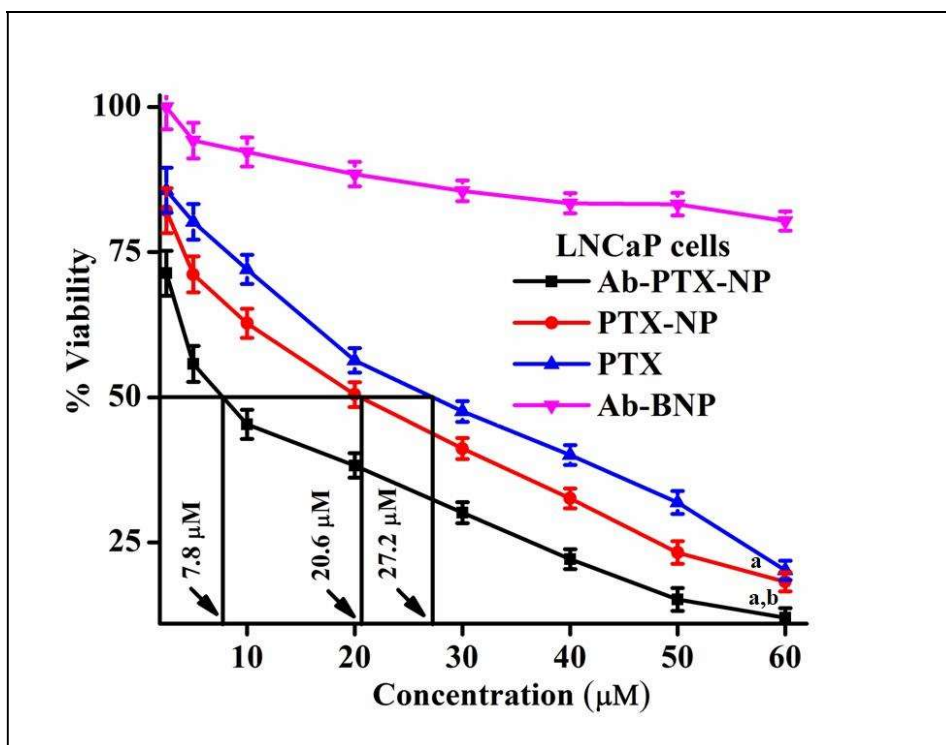


Figure 6.9A In vitro cytotoxicity of PTX, PTX-NP, Ab-PTX-NP and Ab-BNP was determined in LNCaP cells

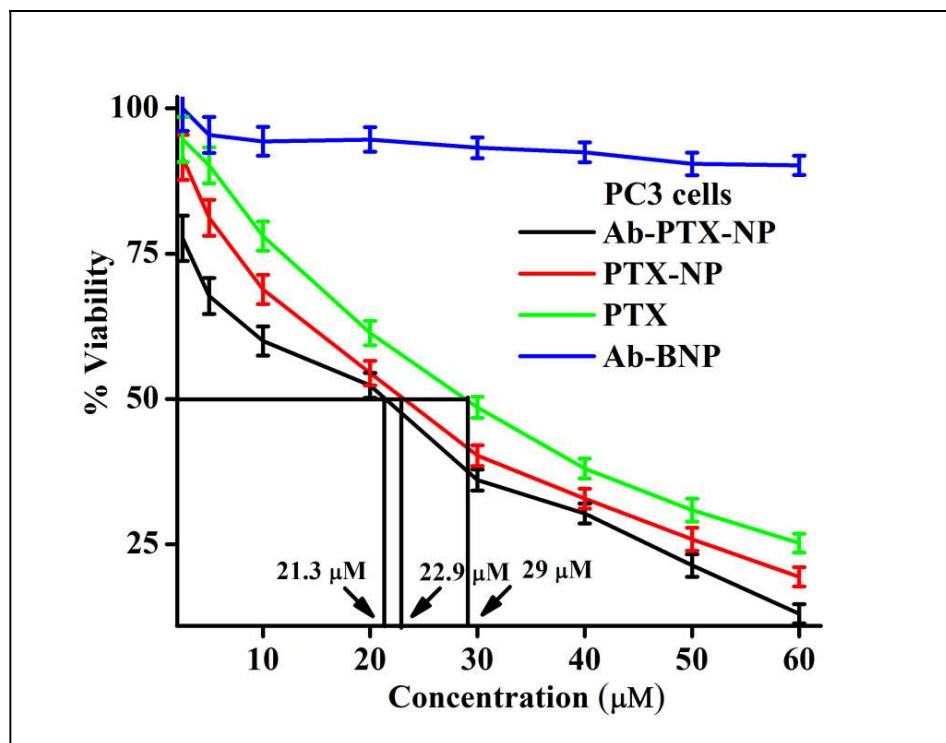


Figure 6.9B In vitro cytotoxicity of PTX, PTX-NP, Ab-PTX-NP and Ab-BNP was determined in PC3 cells.

Table 6.5. IC₅₀ values of PTX, PTX-NP and Ab-PTX-NP on different prostate cancer cells and normal cells.

Cell types	PTX (μM)*	PTX-NP (μM)*	Ab-PTX-NP (μM)*
PC3	35.4 ± 1.5	22.9 ± 2.1 ^a	21.3 ± 1 ^a
LNCaP	27.2 ± 0.3	20.6 ± 3.4 ^a	7.8 ± 0.5 ^{a,b}
HEK 293	>60	>60	>60

NB: LNCaP (+ve PSMA), PC3 (-ve PSMA) prostate cancer cells.

HEK 293: normal kidney cells.

* Each value represents mean ± SD (n = 3).

^a (p<0.05) when PTX is compared with PTX-NP and PTX is compared to Ab-PTX-NP

^b (p<0.05) when PTX-NP is compared to Ab-PTX-NP

6.8.2. Expression analysis of PSMA on LNCaP and PC3 cells by Western blot

PSMA is overexpressed in LNCaP cells. The analysis was done to confirm the expression of PSMA in LNCaP (+ve PSMA), and PC3 (-ve PSMA) prostate cancer cells (**Figure. 6.10**). The results determined that LNCaP cells were found to have a strong level of expression of PSMA, whereas, PC3 cells exhibited no apparent PSMA expression.

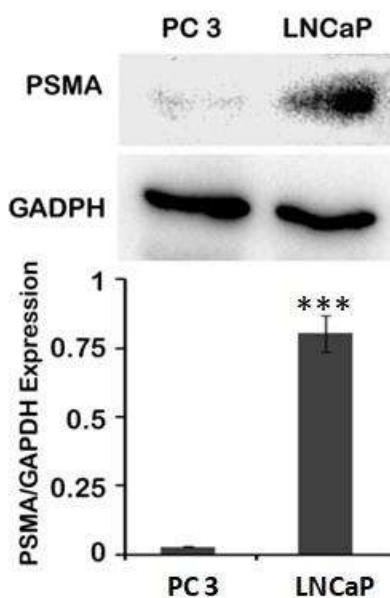


Figure 6.10 PSMA expression in LNCaP and PC3 cells detected by Western blot

PSMA to GADPH ratio is shown graphically

Data shows mean ± SD (n = 3)

*** Statistical significance of PC3 when compared with LNCaP is p<0.001.

6.8.3. Cellular uptake study on PC3 and LNCaP cells *in vitro*

Prostate cancer LNCaP (+ve PSMA) and PC3 (-ve PSMA) cells were used for the purpose of detection of the uptake of FITC tagged PTX-NP and Ab-PTX-NP. The cellular uptake was quantified by flow cytometry, which reveals a steady increase in median fluorescence intensity in LNCaP cells as compared to PC3 and untreated cells with increasing time (**Figure 6.11A and B**). FITC mean median values in LNCaP cells for PTX-NP were 582, 1328, and 2780, and for Ab-PTX-NP were 1322, 2471, and 3818 at time intervals 0.5, 2, and 4 h.

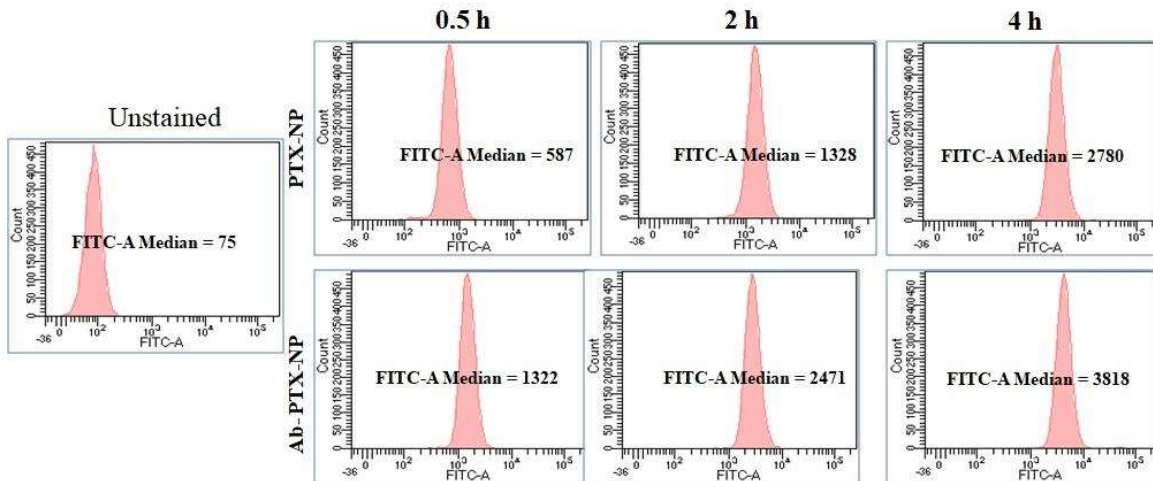


Figure 6.11A. Flow cytometry analysis representing distribution of FITC PTX-NP and FITC Ab-PTX-NP in LNCaP cells after treating them for 0.5 h, 2 h and 4 h, respectively

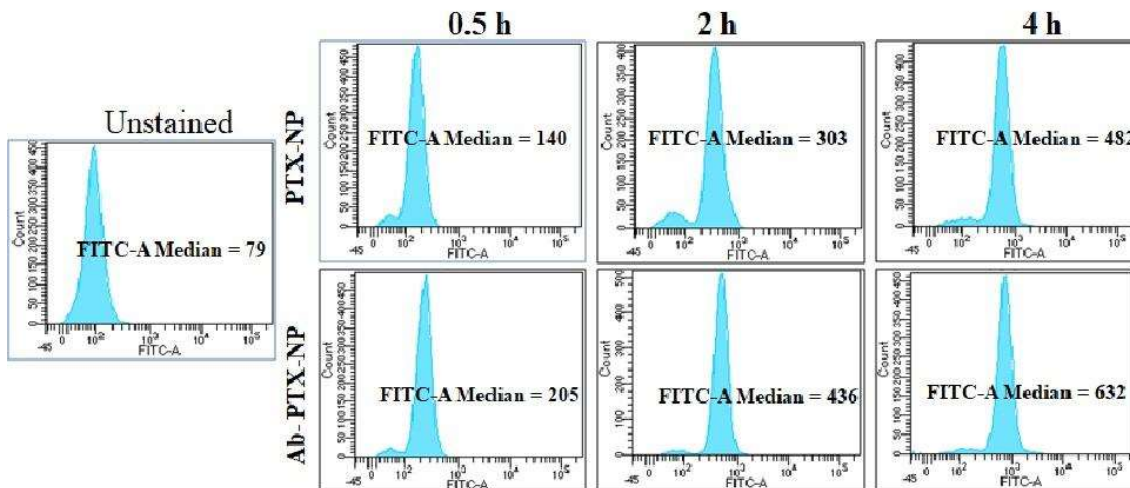


Figure 6.11B. Flow cytometry analysis representing distribution of FITC PTX-NP and FITC Ab-PTX-NP in PC3 cells after treating them for 0.5 h, 2 h and 4 h, respectively

In LNCaP cells, the FITC mean-median values indicate the cellular uptake of experimental nanoparticles in the following Ab-PTX-NP > PTX-NP > PTX sequence. While in PC3 cells at the same time intervals, the cellular internalization was much lower for both PTX-NP and Ab-PTX-NP, respectively.

The quantitative cellular uptake study of FITC labeled PTX-NP and Ab-PTX-NP was backed up by qualitative confocal microscopy images of LNCaP (**Figure. 6.12A**), and PC3 (**Figure. 6.12B**) treated with FITC labeled PTX-NP and Ab-PTX-NP, which revealed time dependent internalization of the experimental formulations within cancerous cells at 4h, respectively. The data suggest maximum internalization of Ab-PTX-NP in LNCaP cells, probably due to maximum affinity of J591 for PSMA, showing site specific potential of J591 antibody in PSMA positive LNCaP cells. Since the objectives were fulfilled by the study, it was not further extended beyond 4h. However, if the cellular uptake continues after 4 h, cellular uptake may increase with time till the duration, the receptors on the cells are saturated by the antibody of Ab-PTX-NP, which further result in a constant plateau of cellular drug concentration, followed by the eventual decrease of the drug in the cells.

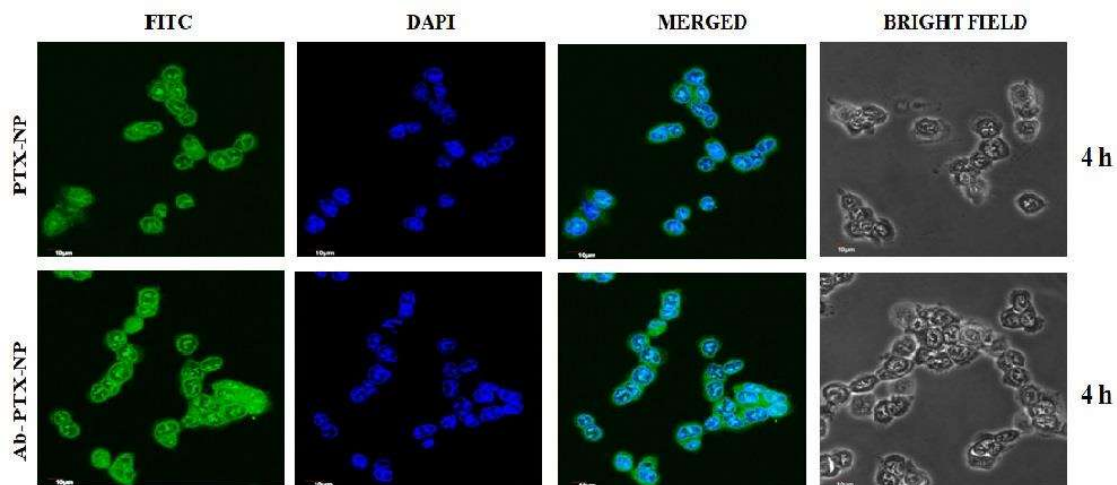


Figure 6.12A. Confocal microscopy images of LNCaP cells after treating with FITC PTX-NP and FITC Ab-PTX-NP for 4 h

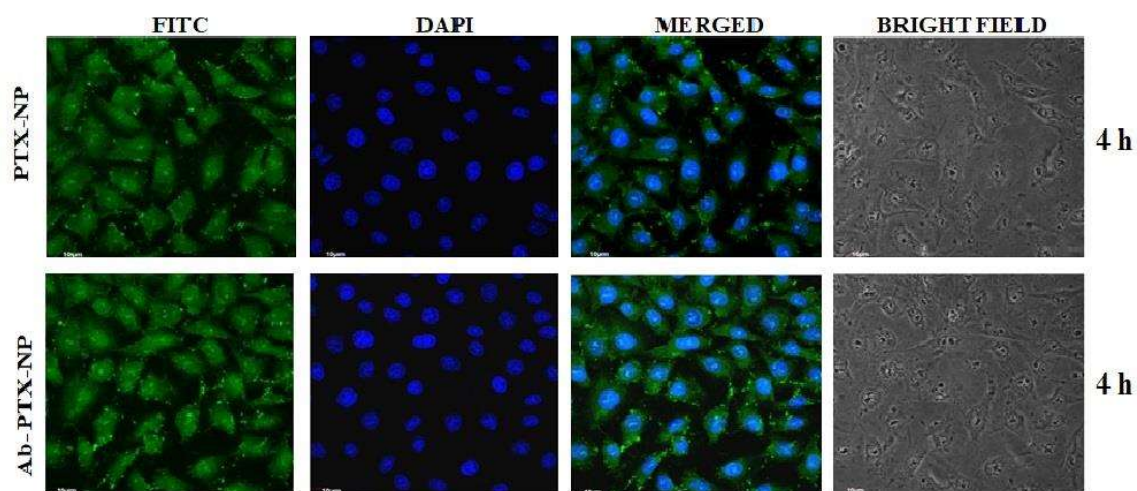


Figure 6.12B. Confocal microscopy images of PC3 cells after treating with FITC PTX-NP and FITC Ab-PTX-NP for 4 h

6.8.4. Induction of cell death by acridine orange/ethidium bromide dual staining

The apoptosis-induced morphological alterations in LNCaP and PC3 prostate cancer cells for 24 h, with IC_{50} values of the experimental formulations, PTX, PTX-NP, and Ab-PTX-NP, were observed upon double staining with AO/EB, which displayed differential uptake of acridine orange and ethidium bromide by live and apoptotic cells as shown in **Figure 6.13A and B**. The healthy condition of control cells appeared green. Acridine orange (AO) was taken up by live cells while ethidium bromide (EB) was used by apoptotic cells due to the loss of integrity of the cellular membrane. The nuclei of LNCaP cells when treated with Ab-PTX-NP appears dark orange to red with condensed or fragmented chromatin due to the major internalization of EB (increased endocytosis leading to apoptosis). Measuring total fluorescence intensity in LNCaP and PC3 revealed conformity with the images in our findings shown in Figure 6.13C. As a result of apoptosis/ necrosis, the reduction in cells via cell counting was observed more in LNCaP as compared with PC3 cells when treated with PTX-NP and Ab-PTX-NP. The staining was observed by Olympus Fluoview 10i confocal microscope. Filters of acridine orange DNA (green) (Excitation (Ex)/Emission (Em) 502/526 nm) and propidium iodide red (Ex/Em 537/619 nm)

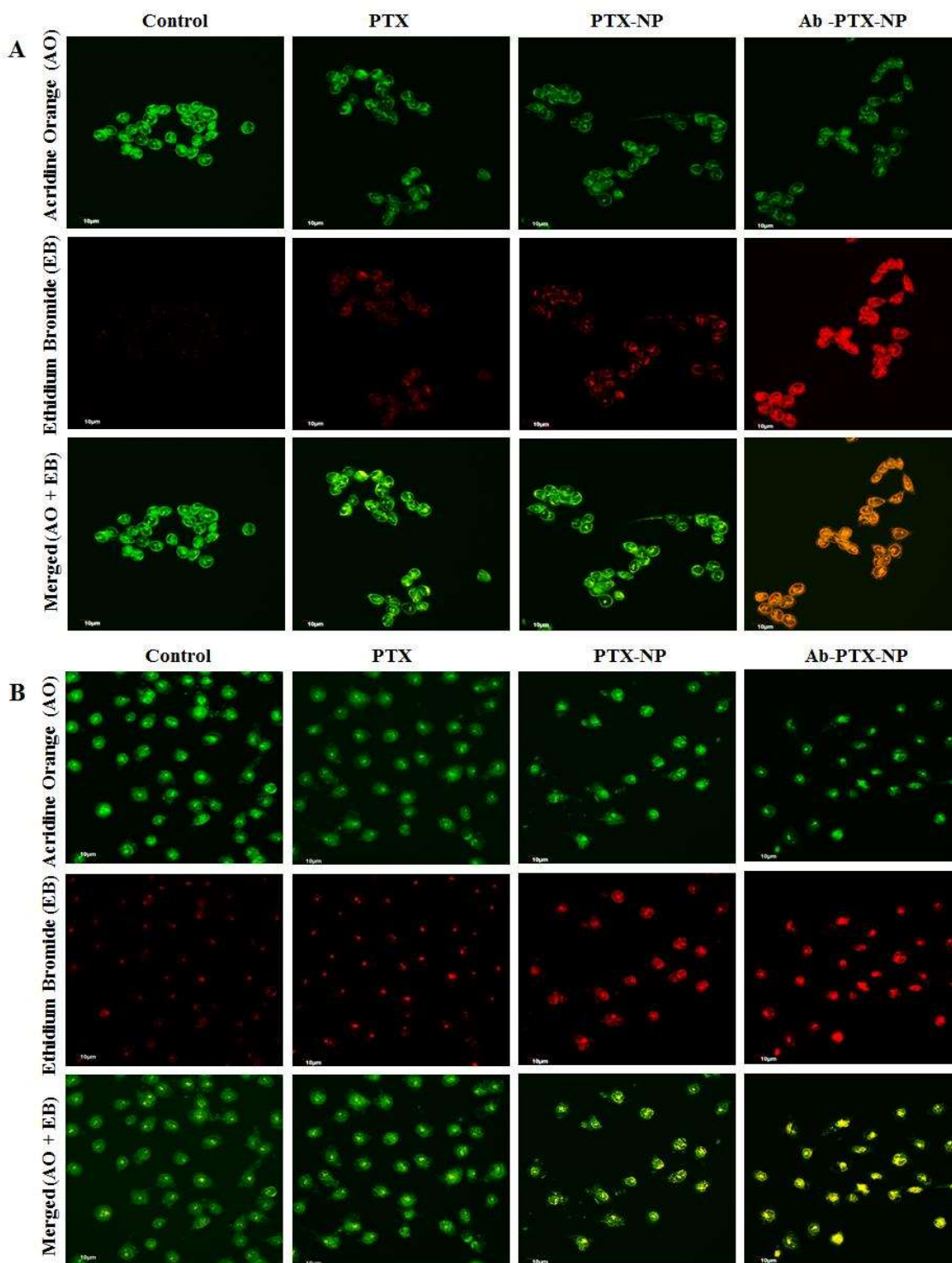


Figure 6.13. Confocal microscopy images of (A) LNCaP cells after treating with PTX , PTX-NP and Ab-PTX-NP (B) PC3 cells after treating PTX , PTX-NP and Ab-PTX-NP, for 24 h followed by staining with acridine orange (4 $\mu\text{g/ml}$) and ethidium bromide (4 $\mu\text{g/ml}$), by acridine orange/ethidium bromide (AO/EB) dual staining.

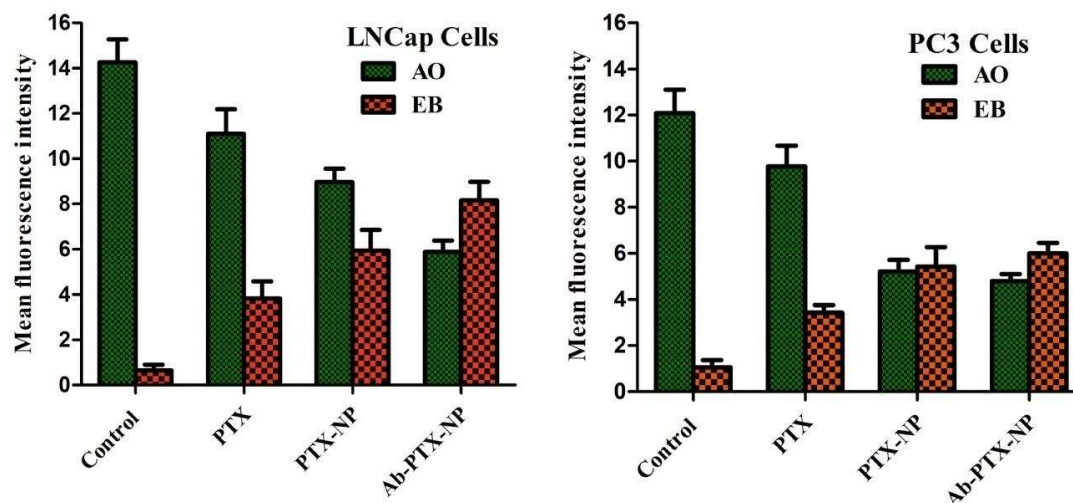


Figure 6.13C. Mean fluorescence intensity percentage obtained by Acridine orange/ethidium bromide dual staining. Image J software was used.

Total cells seeded= 1×10^4

LNCaP cells

Cells in control, PTX, PTX-NP, Ab-PTX-NP is 26,28, 33, 27

PC3 cells

Cell in control, PTX, PTX-NP, Ab-PTX-NP is 50,42,21,27

Data show mean \pm SD (n=3).

6.8.5. Mitochondrial membrane depolarization analysis

The loss and alteration of mitochondrial membrane potential, which is a prerequisite phenomenon of apoptosis, can be quantified by increased monomer/aggregate ratio (green/red ratio), which was observed with the highest percentage of cells with depolarized mitochondria in Ab-PTX-NP. Results yielded 34.1% for PTX-NP and 45.6% for Ab-PTX-NP, respectively, while only 13.8% for the free drug. Further, PTX-NP and Ab-PTX-NP for 24 h, showed lower and marginalized apoptosis in PC3 cancerous cells on the treatment with the IC₅₀ concentration of the experimental formulations as shown in **Figure 6.14**.

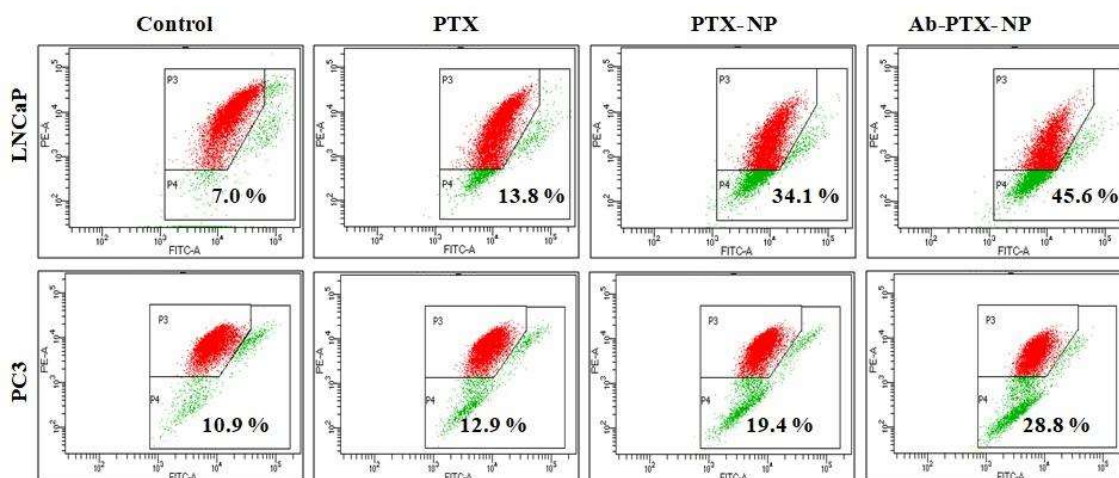


Figure.6.14. Loss of mitochondrial membrane potential as estimated by JC-1 staining analysis after treating the LNCaP (+ve PSMA) and PC3 (-ve PSMA) cells with PTX/ PTX-NP/Ab-PTX-NP for 24 h

6.8.6. Apoptosis Study

In Annexin V-FITC/PI dual staining, annexin V bound with phosphatidylserine helped to quantitatively detect the induction of apoptosis when LNCaP cells on the treatment with PTX, PTX-NP, and Ab-PTX-NP (**Figure 6.15**). The percentage of apoptotic cells was 48.6% for PTX-NP, and 74.1% for Ab-PTX-NP while for free PTX it was 21% for 24 h. Similar treatment on PC3 cells was conducted, which showed the lower apoptotic value of the experimental formulations. Thus, Ab-PTX-NP indicated better efficacy in LNCaP cells.

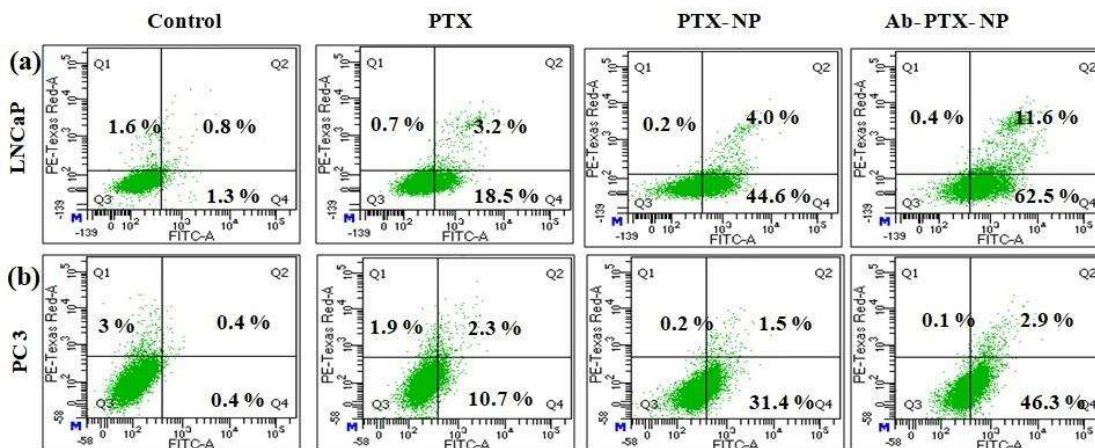


Figure.6.15. Quantification of apoptosis detected in LNCaP (+ve PSMA) and PC3 (-ve PSMA) cells treated with PTX/ PTX-NP/Ab-PTX-NP for 24 h

Data were obtained using a FACS Aria flow cytometer (Becton Dickinson, Holdrege, Nebraska, USA) using channels of FITC (Ex/Em 488 nm/530 nm), and PE-Texas red (Ex/Em 561 nm/616 nm) and post capturing analysis was done with BD FACS Diva software (Becton Dickinson, Holdrege Nebraska, USA)

6.8.7 Nuclear morphology analysis

DAPI staining revealed pronounced morphological changes due to apoptotic body formation in Ab-PTX-NP treated LNCaP (+ve PSMA) cells when studied in both types of prostate cancer cells. The results are shown in **Figure 6.16**.

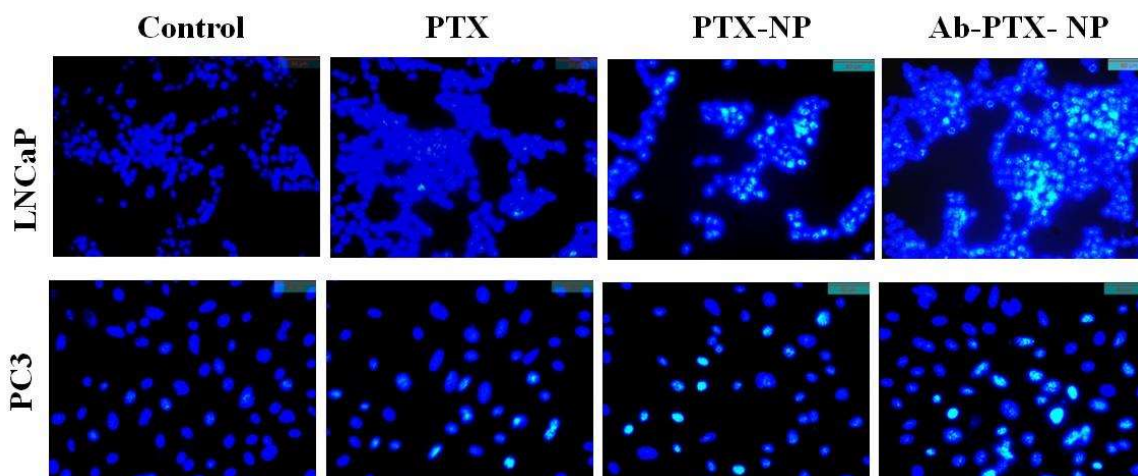


Figure 6.16. Confocal microscopic image (100X) representing DNA degradation and apoptotic body formation upon treatment with PTX/ PTX-NP/Ab-PTX-NP for 24 in LNCaP (+ve PSMA) cells and in PC3 (-ve PSMA) cells

6.9. Hemolysis study

The hemo-compatibility of PTX, PTX-NP, and Ab-PTX-NP at various concentration range (2.5 to 100 μ M) was studied which resulted in minimal erythrocyte damage and negligible hemolytic activity in PTX-NP and Ab-PTX-NP containing PTX (below 50 μ M) as shown in **Figure 6.17**. Sequential rise in hemolysis was observed with the elevated concentration of PTX-NP and Ab-PTX-NP ranging from 50 to 100 μ M. Thus, Ab-PTX-NP can be rendered safe for intravenous administration as the hemolysis rate of the desired formulation was within the permissible range of 5% as per safe critical value for biomaterials (ISO/TR 7406.46) (Anitha et al., 2012; Liu et al., 2017).

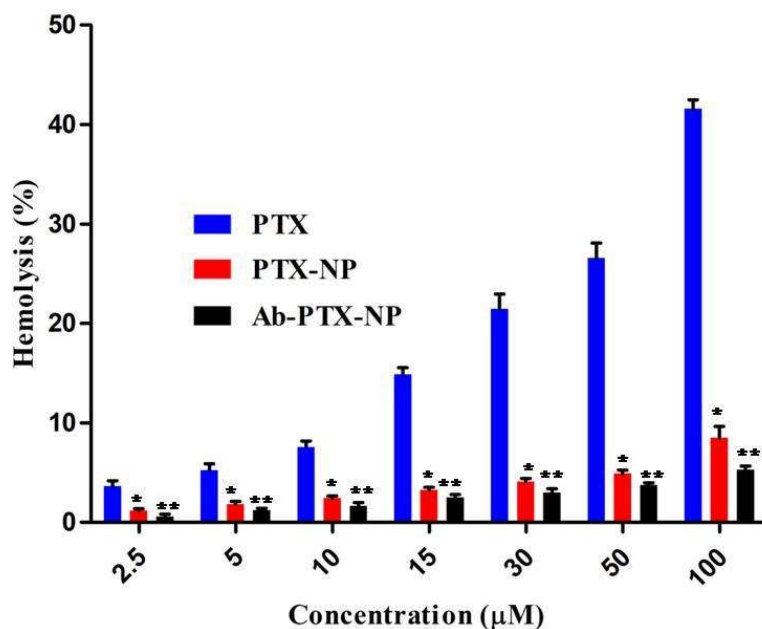


Figure 6.17. Hemolytic activity of PTX/ PTX-NP/ Ab-PTX-NP

*P<0.05 when PTX treated group is compared with PTX-NP treated and Ab-PTX-NP treated group

**P<0.05 PTX-NP treated group is compared with Ab-PTX-NP treated group

6.10. *In vivo* study

6.10.1. Pharmacokinetic study by LC-MS/MS method

The plasma concentration profiles of PTX (free drug), PTX-NP, and Ab-PTX-NP were determined by pharmacokinetic study, plotted on the graph (**Figure 6.18**) and the values of different pharmacokinetic parameters were depicted in Table 6.6. The data depicted that Ab-PTX-NP maintained steady plasma PTX concentration till 96 h of the study with a notably increased half life of the drug. The mean residence time (MRT_{inf}), marked 3-4 time fold increase in AUC_{last} and AUC_{inf} , of the drug from Ab-PTX-NP as compared to data obtained from PTX-NP and PTX. Drug was released from the surface of the engineered Ab-PTX-NP initially. Further, the release was steady for a longer span of time and showed much higher availability of the drug, PTX in plasma on administration of a single intravenous injection of Ab-PTX-NP.

Table 6.6 Plasma pharmacokinetic parameters of paclitaxel released from PTX-NP/ Ab-PTX-NP/ PTX suspension after the intravenous bolus administration of PTX-NP/ Ab-PTX-NP/ PTX with an equivalent amount of drug in BALB/c mice.

Pharmacokinetic parameters	Plasma values of Drug (Paclitaxel)		
	Upon PTX administration*	Upon PTX-NP administration*	Upon Ab-PTX-NP administration*
t _{1/2} (h)	8.309±1.24	18.63±3.11 ^a	20.31±5.86 ^{a,b}
AUC _{0-t} (ng/mL.h)	1134.291±47.46	3254.071±849.93 ^a	7868.208±818.985 ^{a,b}
AUC _{0-∞} (ng/mL.h)	1195.264±58.71	3645.893±1147.267 ^a	8266.213±691.47 ^{a,b}
AUMC _{0-∞} (ng/mL.h ²)	5621.12±665.949	62590.02±42217.51 ^a	258554±16467.68 ^{a,b}
MRT _{0-∞} (h)	4.70±0.40	16.005±5.63 ^a	31.34±1.72 ^{a,b}
CL (L/h/kg)	8.38±0.41	2.2±0.81 ^a	1.21±0.95 ^{a,b}

*Data show mean ± SD (n=3).

^a(p<0.05) The pharmacokinetics data of treatment of PTX-NP treatment group and Ab-PTX-NP treatment group were compared with PTX- treated group

^b(p<0.05) The pharmacokinetic data of PTX-NP and Ab-PTX-NP groups were compared.

[§]Units of AUC in plasma are h.ng/mL.

NB: t_{1/2}, half-life; AUC_{0-t}, area under the plasma concentration–time curve from time 0 to time of last measurable concentration; AUC_{0-∞}, under the plasma concentration–time curve from time 0 to infinity; AUMC_{0-t}, area under the first moment curve from time 0 to time of last measurable concentration; AUMC_{0-∞}, area under the first moment curve from time 0 to infinity; MRT, mean resident time; CL, clearance.

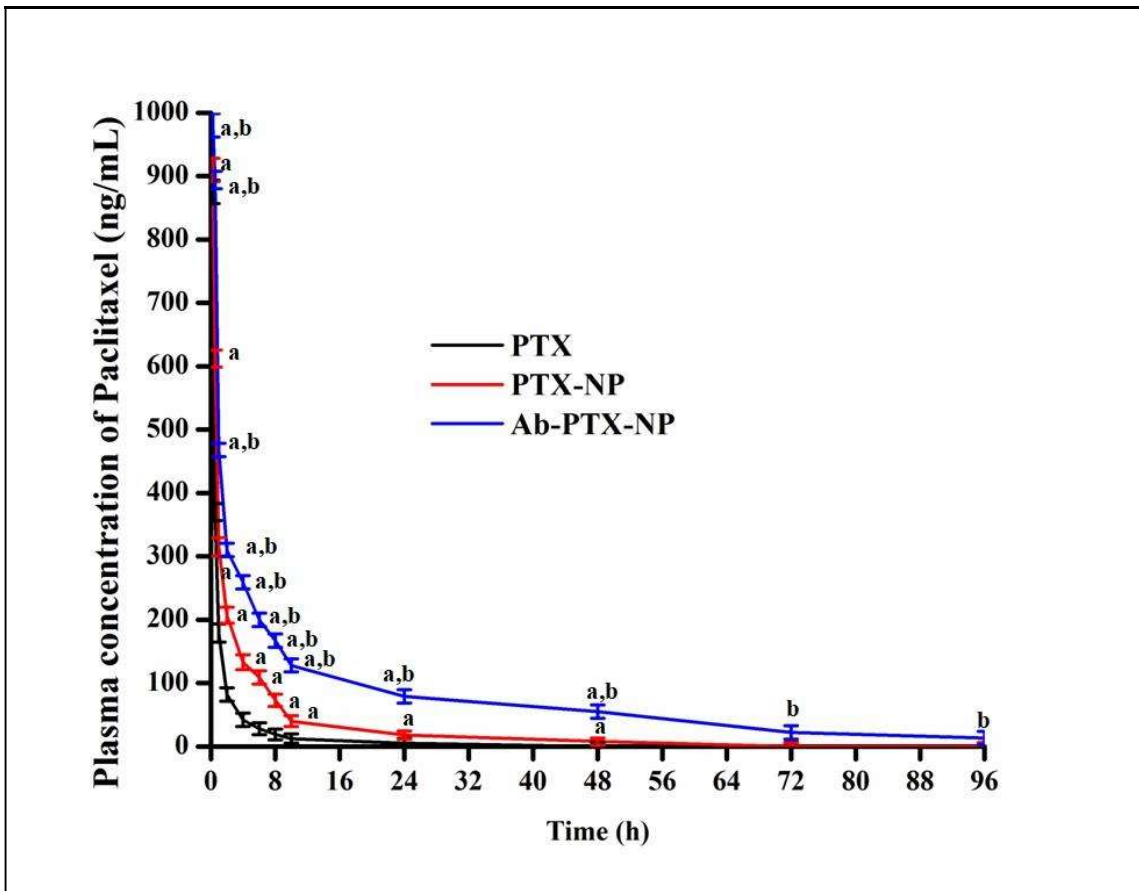


Figure 6.18 Plasma concentration of paclitaxel upon i.v bolus injection (at a dose of 10mg/kg body weight) of PTX/ PTX-NP/ Ab-PTX-NP

7. Discussion

Prostate cancer is one of the major causes of cancer-related mortality in men and is one of the most difficult cancers to cure. Conventional chemotherapy targets cancer cells in a non-specific manner. Nanotechnology is rapidly expanding, and it is expected to have far-reaching consequences for the future of science and medicine. Significant efforts are being made to target cancer-specific cells more effectively with nanoformulations while reducing adverse effects on healthy tissues by adopting active drug delivery vehicles such as ligand attachment. Ligands for active targeting such as antibodies and aptamers are widely used for site-specific targeting of cancer cells, which leads to increased biocompatibility, bioavailability, and active targeting at the cancer site (Wu et al., 2015; Yoo et al., 2019). In recent times, a substantial increase is seen in the fabrication and development of nanoparticles to treat prostate cancer. The use of lower doses of therapeutic agents, increasing efficacy while reducing toxicity, and improved residence time in the body are the ultimate worthy goals of site-specific targeting of nanoparticles for anticancer drug delivery. The preparation, optimization, and evaluation of antibody fabricated Paclitaxel encapsulated nanoparticles (Ab-PTX-NP) was the main goal of this study, and to investigate the ability of attached J591 Ab nanoparticles to reach the PSMA on the cancerous prostate cells, ensuring that non-cancerous cells or healthy tissues remain unaffected. The quest for specific prostate cancer cell targeting by modifying the surface of NP with J591 Ab can avoid nonspecific uptake of the drug by other cells or healthy tissues (Flores et al., 2017). PSMA expression is being actively investigated for theranostic purposes, which correlates with the sensitivity of the androgen and might assist in tumour invasiveness (Chen et al., 2012). The J591 Ab was used to target overexpressed PSMA in LNCaP prostate cancer cells.

We encapsulated Paclitaxel, which is given as the first line of chemotherapy in prostate cancer, often combined with noscapine, quercetin, carboplatin, etc (Mohiuddin et al., 2019) in biodegradable and biocompatible polymeric nanoparticles. Paclitaxel, an anticancer drug, has poor water solubility and absorption, which previously restricted its clinical use. However, the PTX formulation of nanoparticles aids in overcoming these drawbacks.

We used the multiple emulsion solvent evaporation method to prepare stable nanoparticles that could deliver the encapsulated drug sustainably for a longer period of time, as reported (Mandal et al., 2018; Bhattacharya et al., 2018). Additionally, this method has a number of benefits due to its biocompatibility, biodegradability, and adaptability to the various organic

solvents and emulsifiers employed in the preparation. The method creates nanoparticles that can encapsulate and protect a variety of hydrophilic and hydrophobic drugs in a distinctly proficient manner (Nava-Arzaluz et al., 2012; Iqbal et al., 2015).

PVA is utilized in the preparation of nanoparticles as a stabiliser. It offers a variety of beneficial properties to improve the quality of nanoparticles, including biocompatibility, hydrophobicity, adequate mechanical strength, extended temperature, and pH stability (Iqbal et al. 2015). Furthermore, according to Mandal et al., (2018), PVA itself can operate as a cryoprotectant because it contains several hydroxyl groups, which limits the use of other commonly used cryoprotectants like mannitol, sucrose, lactose, etc. Different surfactants were used along with PVA in the preparation of experimental nanoparticles. The nanoparticles with the incorporation of TPGS (which acts as a solubilizer, emulsifier, and stabilizer and is non-toxic and USFDA approved) along with PVA (Chakraborty et al., 2020), show an increase in the solubility of PTX, leading to higher drug loading and preventing crystallization of free drug. Further, PTX-NP chosen as an optimized formulation was conjugated with the J591 antibody to produce Ab-PTX-NP.

The antibody conjugation strategy was based on EDC and NHS chemistry, which forms peptide bonds between the amine groups of the J591 Ab and the carboxyl groups of the PLGA (Lee et al., 2021). The attachment through the amine group to the nanoparticle surface conserves the activity of the antibodies while simultaneously preventing nonspecific protein absorption. Further, increasing the number of ligands per NP might increase the convenience of the ligand binding to the receptors (Tan et al., 2015). The SDS-PAGE analysis for conjugation of J591 Ab validates the feasibility of Ab-PTX-NP for further *in vitro* cellular study as it shows protein band at almost the same level as the monoclonal J541 antibody. The weight of the antibody conjugated nanoparticle, Ab-PTX-NP, moved to the higher side (due to the weight of PTX-NP) in comparison to the free J591.

PTX-NP and Ab-PTX-NP were analysed for physicochemical parameters. Fourier-transform infrared (FTIR) spectroscopy confirmed the nonexistence of the chemical interactions involving the drug and the excipients, while diminutive physical interactions might have helped in the formation of spherical, interstice free, smooth nanoparticle structures. The presence of nitrogen as detected by EDX in Ab-PTX-NP indicated the inclusion of the PTX in the particles. The difference in drug encapsulation of antibody conjugated and unconjugated nanoparticles (Ab-PTX-NP and PTX-NP) was very low. Drug loading was

slightly lower in Ab-PTX-NP due to antibody conjugation that could be considered trivial. The narrow range of distribution of the nanoparticles was indicated by its lower PDI. The zeta potential value proves that Ab-PTX-NP and PTX-NP in their suspended forms would not conglomerate because of the surface charge (Maji et al., 2014). The zeta potential value of the nanoparticles after antibody conjugation preserved their negative zeta-potential, though it shows the drop of negative zeta (less negative) potential in the nanoparticles after conjugation with antibody. Antibody conjugation increased the average particle size (hydrodynamic diameter) slightly. According to the results of the stability study, lyophilized PTX-NP and Ab-PTX-NP were stable at 4-8 °C in a refrigerated condition.

The experimental drug release data explicate that PTX-NP and Ab-PTX-NP had an effective sustained drug release providing, potentially optimal bioavailability of Paclitaxel within the therapeutic window over a prolonged period. The antibody conjugated nanoparticles displayed faster degradation in the acidic medium. Lower pH conditions initiated the hydrolysis of the polymeric core by striking the ester bonds. Dissolution is stable in higher pH media due to the polymer retaining its non-polar property, due to the trapping of hydroxyl groups on its surface, which ultimately lowers the water absorption by the NP. Data suggests that an acidic tumour environment (pH 5) would exhibit faster drug release while the drug release would be slow and sustained in the physiologically neutral media of blood (pH 7.4) (Mondal et al., 2019). The Ab-PTX-NP showed stability in mouse serum, which was observed for 24 h. PTX release from PTX-NP and Ab-PTX-NP denoted good linearity in the Korsmeyer- Peppas kinetics (as supported by R^2 value), suggesting release by Fickian diffusion, which was observed in PBS buffer (pH 7.4) with 0.1% w/v tween 80, citrate buffer, acetate buffer, and bicarbonate buffer.

We have used LNCaP and PC3 prostate cancer cells as LNCaP cells express PSMA while expression of PSMA is absent on PC3 cells. The Western blot analysis further substantiated the higher level of expression of PSMA in LNCaP cells, whereas the expression was insignificant in PC3 cells. A cytotoxicity study and IC_{50} doses on prostate cancer cells using the MTT assay revealed that a lower dose of Ab-PTX-NP was effective in producing a higher cytotoxic effect than PTX suspension and PTX-NP, most likely due to cellular internalisation and ultimately the encapsulated drug being delivered to the cytosol. The cytotoxicity of Ab-PTX-NP cytotoxicity toward LNCaP cells (overexpressing PSMA) was higher due to the presence of the receptor and showed minimum toxicity in HEK 293 cells (human normal kidney cells) and non-cancerous cells. The antibody conjugated blank nanoparticles on

investigation yielded the antibody concentration as non-toxic to prostate cancer cells. The results of cytotoxicity assays that show Ab-PTX-NP nanoparticles internalise substantially more than the other experimental nanoparticles are supported by quantitative and qualitative cellular uptake data of the nanoparticles in prostate cancer cells. PSMA has a substantially higher affinity for LNCaP cells than in PC3 cells. This could explain why Ab-PTX-NP internalised to the greatest extent, highlighting the greater potential of the J591 antibody as a targeted ligand for prostate cancer.

In earlier studies on paclitaxel, it was reported that paclitaxel incorporated polymeric nanoparticles primarily initiated the apoptotic pathway, which showed potent antiproliferative activity by bringing the cell cycle to arrest at G2/M and S phases, which normally activates three principal checkpoints such as G1/S, G2/M, and metaphase/anaphase transitions during mitosis (Chakraborty et al., 2020). The intrinsic pathway of apoptosis is the possible mechanism of cell death induced by paclitaxel, although some recent reports suggest that paclitaxel initiates apoptosis via multiple mechanisms (Vakilinezhada et al., 2019). Paclitaxel is acknowledged to cause both mitotic arrest and apoptotic cell death. It simultaneously acts on mitochondria and microtubule assembly to generate sufficient signals for mitochondrial apoptosis (Wang et al., 2000; Yi et al., 2015). It is also reported to elevate ROS by increasing the activity of the NADPH oxidase (NOX) enzyme (Chakraborty et al., 2020; Yi et al., 2015).

Apoptosis, or programmed cell death, is an extremely controlled physiological response because it results in the death of cells without harming adjacent tissues. Apoptosis is distinguished by the following hallmarks: loss of phospholipid asymmetry; chromatin condensation; nuclear shrinkage; apoptotic body breakdown; and finally, phagocytosis of apoptotic bodies (Indran et al., 2011; Redza-Dutordoir and AverillBates 2016). The apoptosis inducing ability of Ab-PTX-NP shows cell death by AO/EB staining that was visualized by the colour change of apoptotic cells. The total fluorescence intensity and cell counting advocated the effectiveness of Ab-PTX-NP in LNCaP cells. It has distinctly separated normal and cancer cells due to the loss of integrity of the cellular membrane, nuclear fragmentation, and chromatin condensation, while recognizing the difference between early and late apoptotic cells. Mitochondrial membrane depolarization occurs due to changes in mitochondrial transmembrane potential (MMP). During apoptosis, mitochondria undergo depolarization, which finally leads to rupturing of mitochondria, leading to the disruption of Ca^{2+} homeostasis between mitochondria and the endoplasmic reticulum. That indicates a

lowering of MMP in apoptotic cells (Priyadarshini and Keerthi, 2012; Henry-Mowatt et al., 2004)

The data indicates effective depolarization of the mitochondrial membrane in LNCaP cells as the cellular uptake of Ab-PTX-NP increases. It was quantified by determining the decrement in the values of the ratio of green to red fluorescence owing to the transformation of JC-1 aggregates (live healthy cells with high MMP give red colour) to monomers (apoptotic cells with decreased MMP give green colour). The DAPI staining after treating both the prostate cancer types with the experimental formulations pronounced the morphological changes due to apoptotic body formations, which was apparently noticeable in LNCaP (+ve PSMA) cells induced by Ab-PTX-NP as compared to other formulations. Thus, Ab-PTX-NP expedited apoptosis-inducing ability and depicted the highest potency towards PSMA overexpressed prostate cancer cells.

So far, J591 Ab has been successfully utilized for the diagnostic purpose of detecting advanced prostate cancer because of its propensity to attach to abundantly upregulated PSMA on LNCaP cells (Bander et al., 2003). Combining the efficiency of this anti-PSMA antibody J591 with the effectiveness of the anti-cancer drug (paclitaxel) incorporated in the biodegradable (PLGA) nanoparticles has enabled site-specific delivery and showed profound cellular uptake by the prostate cancer cells. Novelty can be interpreted as site and cancer-specific drug delivery. Site specificity causes minimal harm to healthy tissues by avoiding non-specific uptake by healthy tissues, while cancer cell specificity makes the cancer cells less viable and may decrease the ability of the cancer cells to metastasize.

Thus, the prepared optimized formulation Ab-PTX-NP is low in cost, convenient to produce and administer via intravenous route, less invasive due to less frequent dosing, and easy availability to the patients. Furthermore, it is a biodegradable in the human body as well as for the environment. Therefore, the Ab-PTX-NP selected as an escort can be used as a timely and significant therapeutic option for prostate cancer.

8. Conclusion

As a result of the recent explosion in the field of the utility of engineered nanotechnology, our work was motivated to investigate the therapeutic effectiveness of Ab-PTX-NP for site-specific delivery to treat prostate cancer. The developed Ab-PTX-NP was deemed promising due to its biocompatibility, biodegradability, high drug loading capability with acceptable size, prolonged drug release, stability, and non-toxicity to healthy tissues.

Without restricting the use of J591 as a cancer imaging agent, we attempted to selectively employ J591 Ab to target overexpressed PSMA. Patients may benefit from our study as a result of the remarkable characteristics of the nanoparticles and antibody that was attached to them to achieve the intended therapeutic targeting. Enhanced cytotoxic and apoptotic effects and decreased mitochondrial membrane potential at a low dose when compared to PTX and PTX-NP in PSMA-expressing LNCaP cells, the optimized formulation fabricated with J591 antibody demonstrated the ability to concentrate and distribute PTX to prostate cancer cells in vitro and induced apoptosis by reducing MMP. The comparative investigation of several formulations on various prostate cancer cells was conducted to support the rationale, and the results were promising. Patients suffering from prostate cancer with poor prognosis could receive exceptional care from it. To benefit society in the near future, we wish to further investigate our study in an extensive manner preclinically followed by clinical trials.

9. Summary

In recent years, the number of increase in cases, incidence, and mortality associated with malignancy of the prostate has increased largely. Identifying prostate cancer in the early or initial stages is difficult as, in most cases, distinct symptoms are not prominent. Once the disease becomes malignant, the prognosis is poor in most cases, resulting in an increase in fatalities.

Metastasis in later stages often becomes incurable. Androgen deprivation therapy was the only treatment option for men with metastatic disease until quite recently. A variety of treatments in conjunction with surgery or radiotherapy are under research to improve overall survival in newly diagnosed prostate cancer as well as early metastatic prostate cancer. Targeted drug delivery is being focused on developing an overarching treatment for patients with prostate cancer by minimizing toxicity and damage to healthy tissue in order to prevent further metastases, maintain quality of life, and prolong overall survival. Researchers have investigated several ligands in an effort to deliver therapeutic preferential to the affected organ.

A monoclonal antibody, J591, was utilized against prostate-specific membrane antigen (PSMA). PSMA expression is elevated in prostate cancer cells. The conjugated antibody to Paclitaxel nanoparticles would bind with the PSMA highly expressed on prostate cancer cells, delivering the encapsulated drug Paclitaxel (PTX) to the cells. Paclitaxel is an anticancer drug with a broad anti-tumor activity spectrum. PTX promotes and stabilizes microtubules while inhibiting the late G2 or M phases of the cell cycle, thus further causing apoptosis. However, in our study, we tried to use its therapeutic application in cancer therapy, which was limited due to its low water solubility and associated toxicity. We encapsulated the potent drug PTX in poly(d,l)-lactic-*co*-glycolic acid (PLGA) nanoparticles. PLGA is virtuous over other polymers as it is biodegradable, drug release can be manipulated and it produces stable desired nanoparticles.

In the present study, Paclitaxel-loaded PLGA nanoparticles were prepared and conjugated with J591 antibody in order to bind specifically to the specific prostate cancer cell receptor PSMA. The effectiveness of the nanoformulations was further evaluated.

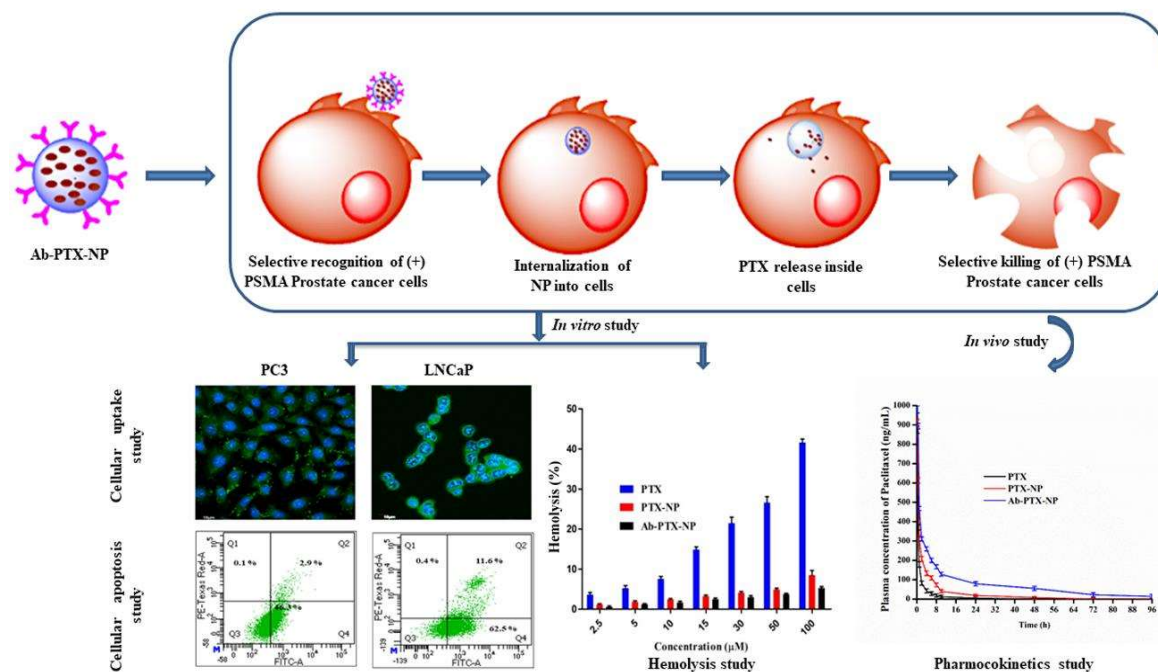


Figure. 9.1 Summarization of the present study, which depicts that the optimized antibody conjugated formulation Ab-PTX-NP recognizes the positive PSMA prostate cancer cells, further internalization of Ab-PTX-NP results in apoptosis of cancerous cells. The hemolysis and pharmacokinetics study reveals the hemo-compatibility and efficiency of the formulation in the form of increased bioavailability and prolonged drug release from Ab-PTX-NP

To obtain the optimum parameters, the PLGA nanoparticles were prepared using the multiple emulsion solvent evaporation technique. The formulations made with different stabilizers were compared. The inclusion of D- α -tocopherol polyethylene glycol succinate (TPGS) improved the solubility, drug loading, and other physicochemical properties of nanoparticles. The optimized PTX-NP was conjugated using EDC and NHS to obtain Ab-PTX-NP. The conjugation was confirmed with the help of SDS-PAGE gel electrophoresis. PTX-NP and Ab-PTX-NP were evaluated on various parameters; the size range obtained was between 200nm and 300nm with a negative zeta charge for both the formulations. The scanning electron microscopy and atomic force microscopy evaluations of the morphological characteristics of the particles revealed distinct, homogenous particles with smooth surface. Transmission electron microscopy revealed a uniform distribution of the drug throughout the nanoparticles. The efficiency of drug loading and entrapment was satisfactory. The experimental data on drug release elucidated that both PTX-NP and Ab-PTX-NP had an

efficient sustained drug release, which could result in optimal bioavailability of PTX within the therapeutic window over a long period of time. Further, the release pattern of paclitaxel from Ab-PTX-NP was evaluated in various release media. The release kinetic study revealed that the PTX release pattern from PTX-NP and Ab-PTX-NP in the respective medium followed the Korsmeyer—Peppas kinetic model. The PTX-NP and Ab-PTX-NP were found to be stable when stored in the refrigerator (at 4–8°C).

The *in vitro* cytotoxicity was analysed by the MTT assay, which displayed that the lower dose of Ab-PTX-NP produced an elevated cytotoxic effect when compared with PTX-NP and free drug in PSMA overexpressing LNCaP cells. The antibody conjugated blank nanoparticles were found to be non-toxic, indicating the antibody in the particular concentration is safe for use. The Ab-PTX-NP cytotoxicity toward LNCaP cells (overexpressing PSMA) was higher due to the presence of the receptor and showed minimum toxicity in non-cancerous cells. Cellular internalization of the formulation in LNCaP cells ensured the encapsulated drug was delivered to the cytosol. The quantitative and qualitative *in vitro* cellular uptake study data of the Ab-PTX-NP in LNCaP cells also support the findings of the cytotoxicity studies, i.e., superior cellular internalizations of antibody conjugated nanoparticles in LNCaP cells. Ab-PTX-NP capacity to induce apoptosis was demonstrated by the colour shift of apoptotic cells as observed by AO/EB staining. According to the total fluorescence intensity and cell count, Ab-PTX-NP appeared to be effective in initiating apoptosis in LNCaP cells. Loss of membrane integrity, nuclear fragmentation, and chromatin condensation have allowed us to distinguish between early and late apoptotic cells, allowing us to identify the state of progress of cancerous cell death by apoptosis. Variations in mitochondrial transmembrane potential (MMP) lead to depolarization of the mitochondrial membrane. Apoptosis is characterized by mitochondrial depolarization and rupturing, which disrupts Ca^{2+} equilibrium between the mitochondria and the endoplasmic reticulum. This suggests that MMP levels were decreased in apoptotic cells.

As shown by the findings, increasing cellular uptake of Ab-PTX-NP correlates with effective depolarization of the mitochondrial membrane in LNCaP cells. It was measured by observing the decrease in the ratio of green to red fluorescence as a result of the transformation of JC-1 aggregates (which, in living cells with high MMP, gives a reddish color) (in apoptotic cells with decreased MMP gives green colour). The morphological alterations owing to apoptotic body formations were evident in LNCaP (+ve PSMA) cells generated by Ab-PTX-NP as compared to other formulations, as shown by DAPI staining after treatment with the

experimental formulations for both PSMA positive LNCaP cells and PSMA negative PC3 prostate cancer cells. Thus, Ab-PTX-NP exhibited the greatest potency and speed in eliciting apoptosis in PSMA prostate cancer cells. This study acknowledges the effectiveness of Ab-PTX-NP *in vitro*, which displays elevated cellular cytotoxicity and internalization, and maximum apoptosis (74.1%) in PSMA-abundant LNCaP cells, in comparison to PSMA negative PC3 cells. Pharmacokinetics data (by LC-MS/MS) for the experimental nanoparticles and free drug at various predefined time points revealed increased bioavailability and prolonged drug release from Ab-PTX-NP and PTX-NP during the study period upon i.v. administration into the systemic circulation of male Balb/c mice. Thus, Ab-PTX-NP exhibited the greatest potency and speed in eliciting apoptosis in PSMA positive prostate cancer cells.

Herein, our formulation Ab-PTX-NP was maneuvered in a neoteric way to carry the prepared chemotherapeutic nanoparticles directly to the affected prostate cancer cells and proved to have greater efficacy than the free drug.

Future Prospects

The present study showed that J591 antibody conjugated Paclitaxel loaded nanoparticles (Ab-PTX-NP) successfully targeted androgen receptor positive prostate cancer cells through Prostate specific membrane antigen (PSMA) - J591 antibody binding.

The pharmacokinetic profile of the J591 antibody conjugated Paclitaxel loaded nanoparticles in male Balb/c mice favoured the stability and long residence time with increased biological half life of the formulation. J591 antibody conjugated Paclitaxel loaded nanoparticles showed its potential for the management of androgen receptor positive prostate cancer. However, further studies are warranted to investigate the therapeutic potential in preclinical (animals) prostate cancer models. Upon success, the formulation can be translated for clinical investigation.

References

A. Ahmad, F. Khan, R.K. Mishra, R. Khan, Precision cancer nanotherapy: evolving role of multifunctional nanoparticles for cancer active targeting, *J. Med. Chem.* 62 (2019) 10475-96.
<https://doi.org/10.1021/acs.jmedchem.9b00511>

A. Anitha, K.P. Chennazhi, S.V. Nair, R. Jayakumar, 5-flourouracil loaded N, O-carboxymethyl chitosan nanoparticles as an anticancer nanomedicine for breast cancer, *J. Biomed. Nanotechnol.* 8 (2012) 29-42.
<https://doi.org/10.1166/jbn.2012.1365>

A. Mahapatro and D.K. Singh, Biodegradable nanoparticles are excellent vehicle for site directed in-vivo delivery of drugs and vaccines, *J. Nanobiotechnology* 9 (2011) 1-1.
<https://doi.org/10.1186/1477-3155-9-55>

A.T. Tawfeeq, N.A.A. Mahmood, Z.S. Abd-Alghni, Starvation contributes to elevated levels of heat shock proteins and cancer stem cell markers in an esophageal cancer cell line, *Biomed. Res.* 29 (2018) 3815-3823.

B. Haley and E. Frenkel, Nanoparticles for drug delivery in cancer treatment, *Urol. Oncol-Semin. Ori. Inv.* 26 (2008) 57-64.
<https://doi.org/10.1016/j.urolonc.2007.03.015>

B. Huang, J. Otis, M. Joice, A. Kotlyar, T.P. Thomas, PSMA-targeted stably linked “dendrimer-glutamate urea-methotrexate” as a prostate cancer therapeutic, *Biomacromolecules* 15 (2014) 915-923.
<https://doi.org/10.1021/bm401777w>

B. Mukherjee, M. Rajagopalan, S. Chakraborty, P. Ghosh, M. Ray, R. Sen, I. Ehsan, Hepatocellular Carcinoma: Diagnosis, Molecular Pathogenesis, Biomarkers, and Conventional Therapy, in: B.Mukherjee, *Nanotherapeutics for the Treatment of Hepatocellular Carcinoma*, Bentham books, 1 (2022) 1-97.
<https://doi.org/10.2174/97898150397401220101>

B. W. Tse, G.J. Cowin, C. Soekmadji, L. Jovanovic, R.S. Vasireddy, M.T. Ling, A. Khatri, T. Liu, B. Thierry, P.J. Russell PJ, PSMA-targeting iron oxide magnetic nanoparticles enhance MRI of preclinical prostate cancer, *Nanomedicine*. 3 (2015) 375-86.
<https://doi.org/10.2217/nmm.14.122>

C. Fornaguera, G. Calderó, M. Mitjans, M.P. Vinardell, C. Solans, C. Vauthier, Interactions of PLGA nanoparticles with blood components: protein adsorption, coagulation, activation of the complement system and hemolysis studies, *Nanoscale* 7 (2015) 6045-6058.
<https://doi.org/10.1039/c5nr00733j>

D. Dutta, B. Paul, B. Mukherjee, L. Mondal, S. Sen, C. Chowdhury, M.C. Debnath, Nanoencapsulated betulinic acid analogue distinctively improves colorectal carcinoma in vitro and in vivo, *Sci. Rep.* 9 (2019) 1-20.
<https://doi.org/10.1038/s41598-019-47743-y>

D. Mandal, T.K. Shaw, G. Dey, M.M. Pal, B. Mukherjee, A.K. Bandyopadhyay, M. Mandal, Preferential hepatic uptake of paclitaxel-loaded poly-(DL-lactide-co-glycolide) nanoparticles—A possibility for hepatic drug targeting: Pharmacokinetics and biodistribution, *Int. J. Biol. Macromol.* 112 (2018) 818-830.
<https://doi.org/10.1016/j.ijbiomac.2018.02.021>

E. Andreopoulou, J.A. Sparano, Chemotherapy in Patients with Anthracycline- and Taxane-Pretreated Metastatic Breast Cancer: An Overview. *Curr. Breast Cancer Rep.* 5 (2013) 42–50.
<https://doi.org/10.1007/s12609-012-0097-1>

E. Ertugen, A. Tunçel, F. Yurt, Docetaxel loaded human serum albumin nanoparticles; synthesis, characterization, and potential of nuclear imaging of prostate cancer, *J. Drug Deliv. Sci. Technol.* 55 (2020) 101410.
<https://doi.org/10.1016/j.jddst.2019.101410>

F. Danhier, A. Le Breton, V. Preat, RGD-based strategies to target alpha(v) beta(3) integrin in cancer therapy and diagnosis, *Mol. Pharm.* 9 (2012) 2961–2973.
<https://doi.org/10.1021/mp3002733>

F. Sanice, N. Shabani Ravari, N. Goodarzi, M. Amini, F. Atyabi, E. Saeedian Moghadam, R. Dinarvand, Glutamate-urea-based PSMA-targeted PLGA nanoparticles for prostate cancer delivery of docetaxel, *Pharm. Dev. Technol.* 26 (2021) 381-389. <https://doi.org/10.1080/10837450.2021.1875238>

F.C. Gaertner, K. Halabi, H. Ahmadzadehfar, S. Kürpig, E. Eppard, C. Kotsikopoulos, N. Liakos, R.A. Bundschuh, H. Strunk, M. Essler, Uptake of PSMA-ligands in normal tissues is dependent on tumor load in patients with prostate cancer, *Oncotarget* 8 (2017) 55094-55103. <https://doi.org/10.18632/oncotarget.19049>

G. Tan, K. Kantner, Q. Zhang, M.G. Soliman, P. Del Pino, W.J. Parak, M.A. Onur, D. Valdeperez, J. Rejman, B. Pelaz, Conjugation of polymer-coated gold nanoparticles with antibodies—Synthesis and characterization, *Nanomaterials* 5 (2015) 1297-1316. <https://doi.org/10.3390/nano5031297>

H. Afrooz, F. Ahmadi, F. Fallahzadeh, S. H. Mousavi-Fard, S. Alipour, Design and characterization of paclitaxel-verapamil co-encapsulated PLGA nanoparticles: Potential system for overcoming P-glycoprotein mediated MDR, *J. Drug Deliv. Sci. Technol.* 41 (2017) 174-181. <https://doi.org/10.1016/j.jddst.2017.06.020>

H. Gelderblom, J. Verweij, K. Nooter, A. Sparreboom, Cremophor EL: the drawbacks and advantages of vehicle selection for drug formulation, *Eur. J. Cancer* 37 (2001) 1590–1598. [https://doi.org/10.1016/s0959-8049\(01\)00171-x](https://doi.org/10.1016/s0959-8049(01)00171-x)

H. Maleki, M. R. H. Najafabadi, T. J. Webster, M. R. Hadjighassem, E. Sadroddiny, H. Ghanbari, M. Khosravani, M. Adabi, Effect of Paclitaxel/etoposide co-loaded polymeric nanoparticles on tumor size and survival rate in a rat model of glioblastoma, *Int. J. Pharm.* 604 (2021) 120722. <https://doi.org/10.1016/j.ijpharm.2021.120722>

I.A. Siddiqui, V.M. Adhami, J. Christopher, H. Mukhtar, Impact of nanotechnology in cancer: emphasis on nanochemoprevention, *Int. J. Nanomedicine* 7 (2012) 591. <https://doi.org/10.2147/IJN.S26026>

I.R. Indran, G. Tufo, S. Pervaiz, C. Brenner, Recent advances in apoptosis, mitochondria and drug resistance in cancer cells, *Biochim. Biophys. Acta* 1807 (2011) 735–745.
<https://doi.org/10.1016/j.bbabi.2011.03.010>

J. Henry-Mowatt, C. Dive, J.C. Martinou, D. James, Role of mitochondrial membrane permeabilization in apoptosis and cancer, *Oncogene* 23 (2004) 2850-2860.
<https://doi.org/10.1038/sj.onc.1207534>

J. Panyam and V. Labhasetwar, Sustained cytoplasmic delivery of drugs with intracellular receptors using biodegradable nanoparticles, *Mol pharm.* 1(2004) 77-84.
<https://doi.org/10.1021/mp034002c>

J. Panyam, W-Z. Zhou, S. Prabha, S.K. Sahoo, V. Labhasetwar, Rapid endolysosomal escape of poly(DL-lactide-co-glycolide) nanoparticles: implications for drug and gene delivery, *The FASEB Journal* 16 (2002) 1217-1226.
<https://doi.org/10.1096/fj.02-0088com>

J. Yoo, C. Park, G. Yi, D. Lee, H. Koo, Active targeting strategies using biological ligands for nanoparticle drug delivery systems, *Cancers* 11 (2019) 640.
<https://doi.org/10.3390/cancers11050640>

J.D. Mangadlao, X. Wang, C. McCleese, M. Escamilla, G. Ramamurthy, Z. Wang, M. Govande, J.P. Basilion, C. Burda, Prostate-specific membrane antigen targeted gold nanoparticles for theranostics of prostate cancer, *ACS Nano* 12 (2018) 3714-3725.
<https://doi.org/10.1021/acsnano.8b00940>

J.J. Pillai, A.K. Thulasidasan, R.J. Anto, N.C. Devika, N. Ashwanikumar, G.V. Kumar, Curcumin entrapped folic acid conjugated PLGA–PEG nanoparticles exhibit enhanced anticancer activity by site specific delivery, *RSC Adv.* 5 (2015) 25518-25524.
<https://doi.org/10.1039/C5RA00018A>

J.M. Gallo, S. Li, P. Guo, K. Reed, J. Ma, The effect of P-glycoprotein on paclitaxel brain and brain tumor distribution in mice, *Cancer Res.* 63 (2003) 5114–5117. PMID: 12941842

J.P. Gillet and M.M. Gottesman, Mechanisms of multidrug resistance in cancer, *Methods Mol. Biol.* 596 (2010) 47–76.

https://doi.org/10.1007/978-1-60761-416-6_4

K. Cho K, X.U. Wang, S. Nie, Z. Chen, D.M. Shin, Therapeutic nanoparticles for drug delivery in cancer, *Clin Cancer Res.* 14 (2008) 1310-6.

<https://doi.org/10.1158/1078-0432.CCR-07-1441>

K. Liu, W. Chen, T. Yang, B. Wen, D. Ding, M. Keidar, J. Tang, W. Zhang, Paclitaxel and quercetin nanoparticles co-loaded in microspheres to prolong retention time for pulmonary drug delivery, *Int. J. Nanomedicine* 12 (2017) 8239–8255.

<https://doi.org/10.2147/IJN.S147028>

K. Omabe, C. Paris, F. Lannes, D. Taïeb, P. Rocchi, Nanovectorization of Prostate Cancer Treatment Strategies: A New Approach to Improved Outcomes. *Pharmaceutics* 13 (2021) 591. <https://doi.org/10.3390/pharmaceutics13050591>

K. Priyadarshini, A.U. Keerthi, Paclitaxel against cancer: a short review, *Med. Chem.* 2 (2012) 139-141.

<https://doi.org/10.4172/2161-0444.1000130>

K. Yifan, Y. Zhang, F. Mao, Z. Zhang, Z. Li, R. Wang, J. Liu, X. Liu, Inhibition of EZH2 Enhances the Antitumor Efficacy of Metformin in Prostate Cancer The Combination of Metformin and GSK126 Is Synergistic, *Mol. Cancer Ther.* 19 (2020) 2490-2501.

<https://doi.org/10.1158/1535-7163>

L.P. Jahromi, M. Ghazali, H. Ashrafi, A. Azadi, A comparison of models for the analysis of the kinetics of drug release from PLGA-based nanoparticles, *Heliyon* 6 (2020) e03451.

<https://doi.org/10.1016/j.heliyon.2020.e03451>

L. Mondal, B. Mukherjee, K. Das, S. Bhattacharya, D. Dutta, S. Chakraborty, M.M. Pal, R.H. Gaonkar, M.C. Debnath, CD-340 functionalized doxorubicin-loaded nanoparticle induces apoptosis and reduces tumor volume along with drug-related cardiotoxicity in mice, *Int. J. Nanomedicine* 14 (2019) 8073-8094.

<https://doi.org/10.2147/IJN.S220740>

L. Yao-Cheng, M. Boone, L. Meuris, I. Lemmens, N. V. Roy, A. Soete, J. Reumers, M. Moisse, S. Plaisance, R. Drmanac, J. Chen, F. Speleman, D. Lambrechts, Y. Van de Peer, J. Tavernier, N. Callewaert N, Genome dynamics of the human embryonic kidney 293 lineage in response to cell biology manipulations, *Nat. Commun.* 5 (2014) 1-12.

<https://doi.org/10.1038/ncomms5767>

M. Redza-Dutordoir, D.A. Averill-Bates, Activation of apoptosis signalling pathways by reactive oxygen species, *Biochim. Biophys. Acta Mol. Cell Res.* 1863 (2016) 2977-2992.

<https://doi.org/10.1016/j.bbamcr.2016.09.012>

M. Sharma, S. Gupta, B. Dhole, A. Kumar, The prostate gland, In: A. Kumar, M. Sharma, *Basics of Human Andrology*, Springer, Singapore, (2017) 17-35.

https://doi.org/10.1007/978-981-10-3695-8_2

M.A. Vakilinezhad, A. Aminic, T. Daraa, S. Alipourb, Methotrexate and Curcumin co-encapsulated PLGA nanoparticles as a potential breast cancer therapeutic system: In vitro and in vivo evaluation, *Colloids Surf. B Biointerfaces* 184 (2019) 110515.

<https://doi.org/10.1016/j.colsurfb.2019.110515>

M.D. Galsky and N.I. Vogelzan, Docetaxel-based combination therapy for castration-resistant prostate cancer, *Ann. Oncol.* 21(2010) 2135–2144.

<https://doi.org/10.1093/annonc/mdq050>.

M.G. Nava-Arzaluz, E. Pinon-Segundo, A. Ganem-Rondero, D. Lechuga-Ballesteros, Single emulsion-solvent evaporation technique and modifications for the preparation of pharmaceutical polymeric nanoparticles, *Recent Pat Drug Deliv Formul.* 6 (2012). 209-223.

<https://doi.org/10.2174/187221112802652633>.

M.L. Hans and A.M. Lowman, Biodegradable nanoparticles for drug delivery and targeting, *Curr Opin Solid State Mater Sci.* 6 (2002) 319-327.

[https://doi.org/10.1016/S1359-0286\(02\)00117-1](https://doi.org/10.1016/S1359-0286(02)00117-1)

M.S. Litwin, H.J. Tan, The diagnosis and treatment of prostate cancer: a review, *JAMA* 317 (2017) 2532-2542.

<https://doi.org/10.1001/jama.2017.7248>

M.S. Tousi, H. Sepehri, S. Khoee, M.M. Farimani, L. Delphi, F. Mansourizadeh, Evaluation of apoptotic effects of mPEG-b-PLGA coated iron oxide nanoparticles as a eupatorin carrier on DU-145 and LNCaP human prostate cancer cell lines, *J. Pharm. Anal.* 11 (2021) 108-121. <https://doi.org/10.1016/j.jpha.2020.04.002>

N. K. Lee, C. J. Wang, J. Lim, W. Park, H. K. Kwon, S. N. Kim, T. H. Kim, C. G. Park, Impact of the conjugation of antibodies to the surfaces of polymer nanoparticles on the immune cell targeting abilities, *Nano Converg.* 8 (2021) 1-11. <https://doi.org/10.1186/s40580-021-00274-7>.

N.H. Bander, E.J. Trabulsi, L. Kostakoglu, D. Yao, S. Vallabhajosula, P. Smith-Jones, M.A. Joyce, M. Milowsky, D.M. Nanus, S.J. Goldsmith, Targeting metastatic prostate cancer with radiolabeled monoclonal antibody J591 to the extracellular domain of prostate specific membrane antigen, *J. Urol.* 170 (2003) 1717-1721. <https://doi.org/10.1097/01.ju.0000091655.77601.0c>

O. Flores, S. Santra, C. Kaittanis, R. Bassiouni, A.S. Khaled, A.R. Khaled, J. Grimm, J.M. Perez, PSMA-targeted theranostic nanocarrier for prostate cancer, *Theranostics* 7 (2017) 2477-2494. <https://doi.org/10.7150/thno.18879>

P. Ghosh, A. Bhoumik, S. Saha, S. Mukherjee, S. Azmi, J.K. Ghosh, S.R. Dungdung, Spermicidal efficacy of VRP, a synthetic cationic antimicrobial peptide, inducing apoptosis and membrane disruption, *J. Cell. Physiol.* 233 (2018) 1041-1050. <https://doi.org/10.1002/jcp.25958>

P. Rawla, Epidemiology of prostate cancer, *World J. Oncol.* 10 (2019) 63-89. <https://doi.org/10.14740/wjon1191>

P.J. Russell, C. Soekmadji, B. Thierry, G. Cowin, T. Strait-Gardner, N. Verma, W. Xiaochun, A. Khatri, Use of targeted magnetic nanoparticles for imaging in prostate cancer, InAACR Special Conference on Advances in Prostate Cancer Research 2013 (pp. Abstract-nr). <https://doi.org/10.1158/1538-7445.PRCA2012-C30>

P.K.B. Nagesh, N.R. Johnson, V.K.N. Boya, P. Chowdhury, S.F. Othman, V. Khalilzad-Sharghi, B.B. Hafeez, A. Ganju, S. Khan, S.W. Behrman, N. Zafar, S.C. Chauhan, M. Jaggi, M.M. Yalla, PSMA targeted docetaxel-loaded superparamagnetic iron oxide nanoparticles for prostate cancer, *Colloids Surf B Biointerfaces*. 144 (2016) 8-20. <https://doi.org/10.1016/j.colsurfb.2016.03.071>.

R. Bazak, M. Hourri, S.El. Achy, Cancer active targeting by nanoparticles: a comprehensive review of literature, *J Cancer Res Clin Oncol* 141, (2015) 769–784. <https://doi.org/10.1007/s00432-014-1767-3>

R.C. Alves, R.P. Fernandes, J.O. Eloy, H.R.N. Salgado, M. Chorilli, Characteristics, properties and analytical methods of Paclitaxel: a review, *Crit Rev Anal Chem*. 48 (2018) 110-118. <https://doi.org/10.1080/10408347.2017.1416283>.

R. Maji, N.S. Dey, B.S. Satapathy, B. Mukherjee, S. Mondal, Preparation and characterization of Tamoxifen citrate loaded nanoparticles for breast cancer therapy, *Int. J. Nanomedicine* 9 (2014) 3107-3118. <https://doi.org/10.2147/IJN.S63535>

R. Mandelkow, D. Guembel, H. Ahrend, A. Kaul, U. Zimmermann, M. Burchardt, M.B. Stope, Detection and quantification of nuclear morphology changes in apoptotic cells by fluorescence microscopy and subsequent analysis of visualized fluorescent signals, *Anticancer Res*. 37 (2017) 2239-2244. <https://doi.org/10.21873/anticancer.11560>

R. Sen, S. Ganguly, S. Ganguly, M.C. Debnath, S. Chakraborty, B. Mukherjee, D. Chattopadhyay, Apigenin-Loaded PLGA-DMSA Nanoparticles: A Novel Strategy to Treat Melanoma Lung Metastasis, *Mol. Pharm.* 18 (2021) 1920-1938. <https://doi.org/10.1021/acs.molpharmaceut.0c00977>

R. Summart, T. Pak, S. Jutharat, M. Puttinan, L.T. Randall, T. Wirote, Superiority of an asymmetric perylene diimide in terms of hydrosolubility, G-quadruplex binding, cellular uptake, and telomerase inhibition in prostate cancer cells, *ACS Omega* 5 (2020) 29733-29745. <https://doi.org/10.1021/acsomega.0c03505>

R.A. Jain, The manufacturing techniques of various drug loaded biodegradable poly(lactide-co-glycolide acid) (PLGA) devices, *Biomaterials* 21 (2000) 2475–2490. [https://doi.org/10.1016/S0142-9612\(00\)00115-0](https://doi.org/10.1016/S0142-9612(00)00115-0).

R.F. Pagels and R.K. Prud'Homme, Polymeric nanoparticles and microparticles for the delivery of peptides, biologics, and soluble therapeutics. *J. Control Release* 219 (2015) 519–35. <https://doi.org/10.1016/j.jconrel.2015.09.001>

R.H. Gaonkar, S. Ganguly, S. Dewanjee, S. Sinha, A. Gupta, S. Ganguly, D. Chattopadhyay, M.C. Debnath, Garcinol loaded vitamin E TPGS emulsified PLGA nanoparticles: preparation, physicochemical characterization, in vitro and in vivo studies, *Sci. Rep.* 7 (2017) 1-14. <https://doi.org/10.1038/s41598-017-00696-6>

R.M. Taylor and L.O. Sillerud, Paclitaxel-loaded iron platinum stealth immunomicelles are potent MRI imaging agents that prevent prostate cancer growth in a PSMA-dependent manner, *Int. J. Nanomedicine* 7 (2012) 4341-4352. <https://doi.org/10.2147%2FIJN.S34381>

S. Bhattacharya, L. Mondal, B. Mukherjee, L. Dutta, I. Ehsan, M.C. Debnath, R.H. Gaonkar, M.M. Pal, S. Majumdar, Apigenin loaded nanoparticle delayed development of hepatocellular carcinoma in rats, *Nanomedicine* 14 (2018) 1905-1917. <https://doi.org/10.1016/j.nano.2018.05.011>

S. Chakraborty, I. Ehsan, B. Mukherjee, L. Mondal, S. Roy, K.D. Saha, B. Paul, M.C. Debnath, T. Bera, Therapeutic potential of andrographolide-loaded nanoparticles on a murine asthma model, *Nanomedicine* 20 (2019) 102006. <https://doi.org/10.1016/j.nano.2019.04.009>

S. Chakraborty, Z.Y. Dlie, B. Mukherjee, S.E. Besra, S. Sengupta, R. Sen, A. Mukherjee, A Comparative Investigation of the Ability of Various Aptamer-Functionalized Drug Nanocarriers to Induce Selective Apoptosis in Neoplastic Hepatocytes: In Vitro and In Vivo Outcome, *AAPS PharmSciTech* 21 (2020) 1-13. <https://doi.org/10.1016/j.omtn.2020.01.034>

S. K. Sriraman, B. Aryasomayajula, V.P. Torchilin, Barriers to drug delivery in solid tumors, *Tissue barriers* 2(3) (2014) e29528.

<https://doi.org/10.4161/tisb.29528>.

S. Maghsoudi, B. T. Shahraki, N. Rabiee, R. Afshari, Y. Fatahi, R. Dinarvand, S. Ahmadi, M. Bagherzadeh, M. Rabiee, L. Tayebi, M. Tahriri, Recent Advancements in aptamer-bioconjugates: Sharpening Stones for breast and prostate cancers targeting, *J. Drug Deliv. Sci. Technol.* 53 (2019) 101146.

<https://doi.org/10.1016/j.jddst.2019.101146>.

S. Moffatt, R.J. Cristiano, PEGylated J591 mAb loaded in PLGA-PEG-PLGA tri-block copolymer for targeted delivery: in vitro evaluation in human prostate cancer cells, *Int. J. Pharm.* 317 (2006) 10-13.

<https://doi.org/10.1016/j.ijpharm.2006.04.01>

S. Rezvantlab, N.I. Drude, M.K. Moraveji, N. Güvener, E.K. Koons, Y. Shi, T. Lammers, F. Kiessling, PLGA-based nanoparticles in cancer treatment, *Front Pharmacol.* 9 (2018) 1260.

S.A.A. Rizvi, A.M. Saleh, Applications of nanoparticole systems in drug delivery technology, *Saudi Pharm J.* 26 (2018) 64-70.

<https://doi.org/10.3389/fphar.2018.01260>

S.K. Sahoo, W. Ma, V. Labhasetwar, Efficacy of transferrin-conjugated paclitaxel-loaded nanoparticles in a murine model of prostate cancer, *Int J Cancer.* 112 (2004) 335-40.

<https://doi.org/10.1002/ijc.20405>.

S.S. Chang, Overview of prostate-specific membrane antigen, *Rev. Urol.* 6 (2004) S13. PMID: 16985927; PMCID: PMC1472940

T. Karantanos, P.G. Corn, T.C. Thompson, Prostate cancer progression after androgen deprivation therapy: Mechanisms of castrate resistance and novel therapeutic approaches, *Oncogene* 32 (2013) 5501–5511.

<https://doi.org/10.1038/onc.2013.206>

T.B Stage, C. Mortensen, S. Khalaf, V. Steffensen, H.S. Hammer, C. Xiong, F. Nielsen, O. Poetz, A.F. Svenningsen, C. Rodriguez-Antona, D.L. Kroetz, P-Glycoprotein Inhibition Exacerbates Paclitaxel Neurotoxicity in Neurons and Patients with Cancer, *Clin Pharmacol Ther.* 108 (2020) 671-680.

<https://doi.org/10.1002/cpt.1847>.

T.H. Wang, H.S. Wang, Y.K. Soong, Paclitaxel-induced cell death: where the cell cycle and apoptosis come together, *Cancer* 88 (2000) 2619-2628.

[https://doi.org/10.1002/1097-0142\(20000601\)88:11<2619::aid-cnrcr26>3.0.co;2-j](https://doi.org/10.1002/1097-0142(20000601)88:11<2619::aid-cnrcr26>3.0.co;2-j)

V. Sanna and M. Sechi, Nanoparticle therapeutics for prostate cancer treatment, *Maturitas.* 73 (2012) 27-32.

<https://doi.org/10.1016/j.maturitas.2012.01.016>.

X. Wu, J. Chen, M. Wu, J.X. Zhao, Aptamers: active targeting ligands for cancer diagnosis and therapy, *Theranostics* 5 (2015) 322-44.

<https://doi.org/10.7150/thno.10257>.

X. Yi, X. Zhang, H. Jeong, Y.M. Shin, D.H. Park, S. You, D.K. Kim, A novel bispidinone analog induces S-phase cell cycle arrest and apoptosis in HeLa human cervical carcinoma cells, *Oncol. Rep.* 33 (2015) 1526-1532.

<https://doi.org/10.3892/or.2015.3722>

Y. Shi, J. Xuea, L. Jia, Q. Dua, J. Niua, D. Zhanga, Surface-modified PLGA nanoparticles with chitosan for oral delivery of tolbutamide, *Colloids Surf. B Biointerfaces* 161 (2018) 67-72. <https://doi.org/10.1016/j.colsurfb.2017.10.037>

Z. Chen, M.F. Penet, S. Nimmagadda, C. Li, S.R. Banerjee, P.T. Winnard Jr, D. Artemov, K. Glunde, M.G. Pomper, Z.M. Bhujwalla, PSMA-targeted theranostic nanoplex for prostate cancer therapy, *ACS Nano* 6 (2012) 7752-7762.

<https://doi.org/10.1021/nn301725w>

Z. Chen, Small-molecule delivery by nanoparticles for anticancer therapy, *Trends. Mol. Med.* 16 (2010) 594-602.

<https://doi.org/10.1016/j.molmed.2010.08.001>

যাদবপুর বিশ্ববিদ্যালয়
কলকাতা-৭০০ ০৩২, ভারত



*JADAVPUR UNIVERSITY
KOLKATA-700032, INDIA

Ref. No. P-1/Rs/80/16
Date: 23.02.2016
০২.০৩.

To
Iman Ehsan,
C/o, Prof. Biswajit Mukherjee,
Pharmacy Department,
Jadavpur University
Kolkata - 700032

Dear Sir/ Madam,

I am pleased to inform you that you have been selected **PURSE FELLOW** to work in the DST PURSE -II Programme in the PHARMACEUTICAL TECHNOLOGY Department, Jadavpur University.

You will be paid a fellowship of **Rs.21,700/-** with admissible allowances as per DST rules. The tenure of your fellowship is two years from the date of joining. You are required to be present in the department on a regular basis during University hours to assist in the on-going projects of the department under DST PURSE -II Programme. The fellowship will be paid to you only on production of Attendance- cum- work certificate as per rules.

Your service will be governed by the same terms and conditions as may be applicable to the temporary staff of the University and you will be under the administrative control of the undersigned.

You are requested to join the post within ten days from the date of receipt of this letter and submit your joining report in duplicate through proper channel to the undersigned with a declaration stating that you are not a recipient of any emoluments from any other source from the date of your joining the Fellowship.

The duplicate copy of this appointment letter duly signed by you should also be submitted at the time of joining the Fellowship.

Yours faithfully,


REGISTRAR

*Established on and from 24th December, 1955 vide Notification No. 10986-Edn/TU-42/55 dated 6th December, 1955 under Jadavpur University Act, 1955 (West Bengal Act XXXIII of 1955) followed by Jadavpur University Act, 1981 (West Bengal Act XXIV of 1981)

দুরভাষ : ২৪১৪-৩৩৩৩/৩১২৪/৩৩৩৩/৩৩৩৩
দুরবার্তা : (৯১)-৩৩৩-২৪১৪-৩৩৩৩/২৪১৩-৭১২১

Website : www.jadavpur.edu
E-mail : registrar@admin.jdvu.ac.in

Phone : 2414-6666/6194/6643/6495/6443
Fax : (91)-033-2414-6414/2413-7121

যাদবপুর বিশ্ববিদ্যালয়
কলকাতা-৭০০০৩২, ভারত



*JADAVPUR UNIVERSITY
KOLKATA-700 032, INDIA

Ref. No. R-11/228/16
Date: 18.03.2016
২৪

To,
Sm. Iman Ehsan,
C/o Prof. Biswajit Mukherjee,
Pharmaceutical Technology Department,
Jadavpur University,
Kolkata -700032

Madam,

I am pleased to inform you that your post of appointment to work in the DST-PURSE- II Program in the Pharmaceutical Technology Department, Jadavpur University has been upgraded from PURSE Fellow to Junior Research Fellow, after examining the propriety of your application that your qualification entitles you to join as 'Junior Research Fellow'. Your appointment will be governed by the same terms & conditions laid down in your appointment letter No. P-1/ RS/ 80/ 16 dated.02.03.2016 with the revision of your fellowship to Rs. 25,000/= per month plus 30% HRA w.e.f. 08.03.2016.

Yours faithfully,


Registrar

*Established on and from 24th December, 1955 vide Notification No.10986-Edn/IU-42/55 dated 6th December, 1955 under Jadavpur University Act, 1955 (West Bengal Act XXXIII of 1955) followed by Jadavpur University Act,1981 (West Bengal Act XXIV of 1981)

দূরভাষ: ২৪১৪-৬৬৬৬/৩১৯৪/৬৬৪৩/৬৪৯৫/৬৪৪৩
দূরবার্তা: (৯১)-০৩৩-২৪১৪-৬৪১৪/২৪১৩-৭১২১

Website : www.jadavpur.edu
E-mail : registrar@admin.jdvv.ac.in

Phone : 2414-6666/6194/6643/6495/6443
Fax : (91)-033-2414-6414/2413-7121

पी ए बी.एक्स./PABX : 6567136, 6963980, 6962794
फैक्स/FAX : 011-6868662, 6856713, 6853292, 6566258

तार / GRAM : विज्ञानी / SCIENTIFIC
Web-site : www.icmr.nic.in
E-mail : icmrhqds@sanspd.nic.in



भारतीय आयुर्विज्ञान अनुसंधान परिषद INDIAN COUNCIL OF MEDICAL RESEARCH

वी. रामलिंगस्वामी भवन, अन्सारी नगर, पोस्ट बॉक्स 4911, नई दिल्ली - 110 029

V. RAMALINGASWAMI BHAWAN, ANSARI NAGAR, POST BOX 4911, NEW DELHI - 110 029

No. 45/41/2018-Nan/BMS

Date: 8.5.2018

To,

Dr. Biswajit Mukherjee
Professor & Head,
Deptt. of Pharmaceutical Technology,
Jadavpur University,
188, Raja SC Mallick Road,
Kolkatta-700032

Subject:- Award of Research Fellowship to **Ms. Iman Ehsan, SRF** on the Research fellowship project entitled "**Design and development of antibody conjugated biodegradable nanoparticles containing paclitaxel for the treatment of prostate cancer**"

Sir,

The Director General, ICMR sanctions Research Fellowship to **Ms. Iman Ehsan, SRF** on a stipend of **Rs. 28,000/-** p.m. to carry out research on the project mentioned above, under your guidance. H.R.A. and Medical reimbursement will be paid as per rules of your University.

The award of SRF will be subject to the following terms and condition:

TENURE: It will be tenable for one year only from the date of joining duty and will be on yearly basis subject to maximum of **three years**.

Its continuance will, however, depend on the satisfactory progress of work and can be terminated at any time on a one month's notice, if the progress is not satisfactory, or on receiving adverse report from the Guide. The Fellow will be required to work on the project for a period at least one year.

The event of his/her leaving before completing one year on the fellowship, he/she may be required to refund the stipend drawn by him/her from the date of joining to the date of leaving the fellowship.

PRIVATE PRACTICE: Private practice of any kind, or taking up any appointment even in an honorary capacity during the fellowship is not permitted.

ADMINISTRATIVE CONTROL: The candidate will be under the administrative control of the Institution where he/she works, and will also be subject to the rules and regulations of the Institute.

LEAVE: Leave will be admissible according to the rules of the Institution, however in the case of female research fellows leave without stipend upto 6 months (in lieu of maternity leave) may be granted. No other kind of leave (such as sick leave) etc. will be admissible. Awardees are not entitled to vacation normally admissible to the staff of an Institution.

HRA: HRA will only be paid, if the fellow is not availing any hostel facility. A certificate to this effect should be sent along with joining report for payment of HRA.

REPORTS: The awardee shall submit 1st annual reports for the first 10 months on the prescribed standard proforma.

The first annual report should be submitted after 10 months from the date of commencement of the fellowship giving complete factual details of the research work done through the Guide alongwith his/her appraisal. Subsequent annual report should be submitted through the Guide two months before the completion of fellowship tenure. Failure to submit reports in time may lead to termination of the award. Six copies of the final report in the prescribed form clearly shall be submitted one month before the date of termination of the award.

A list of the papers published or presented at Scientific Conferences during the tenure of the fellowship should also be furnished with the annual and final reports.

PUBLICATION OF PAPERS: Prior permission for publication of papers based on the research work done during the tenure of the award should be obtained from the Council. The paper should be sent to the Council through the Guide with his/her recommendations. Due acknowledgement to the Council should be made in these papers.

PAYMENT OF FUNDS: The stipend and the funds for contingencies shall be paid as per procedure laid down in the enclosed an annexure.

CONTINGENT EXPENDITURE: An annual contingent grant of Rs. 20000/- p.a. will be admissible. The contingent grant is given to meet petty expenditure for purchase of chemicals, reagents etc. No non-expenditure article or equipment can be purchased out of the grant.

TRAVEL:-

Traveling allowance will not be admissible for joining duty or on termination of the award.

The Council may approve tours of research fellows/associate for:-

1. **Attending symposium/seminar/conference provided the fellow/associate is presenting a paper which has been accepted by the organizers of the symposium/seminar/conference.**
2. **Field work connected with research**
3. **TA/DA would be admissible as per the rules applicable to Central Government Officers with basic pay equivalent to the amount of the fellowship stipend.**

NOTE:- The expenditure on this account will be met

POST FELLOWSHIP CARRIER:-

1. The Research Fellow can register himself/herself for postgraduate qualification and to utilize in his/her the work done by him/her during his/her fellowship tenure. A copy of these submitted for postgraduate degree will have to be sent to the Council for information and record **from the contingent grant sanctioned to the fellow**. Due acknowledgement to the ICMR should be made in the thesis by the research fellows.
2. The Research Fellow should also send to the Council for information a brief report on the post/job taken by him/her after the expiry of the fellowship.

The date indication forenoon/afternoon on which he/she the fellowship may please be intimated to this office. He/she may be asked to report for duty within a month from the date of issue of this letter failing which the award will be treated as cancelled.

Yours faithfully,

(G.S.Sandhu)
Administrative Officer
For Director-General

1. Copy to :- (i) Head of the Institution, The Registrar, Jadavpur University, 188, Raja SC Mallick Road, Kolkatta-700032
2. Ms. Iman Ehsan, SRF, Deptt. of Pharmaceutical Technology, Jadavpur University, 188, Raja SC Mallick Road, Kolkatta-700032
2. Accounts Section – V, ICMR
3. IRIS Cell No. 2017-3968


Administrative Officer
For Director-General



Institutional Animal Ethics Committee (IAEC)

Department of Pharmaceutical Technology

Jadavpur University

Kolkata-700032

Ref No: AEC/PHARM/1702/24/2017

This is to certify that Project title **“Design and development of antibody conjugated biodegradable nanoparticles containing Paclitaxel for the treatment of prostate cancer”** has been approved by the IAEC

Prof. (Dr.) Biswajit Mukherjee


Dr. Kuladip Jana


Name of the Chairman/ Member Secretary IAEC:

Name of the CPSCEA nominee

Chairman/Member Secretary of IAEC

CPSCEA nominee


Signature with date 01/16/2017


Signature with date

Chairman
Institutional Animal Ethics Committee
Jadavpur University
Kolkata-700032



J591 functionalized paclitaxel-loaded PLGA nanoparticles successfully inhibited PSMA overexpressing LNCaP cells

Iman Ehsan^a, Leena Kumari^{a,1}, Ramkrishna Sen^{a,1}, Ashique Al Hoque^a, Biswajit Mukherjee^{a,*}, Alankar Mukherjee^a, Prasanta Ghosh^a, Sanchari Bhattacharya^b

^a Department of Pharmaceutical Technology, Jadavpur University, Kolkata, India

^b Guru Nanak Institute of Pharmaceutical Science and Technology, Panihati, Kolkata, India

ARTICLE INFO

Keywords:

Poly(lactide-co-glycolide) nanoparticles
Paclitaxel
Surface modification
Prostate-specific membrane antigen (PSMA)
Prostate cancer

ABSTRACT

To evaluate the chemotherapeutic efficacy of J591 fabricated poly(D,L)-lactic-co-glycolic acid (PLGA) nanoparticles containing paclitaxel (Ab-PTX-NP) *in vitro* in PSMA (prostate specific membrane antigen) expressing prostate cancer cells, increase the solubility, bioavailability, circulation time, and limit systemic toxicity to achieve the maximum curative effect accompanied by controlled dosing, we formulated Ab-PTX-NP. Physico-chemical characterizations such as Field emission scanning electron microscopy, Transmission electron microscopy, and Atomic force microscopy revealed that the particles were smooth-surfaced, with homogeneous distribution of drug within the particles and size were in the nano range. The encapsulation efficiency of Ab-PTX-NP was found to be 70.85%. This study acknowledges the effectiveness of Ab-PTX-NP *in vitro*, which displays elevated cellular cytotoxicity and internalization, maximum apoptosis (74.1%) in PSMA-abundant LNCaP cells, in comparison to PSMA negative PC3 cells. Pharmacokinetic data revealed the bioavailability of paclitaxel upon i.v. administration in the systemic circulation of male Balb/c mice. Herein, J591 was maneuvered in a neoteric way to carry the prepared chemotherapeutic nanoparticles directly to the affected prostate cancer cells.

1. Introduction

Prostate cancer is a common and recurrent cancer type in males globally, with a growing incidence of mortality [1]. International management of prostate cancer is still obscure and remains a global challenge to manage in spite of our perceptive of its biology and growth regulation. Recent treatments include surgical elimination of the prostate, radiation and androgen ablation (early stage), and chemotherapy (secondary treatment). Normally, androgen regulates the prostate and most of its malignancies, development, growth, and function [2,3]. Our study will utilize the ubiquitous overexpression of the prostate-specific membrane-antigen PSMA on cancerous prostate cells. PSMA plays an imperative role in diagnosis, managing as well as treating prostate cancer. The aggrandized PSMA glutamate carboxypeptidase II, having a molecular weight of about 100 kDa, is enhanced and progressively elevated in prostate adenocarcinoma and in the neovasculature of solid tumors and positively correlates with tumor progression or metastasis in prostate cancer tissue, thus, differentiating benign tumors from

malignant disease [4,5]. More crucially, the presence of internalization motif in the cytoplasmic tail of PSMA might suggest that the ligand-attached nanotherapeutics may get internalised into the cell [6].

J591, an anti-PSMA monoclonal antibody (Ab), has already been developed to target PSMA and has been demonstrated in cellular internalization [7,8]. The absence of the majority of extra-prostatic expression of PSMA on normal vasculature endothelium makes it target-specific. Paclitaxel (PTX) is the best microtubule stabilized drug licensed by the United States Food and Drug Administration (USFDA) for the therapeutic treatment of a range of malignancies, including prostate cancer. PTX inhibits mitosis and is effective in eradicating cancer cells during the interphase of the cell cycle [9]. It can be hypothesized that delivering paclitaxel (PTX) as a chemotherapeutic payload by encapsulating it in a designed PLGA (USFDA approved biodegradable polymer for human use by i.v. route) nanoparticle (PTX-NP), and further conjugating it with J591 Ab (Ab-PTX-NP), aids in the higher cellular internalization of PTX to PSMA expressed prostate cancer cells.

Elevated cellular uptake of PTX by the prostate cancer cells was

* Corresponding author. Department of Pharmaceutical Technology, Jadavpur University, Kolkata, 700032, India.

E-mail address: biswajit.mukherjee@jadavpuruniversity.in (B. Mukherjee).

¹ shares equal authorship.

possible by using the extracellular apical domain of PSMA, which contains binding site for humanized J591 Ab, enabling it as a plausible target, and it may hold potential promise for tumor targeting. Owing to the peculiar pathophysiological features of most solid tumors, such as deficient vasculature and limited lymphatic drainage, PTX-NP helps in overcoming the hydrophobic nature and adverse outcomes such as nephrotoxicity and neurotoxicity, as well as other problems associated with PTX chemotherapy, with a simultaneous enhancement of permeability and retention (EPR) effect [10,11]. Nanoparticles (NPs) enable drugs to release in sustained pattern along with protection of the encased agent from enzymatic degradation, and also prolong pharmacological action, thereby elevating the dose tolerance and minimizing nonspecific drug absorption-associated toxicity to improve safety and efficacy [12,13]. The putative ligand conjugation prevents NPs to cross the blood brain-barrier, consequently, averting any non-selective actions on the central nervous system that results in increased targeting and bioavailability to the affected cells [14]. The current goal of the investigation was to target PSMA positive (+ve) LNCaP cells with J591 conjugated nanoparticles containing paclitaxel. It appraised the selectivity of Ab-PTX-NP to PSMA (+ve) prostate cancer cells, its cellular internalization, and drug related apoptotic activity in those cells. Further, pharmacokinetic assessment of the formulation was conducted in Balb/c mice. J591 has been widely used for imaging [15]. However, in our study, it has been utilized as a ligand, which when conjugated to the drug loaded nanoparticle can be utilized for advanced prostate chemotherapy.

2. Materials and methods

2.1. Materials

Paclitaxel (PTX) with 99.95% purity, commercial formulation (CF) was obtained from Fresenius Kabi Oncology Ltd., Kolkata, India. Acid-terminated PLGA {poly (lactide-coglycolide) ratio 75:25, MW 4000–15,000}, D- α -tocopherol polyethylene glycol succinate (TPGS), Fluorescein isothiocyanate (FITC) were procured from Sigma-Aldrich Co., St Louis, MO, USA. The anti-PSMA J591 monoclonal antibody (J591 Ab) was procured from Dr. Neil Bhandar, San Diego, California, United States. Two different human prostate carcinoma cells, (+ve PSMA) LNCaP cells, (-ve PSMA) PC3 cells were obtained from the National Centre for Cell Sciences, Pune, India. Balb/c male mice were obtained from the National Institute of Nutrition, Hyderabad, India (refer Supplementary material).

2.2. Fourier-transform infrared (FTIR) spectroscopy

To detect possible interactions between PTX and the excipients used for the preparation of PTX-NP were detected via infrared spectra (FTIR spectroscopy), (refer Supplementary material) [16].

2.3. Physicochemical characterization of PTX-NP and Ab-PTX-NP

Paclitaxel encapsulated biodegradable PLGA nanoparticles (PTX-NP) and FITC labeled PTX-NP were prepared by multiple emulsion solvent evaporation method [17,18]. The nanoparticle surface was fabricated with J591 Ab using 1-(3-dimethylaminopropyl)-3-ethylcarbodiimide hydrochloride (EDC) and N-hydroxysuccinimide (NHS) [18–20]. Detailed methodologies related to the preparation, optimization, conjugation, and physicochemical characterizations such as drug loading, particle morphology by Scanning electron microscopy, Transmission electron microscopy, Atomic force microscopy, of the prepared nanoparticles are mentioned in the Supplementary material.

2.4. Energy dispersive X-ray assay (EDX)

It ensures the elemental composition and encapsulation of the drug

in PTX-NP and Ab-PTX-NP [21] (Refer to Supplementary material for details).

2.5. Sodium dodecyl sulfate-polyacrylamide gel electrophoresis (SDS-PAGE)

To confirm the conjugation of antibodies on the surface of PTX-NP, investigation was conducted on SDS-PAGE [22,23] (Details are available in supplementary material).

2.6. In vitro drug release analysis

Evaluation pattern of the drug released from the commercial formulation (CF), PTX suspension, PTX-NP, and Ab-PTX-NP *in vitro* in phosphate buffer saline (PBS, pH 7.4) with 0.1% tween 80 was studied [24]. Further, the release pattern of PTX from Ab-PTX-NP in various buffers of varying pH for duration of 90 days was studied and calculated in the cumulative drug release method [18,25] (Details are given in Supplementary material).

2.7. Stability study

Weighed amounts of PTX-NP and Ab-PTX-NP were stored at different temperatures with variable relative humidities to assess the impact of it, on the nanoparticles. They were stored in a refrigerator (zone III) at 4–8 °C, and at 30 °C, and 40 °C with a relative humidity of 75% for 1, 2, and 3 months following the International Council for Harmonization (ICH, 2003) guidelines and were analyzed for the drug content and morphology at the mentioned time points.

The hydrolytic stability of PTX-NP and Ab-PTX-NP was ascertained in various buffers of different pH for 30 days (refer to Supplementary material for details).

2.8. Cell viability assay

Human prostate carcinoma cells, LNCaP cells, overexpress PSMA (PSMA + ve cells) while PC3 lacks the expression of PSMA (PSMA –ve cells). Same numbers of cells were seeded and the study was conducted for 24h. MTT assay more accurately determines alteration of cell number. The growth rate of the cells does not differ significantly. It measures the number of viable cells in the culture. Upon investigations for a short span of time (as 24 h for present study), the cell sizes are not accountable in the MTT assay, and the cell size does not interfere in the assay results [26]. Several reports [27–32] also suggest that same number of different prostate cancer cells (LNCaP, DU145, LAPC4, and PC3) were seeded in respective studies. The time-dependent cytotoxic effect of PTX, PTX-NP, Ab-PTX-NP, and Ab-BNP on LNCaP cells and PC3 cells was determined for a period of 24 h using MTT dye [33,34] (Supplementary material for detailed methodology). Cell viability assay was done on normal human kidney cells HEK 293, since the human normal prostate cell line such as RWPE-1 was not available in the pandemic situation. The study was conducted on human normal embryonic kidney cell line (HEK 293) to evaluate the effect of the experimental formulation treatment on any normal cell line. HEK 293 cells are one of the most common cell lines used for research purposes due to their easy maintenance, robustness and reliable growth [35,36]. Besides, the cells are also frequently used as a control in many studies to investigate the effects of treatments on cancer-specific cell lines [37].

2.9. PSMA expression of LNCaP/PC3 cells by Western blot

To enquire the expression of PSMA on LNCaP and PC3 cell lines, Western blot analysis was performed as per protocol available [38] (Supplementary material).

2.10. Cellular uptake study of PC3 and LNCaP cells in vitro

In vitro cellular uptake of FITC- labeled PTX-NP and Ab-PTX-NP was investigated in LNCaP and PC3 cells. The uptake was quantified at 0.5, 2 and, 4 h with a flow-cytometer. The qualitative uptake of the above formulations was investigated by confocal laser microscopy in LNCaP and PC3 cells at 4 h [39] (Supplementary material).

2.11. Induction of cell death by acridine orange/ethidium bromide dual staining

The induction of cell death by PTX/PTX-NP/Ab-PTX-NP was detected in confocal laser microscopy in LNCaP and PC3 cells with IC₅₀ concentration of experimental formulations at 24 h. The total fluorescence intensity of each treatment was calculated using ImageJ software, and plotted [40,41].

2.12. Mitochondrial membrane depolarization analysis using JC-1

Variation in the transmembrane potential difference was done using 5,5',6,6'-tetrachloro-1,1',3,3'-tetraethylbenzimidazolyl-carbocyanine iodide (JC-1) and analyzed by flow cytometer [40].

2.13. Apoptosis analysis

Annexin V-FITC/PI (propidium iodide) dual staining was performed to quantify cancer cells upon various treatments to determine the capability of PTX, PTX-NP, and Ab-PTX-NP to activate apoptosis or necrosis in LNCaP and PC3 cells [34,42].

2.14. Nuclear morphology analysis by DAPI (4',6-diamidino-2-phenylindole) staining

LNCaP and PC3 cells were imaged to visualize the apoptotic outcome on the cell morphology after staining with DAPI after treating them with PTX, PTX-NP, and Ab-PTX-NP with their respective IC₅₀ dose for 24 h [43]. The cells were imaged under a confocal laser scanning microscope [44,45].

2.15. Hemolysis analysis

Fresh blood samples from male Balb/c mice were collected in heparinized tubes and the experiment was conducted [44,46,47] (for details please see the Supplementary material).

2.16. Pharmacokinetic study by LC-MS/MS method

The blood was collected from the tail vein of male Balb/c mice (body weight: 25–30 g) and plasma was separated following the experimental treatment. Animals were divided into four groups (each contained 36 mice). At each time point, three animals of each group have been sacrificed. The first group of animals received PTX suspension, the second group received PTX-NP, and the third group of animals received Ab-PTX-NP. The fourth group of animals served as a control group and did not receive any treatment. This study was conducted to compare the bioavailability of paclitaxel upon i.v. bolus administration of the experimental formulations (equivalent to paclitaxel, dose 10 mg/kg body weight) at predetermined time points (0.25, 0.5, 1, 2, 4, 6, 8, 10, 24, 48, 72, and 96 h) post drug administration. The drug content was analyzed by tandem liquid chromatography and mass spectrophotometry (LC-MS/MS) where docetaxel was used as an internal standard. [18, 48] (Supplementary material).

2.17. Statistical analysis

All the data of the experiments are demonstrated as mean \pm standard

deviation (SD). One way analysis of variance (ANOVA) was used, followed by Tukey's test conducted for comparison between the experimental groups. A statistical level of significance of $P < 0.05$ was used.

3. Results

3.1. Fourier-transform infrared (FTIR) spectroscopy

The FTIR spectroscopic investigation unfolded all the characteristic peaks of PTX and the excipients utilized for PTX-NP and depicted no chemical interactions between them (Supplementary Fig. S1). Pure PTX showed peaks of N–H stretching at 3440 cm⁻¹ and asymmetric and symmetric vibrations at 2944 cm⁻¹ for CH₂. The peaks at 1720 cm⁻¹, 1246 cm⁻¹, 1072 cm⁻¹ were observed due to C=O stretching vibrations of the ester group, C=N (imine) stretching, and C=O stretching vibrations, respectively. For C–H in-plane and C–H out-of-plane C–C=O, the peaks were observed at 980 cm⁻¹ and 710 cm⁻¹, respectively. PLGA displayed characteristic peaks of O–H at 3508 cm⁻¹; C–H at 2998 cm⁻¹ and C=O at 1754 cm⁻¹, respectively. The characteristic PVA peaks were observed at 3450 cm⁻¹ with O–H, 2930 cm⁻¹ with C–H, 1738 cm⁻¹, and 1096 cm⁻¹ with C=O stretching vibrations. The physical mixture of PTX-NP and blank formulation shows the signature bands of PVA and PLGA and the absence of PTX, indicating no free drug molecule on the nanoparticle surface. The spherical shape of the nanoparticles might be attributed to physical interactions resulting in minimal peak shifts due to the influence of some weak physicochemical interactions, such as the formation of weak H-bonds, van der Waals attraction force, dipole-dipole interference, etc.

3.2. Physicochemical characterization of prepared nanoparticles

Initially, various paclitaxel loaded nanoparticulate formulations were developed. The formulation (PTX-NP) was optimized after varying different solubilizers such as TPGS, Tween 80, Pluronic-127 and Pluronic-68 with PVA (2.5% w/v). The optimized formulation enhanced the solubility of the PTX, ensued by conjugating with J591 Ab as the ligand attached on the surface of the optimized PTX-NP to obtain Ab-PTX-NP. Therapeutic efficiency such as drug loading is a prerequisite that dictates the amount of formulation to be administered. The drug loading of the optimized formulation without antibody conjugation, designated here as PTX-NP, was found to be 6.96% \pm 0.19% and the encapsulation efficiency as 76.61% \pm 2.09%, respectively. In the case of Ab-PTX-NP, it was found to be 6.44% \pm 0.75%, and its encapsulation efficiency as 70.85% \pm 0.83% (Table 1). The average particle size found with Zetasizer for PTX-NP was 221 nm, while the size increased slightly after antibody conjugation, unveiling the particle size as 295 nm for Ab-PTX-NP (Fig. 1A and B). The values of polydispersity index (PI) of 0.554 \pm 0.06 and 0.512 \pm 0.014 were obtained for PTX-NP and Ab-PTX-NP, respectively (Table 1). The zeta potential of PTX-NP and Ab-PTX-NP was -20 mV and -13.5 mV respectively, (Supplementary Figs. S2A and B). The surface morphology of PTX-NP and Ab-PTX-NP analyzed via FESEM images (Fig. 1C and D) confirmed that the particles were in the nano range and thickly distributed. The drug was homogeneously distributed within the nanoparticle, which was confirmed by TEM analysis (Fig. 1E and F) for both PTX-NP and Ab-PTX-NP without any notable difference. The three dimensional AFM images of PTX-NP and Ab-PTX-NP (Fig. 1G and H) assured the smooth surface of the spherical nanoparticles in a close packed array, distinguished, narrow size distribution with structural integrity without any significant difference between the two formulations.

3.3. Energy dispersive X-ray assay (EDX)

EDX was performed to confirm the elemental composition of the PTX-NP and Ab-PTX-NP, which revealed the weight as well as the atomic percentage of carbon, oxygen, nitrogen, and sulphur. The

Table 1

Composition of optimized experimental nanoparticles with PLGA: drug at the ratio 10:1 along with particle size data, zeta potential, drug loading and encapsulation efficiency.

Formulation	Stabilizer/Solubilizer used	Particle size (Z-average) (nm) ^a	Zeta potential (mV) ^a	Polydispersity index ^a	Drug loading (%) ^a	Encapsulation efficiency (%) ^a
PTX-NP (optimized formulation)	PVA (2.5% w/v) & TPGS (0.03% w/v)	221 ± 1.2	-20 ± 1.6	0.554 ± 0.060	6.96% ± 0.19%	76.71% ± 2.09%
Ab-PTX-NP (optimized formulation with antibody conjugation)	PVA (2.5% w/v) & TPGS (0.03%w/v)	295 ± 0.18	-13.5 ± 3.3	0.512 ± 0.014	6.44% ± 0.75%	70.85% ± 0.83%
PTX-NP1	PVA (2.5% w/v) & Tween 80 (14% v/v)	349.2 ± 26	-8.39 ± 2.9	0.120 ± 0.011	5.19% ± 0.11%	57.09% ± 1.22%
PTX-NP2	PVA (2.5% w/v) & Pluronic-127 (0.5% w/v)	409.1 ± 18	-5.46 ± 2.3	0.181 ± 0.03	5.06% ± 0.05%	55.73% ± 0.50%
PTX-NP3	PVA (2.5% w/v) & Pluronic-68 (0.5% w/v)	418.4 ± 33	-4.97 ± 0.07	0.305 ± 0.039	4.72% ± 0.07%	51.92% ± 0.78%

NB: PTX-NP, PLGA nanoparticle loaded with paclitaxel; Ab-PTX-NP, Antibody conjugated PLGA nanoparticle loaded with paclitaxel; PLGA, poly (lactide-co-glycolide); PVA, poly vinyl alcohol; TPGS, D - α -tocopherol polyethylene glycol succinate.

^a Each value represents mean ± SD (n = 3).

presence of nitrogen in PTX is shown in PTX-NP and Ab-PTX-NP, thus it can be presumed that the nanoparticles were encapsulated with paclitaxel, and the lack of nitrogen in blank nanoparticles advocates the absence of paclitaxel in them, respectively (Supplementary Table S1).

3.4. SDS-PAGE

The SDS-PAGE was carried for PTX-NP and Ab-PTX-NP and compared with J591 Ab which demonstrated that the integrity of J591 Ab was ensured in Ab-PTX-NP after conjugation (Fig. 2G). Furthermore, nanoparticles were conjugated well with the antibody, and the antibody-conjugated particles ran comparatively slowly.

3.5. In vitro drug release analysis

The PTX release profiles from paclitaxel suspension (PS), commercial formulation of PTX (CF), Ab-PTX-NP, and PTX-NP were studied for 90 days (Fig. 2A). The release profile of PTX from unconjugated PTX-NP followed a similar middling pattern to its release from Ab-PTX-NP. A variable drug release of 74.56% ± 2.35% and 68.83% ± 3.07% was depicted from PTX-NP and Ab-PTX-NP, respectively, in phosphate buffer saline (pH 7.4) with 0.1% w/v of tween 80 that imitates the minimally alkaline environment of the blood.

Hence, further drug release of PTX from our decider nanoparticles Ab-PTX-NP for 90 days in various buffers of varying pH was studied cumulatively (Fig. 2B). It was observed that the release of PTX from Ab-PTX-NP was increased in lower pH media, i.e. PTX release in citrate buffer (pH 3) was rapid 96.56% ± 1.02%. The release of PTX in acetate buffer (pH 5) was 92.43% ± 1.81%, which might assert steady, and prolonged drug distribution in the acidic environment of tumor cells (pH around 4.5–5.5). The release was lower in the bicarbonate buffer 29.30% ± 1.43% medium (pH 10). It was noted that in different buffers utilized to examine the release of Ab-PTX-NP, an initial burst release for 24 h was manifested, subsequently releasing the drug in sustained manner for 90 days (period of the current study). PTX-NP delineated stability in mouse serum for at least 24 h in our previous studies [49]. PLGA nanoparticle-stability in serum condition (100% Fetal Bovine Serum) was seen in the present study. It can be summarized that in various pH media, the stability of PLGA nanoparticles was variably maintained during the study period.

Different kinetic models were used to assess drug release kinetic data. Various regression coefficient (R^2) data showed that the PTX release for both PTX-NP and Ab-PTX-NP in PBS (pH 7.4) with 0.1% w/v tween 80 complied with Korsmeyer-Peppas kinetics It depicted good linearity ($R^2 = 0.9179$) and the release exponent (n) value of the drug was 0.21 for PTX-NP, while for Ab-PTX-NP it was ($R^2 = 0.9185$) and n

value 0.18, suggesting release by Fickian diffusion [50]. PTX release from Ab-PTX-NP in acetate buffer, bicarbonate buffer, and citrate buffer also followed Korsmeyer-Peppas kinetic model, suggesting diffusion release pattern of paclitaxel with the erosion of the matrix from Ab-PTX-NP (Table 2).

3.6. Stability study

Physicochemical and morphological characteristics of PTX-NP and Ab-PTX-NP stored at 4–8 °C remained unchanged, while at 30 °C and 40 °C, PTX-NP and Ab-PTX-NP retained its PTX content but spherical morphology was distorted, when kept for 90 days (3 months). Studies on the stability requirements of these samples were performed and drug assay (drug content analysis) where drug content remained nearly unchanged (6.3–6.8%) (Supplementary Table S2).

3.7. Hydrolytic stability study

The hydrolytic stability study for 4 weeks revealed an increment of weight loss with a lowering of pH. Different pH buffers yielded the mass loss of Ab-PTX-NP as 14.53% ± 1.33% at pH 10, 25.73% ± 1.55% at pH 7.8, 35.83% ± 1.61% at pH 5 and 56.97% ± 1.55% at pH 3, respectively (Supplementary Fig. S4). The Ab-PTX-NP displayed a weight loss of 3.1% ± 0.15% after 24 h in mouse serum (pH 7.3) at 24h.

3.8. Cell viability assay

In vitro cytotoxic potential of PTX, PTX-NP, and Ab-PTX-NP determined by MTT assay shows that the Ab-PTX-NP lowest IC₅₀ doses, exhibited the highest cytotoxicity toward LNCaP cells (+PSMA) than in PC3 (-PSMA), as portrayed in Fig. 2C and D. Reports prior to this study highlight that PTX effectively reduces cell viability and controls proliferation of LNCaP and PC3 cell lines [51]. At different concentrations (0–60 μ M) taken for 24 h (Supplementary Table S3), the IC₅₀ values of PTX-NP and Ab-PTX-NP revealed as 20.6 μ M and 7.8 μ M which were evidently much less than the IC₅₀ value of PTX (27.2 μ M) in LNCaP cells. A narrow difference in the IC₅₀ values of PTX-NP and Ab-PTX-NP (22.9 μ M and 21.3 μ M) may be due to the lack of PSMA, in PC3 cells. The Ab-BNP (antibody conjugated nanoparticle without containing any drug) on investigation yielded the antibody concentration as non toxic to prostate cancer cells. Ab-PTX-NP showed negligible antiproliferative activity in normal kidney cells, HEK 293. Since it showed no toxic manifestation in HEK 293, we may assume that Ab-PTX-NP possibly has less or negligible toxicity towards other normal cells also (Supplementary Table S4).

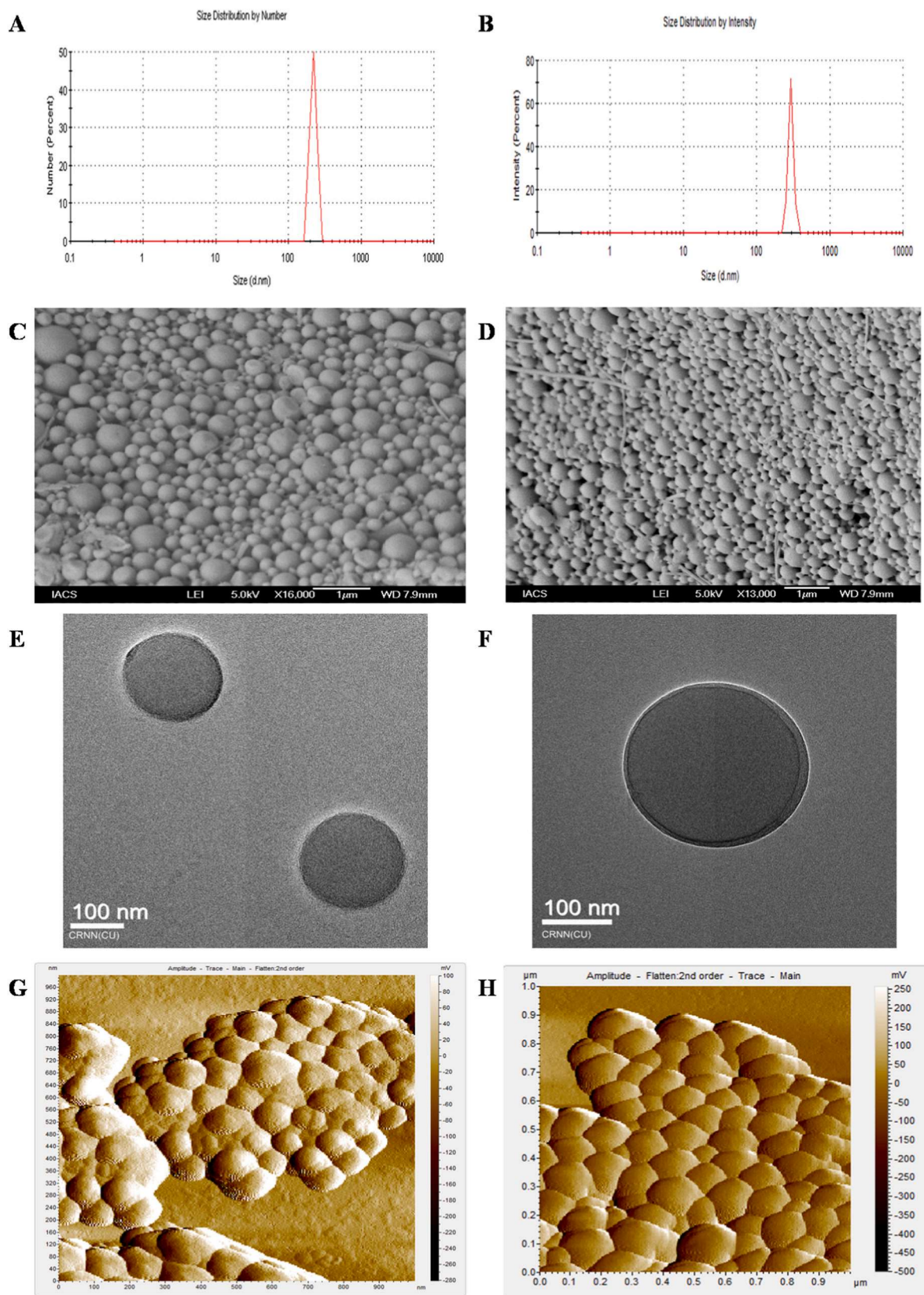


Fig. 1. Average particle size distribution of (A) PTX-NP (B) Ab-PTX-NP; Field emission scanning electron microscopy (C) PTX-NP at 16,000 × magnification (D) Ab-PTX-NP at 13,000 × magnification; Transmission electron microscopy (E) PTX-NP (F) Ab-PTX-NP; Atomic force microscopy (G) PTX-NP and (H) Ab-PTX-NP.

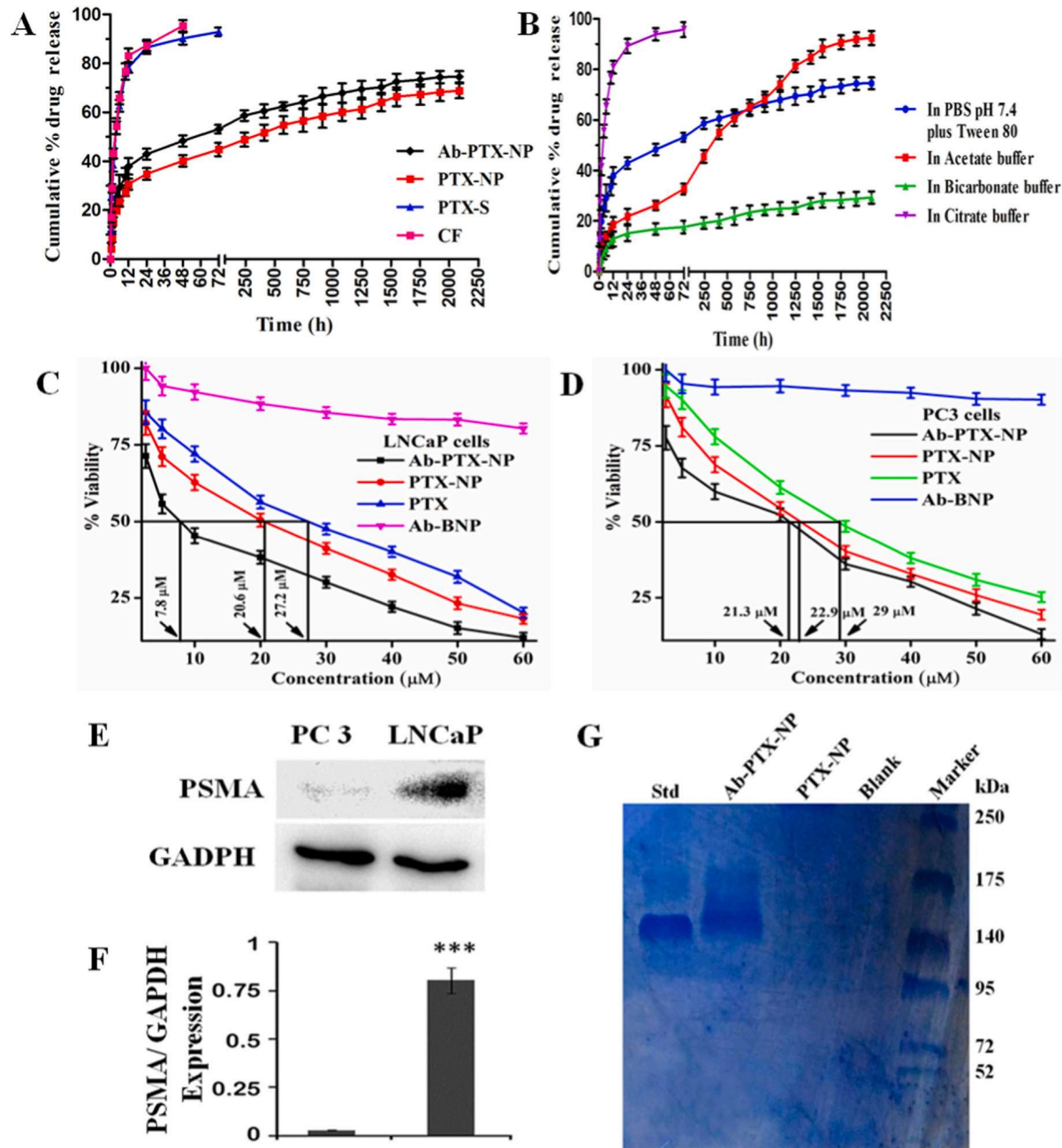


Fig. 2. *In vitro* drug release profile of (A) experimental formulations in phosphate buffer saline (pH 7.4) with 0.1% w/v tween 80 (B) Ab-PTX-NP in different pH (pH 3, 5, 7.4 and 10) media. *In vitro* cytotoxicity of PTX, PTX-NP, Ab-PTX-NP and Ab-BNP was determined in (C) LNCaP and (D) PC3 cells. PSMA expression (E) in LNCaP and PC3 cells detected by Western blot (F) PSMA to GAPDH ratio was shown graphically (G) SDS-PAGE gel electrophoresis, Lane 1 in the SDS-PAGE gel showed the standard anti PSMA monoclonal antibody Ab (J591), lane 2 represents for Antibody conjugated PTX-NP, and lane 3 shows PAGE run of unconjugated NP followed by Blank in lane 4, and then the protein marker in lane 5. NB: PTX, Paclitaxel; NP, nanoparticle; Ab, J591 antibody; BNP blank nanoparticles. Each value in the graphical presentation represents mean \pm SD (n = 3). *** Statistical significance of PC3 when compared with LNCaP is $p < 0.001$.

3.9. PSMA expression of LNCaP/PC3 cells by Western blot

The analysis was done to examine the expression of PSMA in LNCaP (+ve PSMA), and PC3 (-ve PSMA) cells. The results determined that LNCaP cells were found to have the highest level of expression of PSMA, whereas, PC3 cells exhibited no apparent PSMA expression (Fig. 2E and F).

3.10. Cellular uptake study on PC3 and LNCaP cells *in vitro*

LNCaP (+ve PSMA) and PC3 (-ve PSMA) cells were used to detect the

uptake of FITC tagged PTX-NP/Ab-PTX-NP. The cellular uptake quantified by flow cytometry revealed a steady increase in median fluorescence intensity in LNCaP cells as compared to PC3 and untreated cells with increasing time (Fig. 3A and C). FITC mean median values in LNCaP cells for PTX-NP were 587, 1328, and 2780, and for Ab-PTX-NP were 1322, 2471, and 3818 at the time intervals 0.5, 2, and 4 h, respectively.

In LNCaP cells, the FITC mean-median values indicate the cellular uptake of experimental nanoparticles in the sequence of Ab-PTX-NP > PTX-NP > PTX. While in PC3 cells at the same time intervals, the cellular internalization was much lower for both PTX-NP and Ab-PTX-NP,

Table 2

In vitro drug release kinetic equations tested on different release kinetic models along with corresponding R² values and release exponent (n) (Korsmeyer–Peppas model).

Kinetic models	Ab-PTX-NP in Phosphate buffer saline pH 7.4 (with 0.1% tween 80)	Ab-PTX-NP in Citrate buffer	Ab-PTX-NP in Acetate buffer	Ab-PTX-NP in Bicarbonate buffer	PTX-NP in Phosphate buffer saline pH 7.4 (with 0.1% tween 80)
Zero order	y = 0.026x + 32.946 R ² = 0.6334	y = 0.2626x + 52.126 R ² = 0.2804	y = 0.0436x + 19.109 R ² = 0.8823	y = 0.0111x + 10.601 R ² = 0.7194	y = 0.0257x + 26.689 R ² = 0.6951
First order	y = 0.0002x + 1.8123 R ² = 0.78	y = 0.0056x + 1.5595 R ² = 0.5395	y = 0.0005x + 1.9309 R ² = 0.9878	y = 6E-05x + 1.9504 R ² = 0.7588	y = 0.0002x + 1.8576 R ² = 0.8182
Higuchi model	y = 1.2664x + 25.344 R ² = 0.7976	y = 5.7801x + 37.223 R ² = 0.5591	y = 1.8066x + 15.394 R ² = 0.9442	y = 0.5249x + 7.6348 R ² = 0.8572	y = 1.2283x + 19.569 R ² = 0.8473
Korsmeyer–Peppas model	y = 0.1831x + 1.2968 R ² = 0.9185 n = 0.18	y = 0.2216x + 1.5847 R ² = 0.7956 n = 0.22	y = 0.3499x + 0.825 R ² = 0.99 n = 0.34	y = 0.228x + 0.7338 R ² = 0.8943 n = 0.22	y = 0.2122x + 1.1616 R ² = 0.9179 n = 0.21
Hixson–Crowell model	y = 0.0007x + 0.6091 R ² = 0.7326	y = 0.0108x + 1.2137 R ² = 0.4403	y = 0.0013x + 0.2878 R ² = 0.9691	y = 0.0002x + 0.1723 R ² = 0.7458	y = 0.0006x + 0.4734 R ² = 0.779

respectively.

The quantitative cellular uptake study of FITC labeled PTX-NP and Ab-PTX-NP was backed up by qualitative confocal microscopy images of LNCaP (Fig. 3B), and PC3 (Fig. 3D) treated with FITC labeled PTX-NP/Ab-PTX-NP, which revealed time dependent internalization of the experimental formulations within the cancerous cells at 4h, respectively. The data suggest maximum internalization of Ab-PTX-NP in LNCaP cells, probably due to maximum affinity of J591 for PSMA, showing site specific potential of J591 antibody in PSMA positive LNCaP cells. Since the objectives were fulfilled by the study, it was not further extended beyond 4h. However, If the cellular uptake continues after 4 h, cellular uptake may increase with time till the duration, the receptors on the cells are saturated by the antibody of Ab-PTX-NP. It further results in a constant plateau of cellular drug concentration.

3.11. Induction of cell death by acridine orange/ethidium bromide (AO/EB) dual staining

The apoptosis-induced morphological alterations in prostate cancer cells, treated with the respective IC₅₀ value of PTX, PTX-NP, and Ab-PTX-NP for 24h, were observed upon double staining with AO/EB in LNCaP and PC3 cells. The data showed that differential values of uptake of acridine orange and ethidium bromide by live and apoptotic cells were observed (Fig. 4). The control cells appeared green with normal nucleus structure, which indicates its healthy condition. Acridine orange (AO) was taken up by live cells while ethidium bromide (EB) was used by apoptotic cells because of the loss of integrity of the cellular membrane. The nuclei of LNCaP cells when treated with Ab-PTX-NP appeared dark orange to red with condensed or fragmented chromatin due to the major internalization of EB (increased endocytosis leading to apoptosis). Measuring total fluorescence intensity in LNCaP and PC3 revealed conformity with the images in our findings. As a result of apoptosis/necrosis, the reduction in cells via cell counting was observed more in LNCaP as compared with PC3 cells when treated with PTX-NP/Ab-PTX-NP (Supplementary Fig. S5).

3.12. Mitochondrial membrane depolarization analysis

The loss and alteration of mitochondrial membrane potential, which is a prerequisite phenomenon of apoptosis, can be quantified by increased monomer/aggregate ratio (green/red ratio), which was observed with the highest percentage of cells with depolarized mitochondria upon Ab-PTX-NP treatment. Results (mitochondrial depolarization) yielded 34.1% for PTX-NP and 45.6% for Ab-PTX-NP, respectively, while only 13.8% for the free drug. Further, PTX-NP/Ab-PTX-NP treatment for 24 h showed lower and marginalized apoptosis

in PC3 cancerous cells on treatment with the IC₅₀ concentration of the experimental formulations (Fig. 5A).

3.13. Apoptosis study

Annexin V-FITC/PI staining, annexin V bound with phosphatidylserine quantitatively detected the variable induction of apoptosis when LNCaP cells were treated with PTX/PTX-NP/Ab-PTX-NP (Fig. 5B). The percentage of apoptotic cells was 48.6% for PTX-NP, and 74.1% for Ab-PTX-NP while for free PTX it was 21% in 24 h. Similar treatment on PC3 cells showed the lower apoptotic value with the experimental formulations. Thus, Ab-PTX-NP indicated better efficacy in LNCaP cells.

3.14. Nuclear morphology analysis

DAPI staining revealed pronounced morphological changes due to apoptotic body formation in Ab-PTX-NP treated LNCaP (+ve PSMA) cells when studied for both the types of prostate cancer cells (Fig. 5C).

3.15. Hemolysis study

The hemo-compatibility of PTX, PTX-NP, and Ab-PTX-NP at different concentration range (2.5–100 μM) showed minimal erythrocyte damage and negligible hemolytic activity in PTX-NP and Ab-PTX-NP containing PTX (below 50 μM) as shown in Fig. 6A. Elevated concentration ranging from 50 to 100 μM resulted in consequential rise in hemolysis. Thus, Ab-PTX-NP can be rendered safe for intravenous administration as the hemolysis rate of the desired formulation was within the permissible range of 5% that is considered safe critical value for biomaterials by the International Organization for Standardization/Technical report (ISO/TR 7406.46) [47,52].

3.16. Pharmacokinetic study by LC-MS/MS method

The plasma concentration profiles of PTX (free drug), PTX-NP, and Ab-PTX-NP were plotted on the graph (Fig. 6B) and the values of different pharmacokinetic parameters depicted in Table 3, showed that Ab-PTX-NP maintained steady plasma PTX concentration till 96 h of the study with a notably longer and increased half life of the drug, mean residence time (MRT_{inf}), marked 3–4 fold increase in AUC_{last} and AUC_{inf} of the drug from Ab-PTX-NP as compared to those of PTX-NP and PTX. Drug was released from the surface of the engineered Ab-PTX-NP initially. Further, the drug release was steady for a longer span of time and showed much higher PTX availability in plasma following a single i. v. injection of Ab-PTX-NP.

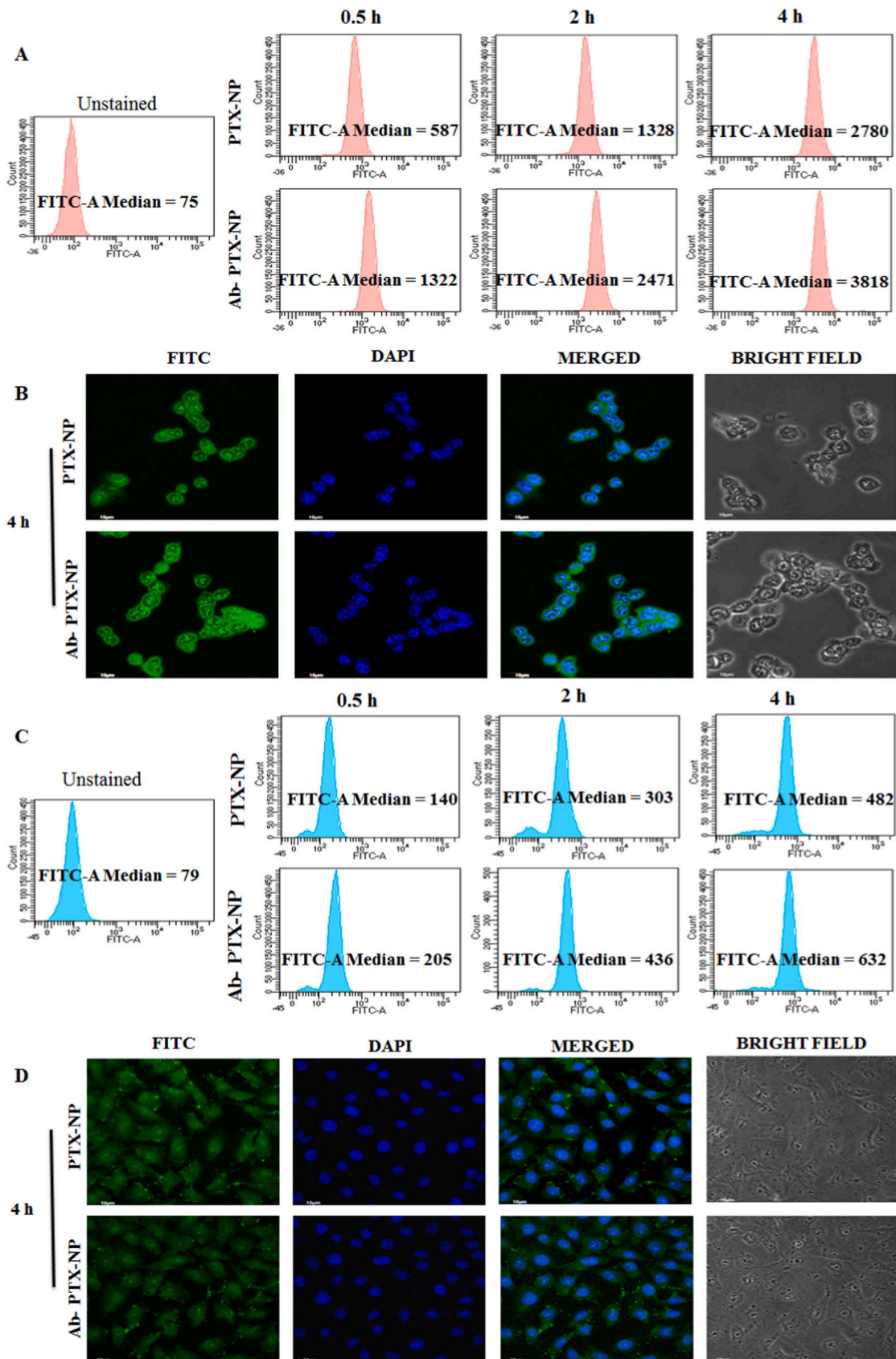


Fig. 3. Cellular uptake study. (A) Flow cytometry analysis representing distribution of FITC PTX-NP and FITC Ab-PTX-NP in LNCaP cells after treating them for 0.5h, 2 h and 4 h respectively. (B) Confocal microscopy images of LNCaP cells after treating with FITC PTX-NP and FITC Ab-PTX-NP for 4 h (C) Flow cytometry analysis representing distribution of FITC PTX-NP and FITC Ab-PTX-NP in PC3 cells after treating them for 0.5h, 2 h and 4 h respectively. (D) Confocal microscopy images of PC3 cells after treating with FITC PTX-NP and FITC Ab-PTX-NP at 4 h (FluoView FV10i, Olympus) using channels FITC (excitation/emission 495nm/519 nm) and DAPI (excitation/emission 359nm/461 nm) with an objective magnification of 60 \times .

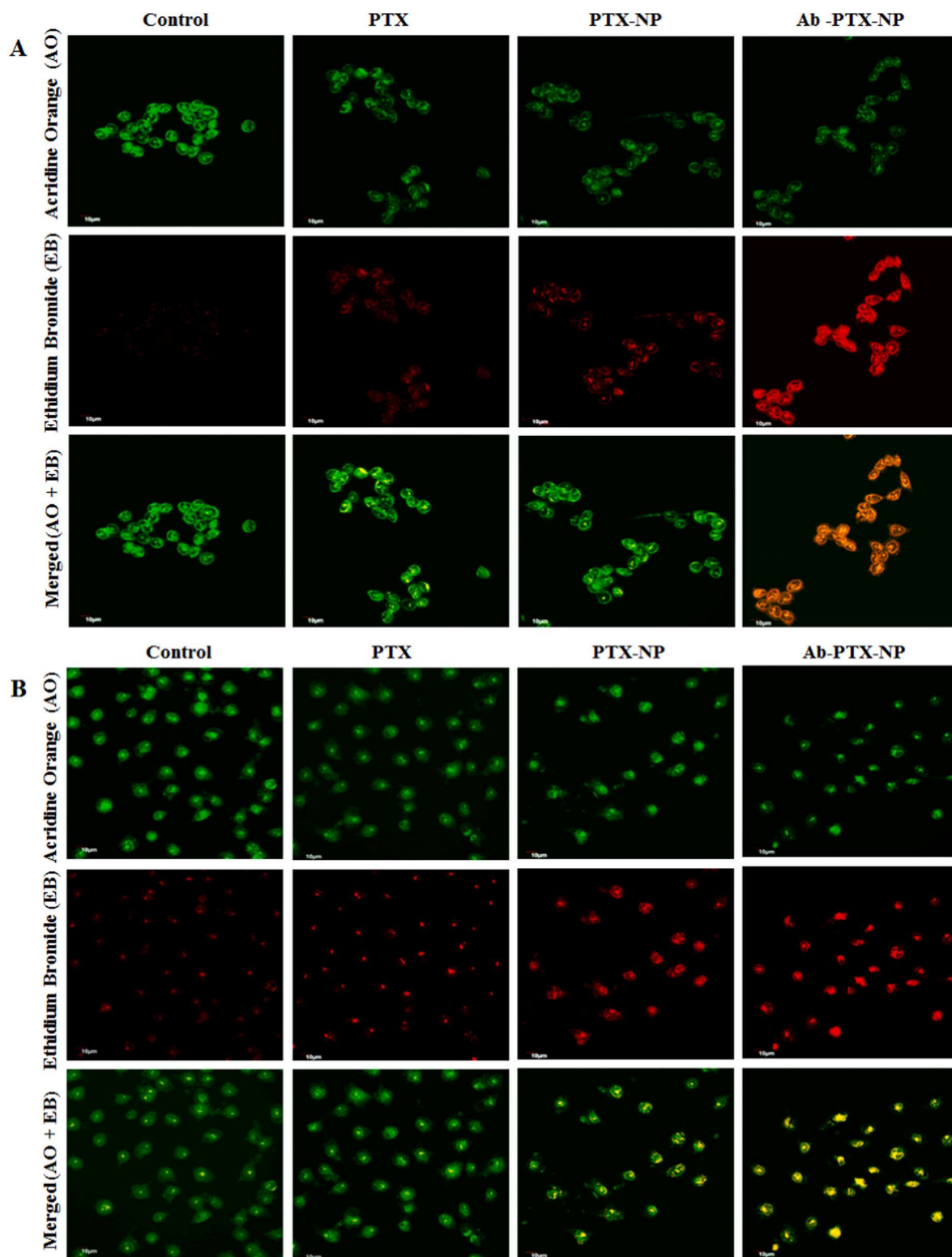


Fig. 4. Acridine Orange/Ethidium bromide (AO/EB) dual staining Confocal microscopy images of (A) LNCaP cells after treating with PTX, PTX-NP and Ab-PTX-NP (B) PC3 cells after treating PTX, PTX-NP and Ab-PTX-NP, for 24 h followed by staining with acridine orange (4 µg/ml) and ethidium bromide (4 µg/ml), by acridine orange/ethidium bromide (AO/EB) dual staining as observed by Olympus Fluoview 10i confocal microscope using the channels of acridine orange DNA (green) (excitation/emission) (502 nm/526 nm) and propidium iodide red (537 nm/619 nm). (For interpretation of the references to colour in this figure legend, the reader is referred to the Web version of this article.)

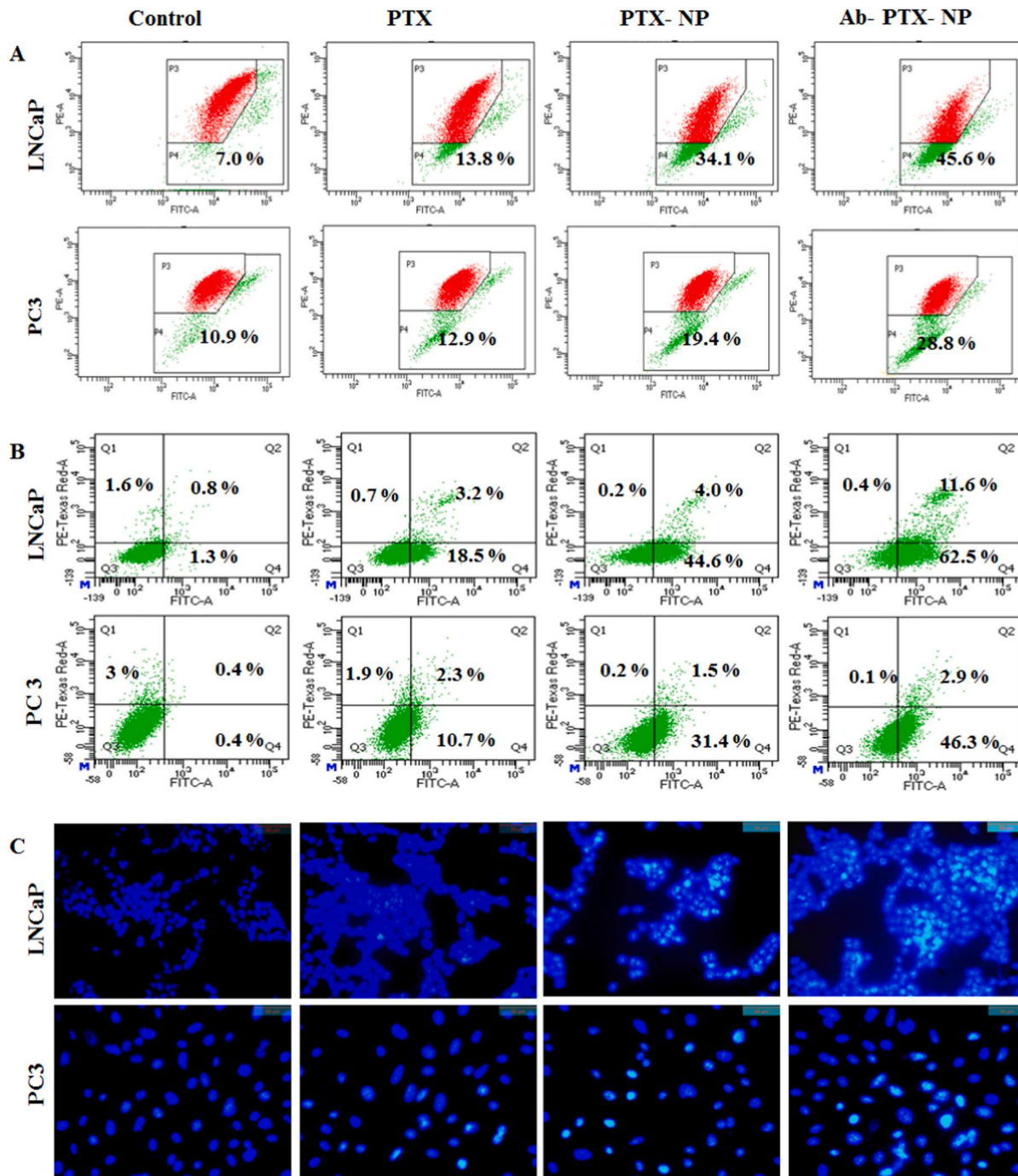


Fig. 5. Mitochondrial membrane depolarization, apoptosis and nuclear morphology of LNCaP (+ve PSMA) and PC3 (-ve PSMA) cells. (A) Loss of mitochondrial membrane potential as estimated by JC-1 staining analysis after treating the LNCaP (+ve PSMA) and PC3 (-ve PSMA) cells with PTX/PTX-NP/Ab-PTX-NP for 24 h, (B) Apoptosis detected with the help of Annexin V/PI in LNCaP (+ve PSMA) and PC3 (-ve PSMA) cells treated with PTX/PTX-NP/Ab-PTX-NP for 24 h, Data were obtained using a FACS Aria flow cytometer (Becton Dickinson, Holdrege, Nebraska, USA) using channels of FITC (Ex/Em 488 nm/530 nm), and PE-Texas red (Ex/Em 561 nm/616 nm) post capturing analysis was done with BD FACS Diva software (Becton Dickinson, Holdrege Nebraska, USA) (C) Image representing DNA degradation and apoptotic bodies formation upon treatment with PTX/PTX-NP/Ab-PTX-NP for 24 h in LNCaP (+ve PSMA) cells and in PC3 (-ve PSMA) cells under confocal microscope (100X). (For interpretation of the references to colour in this figure legend, the reader is referred to the Web version of this article.)

4. Discussion

The foremost target of this research was to prepare, optimize and evaluate Ab-PTX-NP and investigate the ability of attached J591 Ab nanoparticles to reach the PSMA on the cancerous prostate cells. Thus, non-cancerous cells remain unaffected. The quest for specific prostate cancer cell targeting by modifying the surface of NP with J591 Ab can avoid nonspecific uptake of the drug by other cells or healthy tissues. PSMA expression is being actively investigated for theranostic purposes,

which correlate with the sensitivity of the androgen and might assist in tumor invasiveness [53]. In recent times, anti-androgen therapy can be tracked via the virtue of PSMA expression measurement by molecular imaging *in vivo* [53].

Paclitaxel is given as the first line of chemotherapy in prostate cancer, often combined with noscapine, quercetin, carboplatin, etc [54], in biodegradable and biocompatible polymeric nanoparticles. The incorporation of TPGS [11] shows an increase in the solubility of PTX, leading to higher drug loading and preventing crystallization of free drug. The

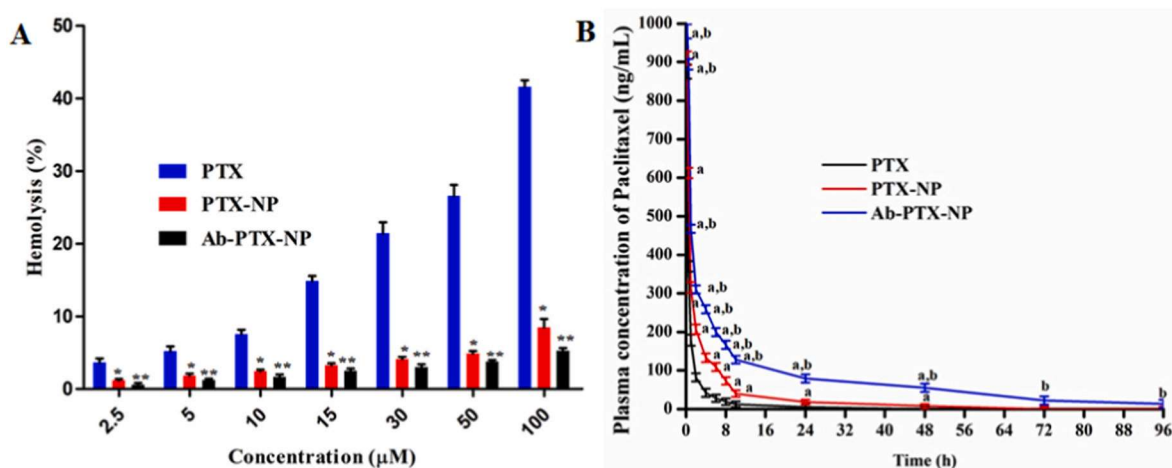


Fig. 6. (A) Hemolytic activity of PTX/PTX-NP/Ab-PTX-NP. Data show mean \pm SD (n = 3)

*P < 0.05 when PTX data were compared with those of PTX-NP and Ab-PTX-NP

**P < 0.05 PTX-NP data were compared with those of Ab-PTX-NP

(B) Plasma concentration of paclitaxel upon i.v bolus injection (at an equivalent dose of 10 mg/kg body weight) of PTX/PTX-NP/Ab-PTX-NP

Data show mean \pm SD (n = 3).

^aP<0.05 when PTX data were compared with those of PTX-NP and Ab-PTX-NP

^bP<0.05 PTX-NP data were compared with those of Ab-PTX-NP.

Table 3

Plasma pharmacokinetic parameters of free paclitaxel, and paclitaxel released from PTX-NP/Ab-PTX-NP/PTX suspension after the intravenous bolus administration of PTX/PTX-NP/Ab-PTX-NP with an equivalent amount of drug in Balb/c mice.

Pharmacokinetic parameters (respective unit)	Plasma values of Drug (Paclitaxel)		
	Upon PTX administration ^c	Upon PTX-NP administration ^c	Upon Ab-PTX-NP administration ^c
t _{1/2} (h)	8.309 \pm 1.24	18.63 \pm 3.11 ^a	20.31 \pm 5.86 ^{a,b}
AUC _{0-t} (ng/mL.h)	1134.291 \pm 47.46	3254.071 \pm 849.93 ^a	7868.208 \pm 818.985 ^{a,b}
AUC _{0-∞} (ng/mL.h)	1195.264 \pm 58.71	3645.893 \pm 114.7267 ^a	8266.213 \pm 691.47 ^{a,b}
AUMC _{0-∞} (ng/mL.h ²)	5621.12 \pm 665.949	62590.02 \pm 4221.751 ^a	258554 \pm 164.6768 ^{a,b}
MRT _{0-∞} (h)	4.70 \pm 0.40	16.005 \pm 5.63 ^a	31.34 \pm 1.72 ^{a,b}
CL _t (L/h/kg)	8.38 \pm 0.41	2.2 \pm 0.81 ^a	1.21 \pm 0.95 ^{a,b}

NB: t_{1/2}, half-life; AUC_{0-t}, area under the plasma concentration–time curve from time 0 to time of last measurable concentration; AUC_{0-∞}, under the plasma concentration–time curve from time 0 to infinity; AUMC_{0-t}, area under the first moment curve from time 0 to time of last measurable concentration; AUMC_{0-∞}, area under the first moment curve from time 0 to infinity; MRT, mean resident time; CL, clearance.

^c Data show mean \pm SD (n = 3).

^a (p < 0.05) The pharmacokinetic data of treatment of PTX group was compared with PTX-NP treatment group and PTX treatment group was compared with Ab-PTX-NP treatment group.

^b (p < 0.05) The pharmacokinetic data of PTX-NP and Ab-PTX-NP groups were compared.

nonexistence of the chemical interactions involving the drug and the excipients was assured by FTIR, while diminutive physical interactions might have helped in the formation of spherical, interstice free, smooth nanoparticle structures. The presence of nitrogen as detected by EDX in Ab-PTX-NP indicated the inclusion of the PTX in the particles.

The antibody conjugation strategy was based on EDC/NHS chemistry, which forms peptide bonds between the amine groups of the J591 Ab and the carboxyl groups of the PLGA [55]. The attachment through the amine group to the nanoparticle surface conserves the activity of the antibodies while simultaneously preventing nonspecific protein absorption. Further, increasing the number of ligands per NP might

increase the convenience of the ligand to bind to the receptors [56].

The difference in drug encapsulation of Ab-PTX-NP and PTX-NP were very low. Drug loading was slightly lower in Ab-PTX-NP due to Ab-conjugation that could be considered trivial. The narrow range of distribution of the NP was indicated by its lower PDI. The zeta potential value proves that Ab-PTX-NP and PTX-NP in their suspended forms would not conglomerate because of the surface charge [21]. The zeta potential value of NP after antibody conjugation preserved their negative zeta-potential, though it shows the drop of negative zeta (less negative) potential in the nanoparticles after conjugation with antibody. Ab-conjugation increased the average particle size (hydrodynamic diameter) slightly. The data of the zeta potential of the formulation in the stability study indicate that the stability of lyophilized PTX-NP and Ab-PTX-NP existed at 4–8 °C in a refrigerated condition.

The SDS-PAGE analysis for conjugation of J591 Ab validates the feasibility of Ab-PTX-NP for further *in vitro* cellular study as it shows protein band at almost the same level as the monoclonal J541 antibody. The weight of the antibody conjugated nanoparticle, Ab-PTX-NP, moved to the higher side (due to the weight of PTX-NP) in comparison to the free J591 Ab. The Western blot analysis further substantiated the higher level of expression of PSMA in LNCaP cells, whereas the expression was insignificant in PC3 cells.

The experimental drug release data explicate that PTX-NP and Ab-PTX-NP had an effective sustained drug release providing potentially optimal bioavailability of PTX within the therapeutic window over a prolonged period. Ab-PTX-NP showed faster degradation in the acidic medium. Lower pH conditions initiated the hydrolysis of the polymeric core by striking the ester bonds. Dissolution is stable in higher pH media due to the polymer retaining its non-polar property, due to the trapping of hydroxyl groups on its surface, which ultimately lowers the water absorption by the NP. Data suggests that an acidic tumor environment (pH 5) would exhibit faster drug release while the drug release would be slow and sustained in physiologically neutral media of blood (pH 7.4) [18]. The Ab-PTX-NP showed stability in mouse serum which was observed for 24 h. PTX release from PTX-NP and Ab-PTX-NP denoted good linearity in the kinetics (as supported by R² value) which was observed in PBS (pH 7.4) with 0.1% w/v tween 80, citrate buffer, acetate buffer and bicarbonate buffer. The MTT assay revealed that less dose of Ab-PTX-NP was effective in producing a higher cytotoxic effect than PTX-NP, probably due to greater cellular internalization and ultimately

the encapsulated drug was delivered to the cytosol. Ab-PTX-NP cytotoxicity toward LNCaP cells (overexpressing PSMA) was higher due to the presence of the receptor and showed minimum toxicity in non-cancerous cells. The quantitative and qualitative cellular uptake data of the Ab-PTX-NP in LNCaP cells also support the findings of the cytotoxicity studies.

In earlier studies on paclitaxel, it was reported that paclitaxel incorporated polymeric nanoparticles primarily initiated the apoptotic pathway which showed potent antiproliferative activity by arresting the cell cycle at G2/M and S phase, which normally activates three principal checkpoints such as G1/S, G2/M, and metaphase/anaphase transitions during mitosis [57]. The intrinsic pathway of apoptosis is the possible mechanism of cell death induced by paclitaxel, although some recent reports suggest that paclitaxel initiates apoptosis via multiple mechanisms [58]. Paclitaxel is acknowledged to cause both mitotic arrest and apoptotic cell death. It simultaneously acts on mitochondria and microtubule assembly to generate sufficient signals for mitochondrial apoptosis [59]. It is also reported to elevate ROS by increasing the activity of the NADPH oxidase (NOX) enzyme [57,60].

The apoptosis inducing ability of Ab-PTX-NP shows cell death by AO/EB staining that was visualized by the colour change of apoptotic cells. The total fluorescence intensity and cell counting advocated the effectiveness of Ab-PTX-NP in LNCaP cells. It has distinctly separated normal and cancer cells due to the loss of integrity of the cellular membrane, nuclear fragmentation, and chromatin condensation, while recognizing the difference between early and late apoptotic cells. Mitochondrial membrane depolarization occurs due to changes in mitochondrial transmembrane potential (MMP). During apoptosis, mitochondria undergo depolarization, which finally leads to rupturing of mitochondria, leading to the disruption of Ca^{+2} homeostasis between mitochondria and endoplasmic reticulum. That indicates lowering of MMP in apoptotic cells [61,62].

The data indicates effective depolarization of the mitochondrial membrane in LNCaP cells as the cellular uptake of Ab-PTX-NP increased. It was quantified by determining the values of the ratio of green to red fluorescence owing to the transformation of JC-1 aggregates (in live cells with high MMP gives red colour) to monomers (in apoptotic cells with decreased MMP gives green color). The DAPI staining after treating both the prostate cancer types with the experimental formulations pronounced the morphological changes due to apoptotic body formations, which was apparently noticeable in LNCaP (+ve PSMA) cells induced by Ab-PTX-NP as compared to other formulations. Thus, Ab-PTX-NP expedited apoptosis-inducing ability and depicted the highest potency towards PSMA prostate cancer cells.

J591 Ab, so far, has been successfully utilized for the diagnostic purpose of detecting advanced prostate cancer because of its propensity to attach to abundantly upregulated PSMA on LNCaP cells [63]. Combining the efficiency of this anti-PSMA antibody J591 with the effectiveness of the anti cancer drug (paclitaxel) incorporated in the biodegradable (PLGA) nanoparticles has enabled site-specific delivery and shows profound cellular uptake by the prostate cancer cells [64]. Novelty can be interpreted as site and cancer specific drug delivery. Site specificity causes minimal harm to healthy tissues by avoiding the non specific uptake by healthy tissues, while cancer cell specificity makes the cancer cells less viable and it may decrease the ability of the cancer cells to metastasize [65].

Thus, the prepared optimized formulation Ab-PTX-NP is low in cost, convenient to produce and administer via intravenous route, less invasive due to less frequent dosing, and easy availability to the patients. Furthermore, it is a biodegradable approach for treatment in the human body as well as for the environment. Therefore, the Ab-PTX-NP selected as an escort can be used as a timely and significant therapeutic option for prostate cancer.

5. Conclusion

Recently, with an explosion in the field of the utility of engineered nanotechnology, our study was inspired to explore the therapeutic efficiency of Ab-PTX-NP for site-specific delivery to treat prostate cancer. The prepared Ab-PTX-NP was found to be promising owing to its biocompatibility, biodegradability, high drug loading capability with suitable size, sustained drug release, stability, and non-toxicity to the healthy tissues. We tried to utilize J591 Ab strategically to target overexpressed PSMA, without limiting the use of J591 as a cancer imaging agent. Our study might benefit the patients as the exceptional qualities of nanoparticles and the respective antibody was attached to them to attain the desired drug targeting.

The Ab-PTX-NP fabricated with J591 showcased the potential to accumulate and deliver PTX *in vitro* to prostate cancer cells, providing improved cytotoxic and apoptotic effects and increased mitochondrial membrane potential at a low dose when compared to PTX and PTX-NP in PSMA expressing LNCaP cells. The results are potentially attractive as the comparative study of different formulations on different prostate cancer cells was done to brace the rationale. It might provide superlative treatment for patients suffering from prostate cancer with a poor prognosis. Extension of *in vivo* studies of this work is being initiated. We wish to further investigate its application, to benefit the society in the near future.

Ethical conduct of research

All animal experiments were carried out in accordance with protocols approved by the Institutional Animal Ethics Committee of Jadavpur University, Kolkata.

Authors statement

Iman Ehsan- Conducting experiments, collection of data, analysis of data, writing of the draft manuscript, and fund acquisition. Leena Kumari- Conducting some experiments. Ramkrishna Sen – Conducting some experiments. Ashique al Hoque- Conducting some experiments and statistical analysis. Biswajit Mukherjee- Conceptualization of the project, supervising the research activity, mentoring the researchers, writing, reviewing and editing the manuscript, and fund acquisition. Alankar Mukherjee- Conducting some experiments Prasanta Ghosh- Conducting some experiments. Sanchari Bhattacharya- Conducting some experiments.

Declaration of competing interest

The authors declare the following financial interests/personal relationships which may be considered as potential competing interests: Iman Ehsan reports financial support was provided by Jadavpur University.

Data availability

Data will be made available on request.

Acknowledgment

Authors are grateful to the Indian Council of Medical Research for providing the financial support to accomplish this work (Ref No 45/41/2018-Nan/BMS dated 14.05.2018).

Authors are thankful to Hemant R. Badwaik and Brahamachary Paul.

Appendix A. Supplementary data

Supplementary data to this article can be found online at <https://doi.org/10.1016/j.jddst.2022.103689>.

- exhibit enhanced anticancer activity by site specific delivery, *RSC Adv.* 5 (2015) 25518–25524, <https://doi.org/10.1039/C5RA00018A>.
- [44] R.H. Gaonkar, S. Ganguly, S. Dewanjee, S. Sinha, A. Gupta, S. Ganguly, D. Chattopadhyay, M.C. Debnath, Garcinol loaded vitamin E TPGS emulsified PLGA nanoparticles: preparation, physicochemical characterization, in vitro and in vivo studies, *Sci. Rep.* 7 (2017) 1–14, <https://doi.org/10.1038/s41598-017-00696-6>.
- [45] R. Mandelkow, D. Guembel, H. Ahrend, A. Kaul, U. Zimmermann, M. Burchardt, M. B. Stope, Detection and quantification of nuclear morphology changes in apoptotic cells by fluorescence microscopy and subsequent analysis of visualized fluorescent signals, *Anticancer Res.* 37 (2017) 2239–2244, <https://doi.org/10.21873/anticancer.11560>.
- [46] C. Fornaguera, G. Calderó, M. Mitjans, M.P. Vinardell, C. Solans, C. Vauthier, Interactions of PLGA nanoparticles with blood components: protein adsorption, coagulation, activation of the complement system and hemolysis studies, *Nanoscale* 7 (2015) 6045–6058, <https://doi.org/10.1039/c5nr00733j>.
- [47] K. Liu, W. Chen, T. Yang, B. Wen, D. Ding, M. Keidar, J. Tang, W. Zhang, Paclitaxel and quercetin nanoparticles co-loaded in microspheres to prolong retention time for pulmonary drug delivery, *Int. J. Nanomed.* 12 (2017) 8239–8255, <https://doi.org/10.2147/IJN.S147028>.
- [48] N. Karra, T. Nassar, A.N. Ripin, O. Schwob, J. Borlak, S. Benita, Antibody conjugated PLGA nanoparticles for targeted delivery of paclitaxel palmitate: efficacy and biofate in a lung cancer mouse model, *Small* 9 (2013) 4221–4236, <https://doi.org/10.1002/sml.201301417>.
- [49] S. Bhattacharya, L. Mondal, B. Mukherjee, L. Dutta, I. Ehsan, M.C. Debnath, R. H. Gaonkar, M.M. Pal, S. Majumdar, Apigenin loaded nanoparticle delayed development of hepatocellular carcinoma in rats, *Nanomedicine* 14 (2018) 1905–1917, <https://doi.org/10.1016/j.nano.2018.05.011>.
- [50] L.P. Jahromi, M. Ghazali, H. Ashrafi, A. Azadi, A comparison of models for the analysis of the kinetics of drug release from PLGA-based nanoparticles, *Heliyon* 6 (2020), e03451, <https://doi.org/10.1016/j.heliyon.2020.e03451>.
- [51] A.E. Machulkin, D.A. Skvortsov, Y.A. Ivanenkov, A.P. Ber, M.V. Kavalchuk, A. V. Aladinskaya, A.A. Uspenskaya, R.R. Shafikov, E.A. Plotnikova, R. I. Yakubovskaya, E.A. Nimenko, Synthesis and biological evaluation of PSMA-targeting paclitaxel conjugates, *Bioorg. Med. Chem. Lett.* 29 (2019) 2229–2235, <https://doi.org/10.1016/j.bmcl.2019.06.035>.
- [52] A. Anitha, K.P. Chennazhi, S.V. Nair, R. Jayakumar, 5-flourouracil loaded N, O-carboxymethyl chitosan nanoparticles as an anticancer nanomedicine for breast cancer, *J. Biomed. Nanotechnol.* 8 (2012) 29–42, <https://doi.org/10.1166/jbn.2012.1365>.
- [53] Z. Chen, M.F. Penet, S. Nimmagadda, C. Li, S.R. Banerjee, P.T. Winnard Jr., D. Artemov, K. Glunde, M.G. Pomper, Z.M. Bhujwalla, PSMA-targeted theranostic nanoplex for prostate cancer therapy, *ACS Nano* 6 (2012) 7752–7762, <https://doi.org/10.1021/nn301725w>.
- [54] A.K. Mohiuddin, Complementary and alternative treatments for cancer prevention and cure [Part 1], *J. Med. Care Res. Rev.* 2 (2019) 228–286, <https://doi.org/10.23880/apct-16000168>.
- [55] N.K. Lee, C.J. Wang, J. Lim, W. Park, H.K. Kwon, S.N. Kim, T.H. Kim, C.G. Park, Impact of the conjugation of antibodies to the surfaces of polymer nanoparticles on the immune cell targeting abilities, *Nano Converg.* 8 (2021) 1–11, <https://doi.org/10.1186/s40580-021-00274-7>.
- [56] G. Tan, K. Kantner, Q. Zhang, M.G. Soliman, P. Del Pino, W.J. Parak, M.A. Onur, D. Valdeperez, J. Rejman, B. Pelaz, Conjugation of polymer-coated gold nanoparticles with antibodies—synthesis and characterization, *Nanomaterials* 5 (2015) 1297–1316, <https://doi.org/10.3390/nano5031297>.
- [57] S. Chakraborty, Z.Y. Dlie, S. Chakraborty, S. Roy, B. Mukherjee, S.E. Besra, S. Dewanjee, A. Mukherjee, P.K. Ojha, V. Kumar, R. Sen, Aptamer-functionalized drug nanocarrier improves hepatocellular carcinoma toward normal by targeting neoplastic hepatocytes, *Mol. Ther. Nucleic Acids* 20 (2020) 34–49, <https://doi.org/10.1016/j.omtn.2020.01.034>.
- [58] M.A. Vakilinezhada, A. Aminic, T. Daraa, S. Alipourb, Methotrexate and Curcumin co-encapsulated PLGA nanoparticles as a potential breast cancer therapeutic system: in vitro and in vivo evaluation, *Colloids Surf. B Biointerfaces* 184 (2019), 110515, <https://doi.org/10.1016/j.colsurfb.2019.110515>.
- [59] T.H. Wang, H.S. Wang, Y.K. Soong, Paclitaxel-induced cell death: where the cell cycle and apoptosis come together, *Cancer* 88 (2000) 2619–2628, [https://doi.org/10.1002/1097-0142\(20000601\)88:11<2619::aid-cnrc26>3.0.co;2-j](https://doi.org/10.1002/1097-0142(20000601)88:11<2619::aid-cnrc26>3.0.co;2-j).
- [60] X. Yi, X. Zhang, H. Jeong, Y.M. Shin, D.H. Park, S. You, D.K. Kim, A novel bispindinone analog induces S-phase cell cycle arrest and apoptosis in HeLa human cervical carcinoma cells, *Oncol. Rep.* 33 (2015) 1526–1532, <https://doi.org/10.3892/or.2015.3722>.
- [61] K. Priyadarshini, A.U. Keerthi, Paclitaxel against cancer: a short review, *Med. Chem.* 2 (2012) 139–141, <https://doi.org/10.4172/2161-0444.1000130>.
- [62] J. Henry-Mowatt, C. Dive, J.C. Martinou, D. James, Role of mitochondrial membrane permeabilization in apoptosis and cancer, *Oncogene* 23 (2004) 2850–2860, <https://doi.org/10.1038/sj.onc.1207534>.
- [63] M. Redza-Dutordoir, D.A. Averill-Bates, Activation of apoptosis signalling pathways by reactive oxygen species, *Biochim. Biophys. Acta Mol. Cell Res.* 1863 (2016) 2977–2992, <https://doi.org/10.1016/j.bbamcr.2016.09.012>.
- [64] N.H. Bander, E.J. Trabulsi, L. Kostakoglu, D. Yao, S. Vallabhajosula, P. Smith-Jones, M.A. Joyce, M. Milowsky, D.M. Nanus, S.J. Goldsmith, Targeting metastatic prostate cancer with radiolabeled monoclonal antibody J591 to the extracellular domain of prostate specific membrane antigen, *J. Urol.* 170 (2003) 1717–1721, <https://doi.org/10.1097/01.ju.0000091655.77601.0c>.
- [65] O. Flores, S. Santra, C. Kaittanis, R. Bassiouni, A.S. Khaled, A.R. Khaled, J. Grimm, J.M. Perez, PSMA-targeted theranostic nanocarrier for prostate cancer, *Theranostics* 7 (2017) 2477–2494, <https://doi.org/10.7150/thno.18879>.

Therapeutic potential of andrographolide-loaded nanoparticles on a murine asthma model

Shreyasi Chakraborty, M.Pharm^a, Iman Ehsan, M.Pharm^a, Biswajit Mukherjee, Ph.D^{a,*},
Laboni Mondal, M.Pharm^a, Saheli Roy, M.Pharm^b, Krishna Das Saha, Ph.D^b,
Brahamachary Paul, M.Pharm^c, Mita Chatterjee Debnath, Ph.D^c, Tanmoy Bera, Ph.D^a

^aDepartment of Pharmaceutical Technology, Jadavpur University, Kolkata, India

^bCancer and Inflammatory Disorder Division, CSIR-Indian Institute of Chemical Biology, Kolkata, India

^cInfectious Diseases and Immunology Division, CSIR-Indian Institute of Chemical Biology, Kolkata, India

Revised 27 February 2019

Abstract

Corticosteroids commonly prescribed in asthma show several side-effects. Relatively non-toxic andrographolide (AG) has an anti-asthmatic potential. But its poor bioavailability and short plasma half-life constrain its efficacy. To overcome them, we encapsulated AG in nanoparticle (AGNP) and evaluated AGNP for anti-asthmatic efficacy on murine asthma model by oral/pulmonary delivery. AGNP had 5.47% drug loading with a sustained drug release *in vitro*. Plasma and lung pharmacokinetic data showed predominantly improved AG-bioavailability upon AGNP administered orally/by pulmonary route. Cell numbers, IL-4, IL-5, and IL-13 levels in broncho-alveolar lavage fluid and serum IgE content were reduced significantly after administration of AGNP compared to free-AG treatment. AGNP-mediated suppression of NF- κ B was predominantly more compared to free-AG. Further, pulmonary route showed better therapeutic performance. In conclusion, AGNP effectively controlled mild and severe asthma and the pulmonary administration of AGNP was more efficacious than the oral route.

© 2019 Elsevier Inc. All rights reserved.

Key words: Andrographolide; Nanoparticle; Murine asthma model; Ovalbumin; Eosinophilia

Allergic asthma is a chronic airway disorder characterized by airway inflammation, mucus hyper-secretion, airway hyper-responsiveness followed by shortness in breathing¹ and approximately three hundred million people around the world suffer from asthma.² Many inflammatory cells such as Th2 cells, B-cells, mast cells and a number of cytokines are involved in the allergic cascade.^{1,3} Allergen induces crosslinking of IgE with IgE-receptor (Fc ϵ RI) on mast cells, releasing histamine, leukotrienes, interleukins (ILs) and other inflammatory mediators.^{4,5} Airway eosinophilia together with Th2 cytokines, IL-4, IL-5 and IL-13, may ultimately contribute to airway hyper-

responsiveness in asthma.⁶ Treatment with corticosteroids is a common therapeutic strategy for asthma but has severe side-effects.^{7–9} Novel therapeutic agents with their effective route of administration and prolonged action may be an alternative to corticosteroids for management of asthma.

Nanoparticles are frequently used for loading different types of drug due to the several advantages such as improved bioavailability, sustained release, tissue targeted delivery, improved permeability to biological membranes, and usefulness in different routes of administration.^{10–14} In the past few decades, biodegradable polylactide-co-glycolide (PLGA), approved by the US Food and Drug Administration and European Medicine Agency, has been extensively used to develop sustained release nanoparticles to treat various diseases including pulmonary diseases in animals^{15–17} and humans.^{18,19}

Andrographolide (AG), a labdane diterpene lactone,²⁰ attenuates ovalbumin (OVA) induced allergic asthma.^{21–24} But poor water solubility,²⁵ and very short biological half-life in gastrointestinal acidic and alkaline conditions due to its

Funding Source: This work was supported by Department of Science and Technology, Government of India [NSTMIS/Inspire Fellowship/2015/150019], and [NSTMIS/NSTMIS/05/207-1/2016-17].

*Corresponding author at: Department of Pharmaceutical Technology, Jadavpur University, Kolkata, India.

E-mail addresses: biswajit.mukherjee@jadavpuruniversity.in
biswajit55@yahoo.com (B. Mukherjee).

<https://doi.org/10.1016/j.nano.2019.04.009>

1549-9634/© 2019 Elsevier Inc. All rights reserved.



Apigenin loaded nanoparticle delayed development of hepatocellular carcinoma in rats

Sanchari Bhattacharya, M.Pharm^a, Laboni Mondal, M.Pharm^a, Biswajit Mukherjee, Ph.D^{a,*},
Lopamudra Dutta, M.Pharm^a, Iman Ehsan, M.Pharm^a, Mita C. Debnath, Ph.D^b,
Raghuvir H. Gaonkar, M.Pharm^b, Murari M. Pal, M.Pharm^a, Subrata Majumdar, Ph.D^c

^aDepartment of Pharmaceutical Technology, Jadavpur University, Kolkata, West Bengal, India

^bInfectious Diseases and Immunology Division, CSIR-Indian Institute of Chemical Biology, Kolkata, West Bengal, India

^cDivision of Molecular Medicine, Bose Institute, Kolkata, West Bengal, India

Received 30 April 2018; accepted 5 May 2018

Abstract

Hepatocellular carcinoma (HCC) is one of the major causes of cancer related death globally. Apigenin, a dietary flavonoid, possesses anti-tumor activity against HCC cells *in-vitro*. Development, physicochemical characterization of apigenin loaded nanoparticles (ApNp), biodistribution pattern and pharmacokinetic parameters of apigenin upon intravenous administration of ApNp, and effect of ApNp treatment in rats with HCC were investigated. Apigenin loaded nanoparticles had a sustained drug release pattern and successfully reached the hepatic cancer cells *in-vitro* as well as in liver of carcinogenic animals. ApNp predominantly delayed the progress of HCC in chemical induced hepatocarcinogenesis in rats. Quantification of apigenin by liquid chromatography–mass spectroscopy (LC-MS/MS) showed that apigenin availability significantly increased in blood and liver upon ApNp treatment. Apigenin loaded nanoparticle delivery substantially controlled the severity of hepatocellular carcinoma and could be a future hope for lingering the survival in hepatic cancer patients.

© 2018 Elsevier Inc. All rights reserved.

Key words: Apigenin nanoparticles; Hepatocellular carcinoma; Pharmacokinetics; Gamma scintigraphy; Histopathology; LC-MS/MS

Hepatocellular carcinoma (HCC) is one of the most common malignant solid tumors with a very poor prognosis¹ and survival rate² in humans and HCC-related death has been reported as the second highest among the all cancer related deaths worldwide.³ Treatment of this life-threatening disease includes surgical (liver resection and transplantation) and non-surgical (chemotherapy) techniques.⁴ Liver cirrhosis is the most common underlying cause leading to HCC related deaths in patients.⁵ Dietary supplements along with the medicines are always under research

to combat this serious health condition and improve patient-compliance.⁶ Drug resistance and drug-induced toxicity in patients and often failure of early detection of HCC make it very tough to get cure.⁷ Dietary supplements have been reported to improve the condition of HCC in patients as they possess anti-proliferative and anti-tumor effect on malignancies including HCC.⁸ Apigenin is a dietary flavonoid found in various vegetable sources such as parsley leaves, chamomile tea, celery, kumquats, dried Mexican oregano, peppermint, vinespinach *etc.*⁹ It has effective chemo-preservative and/or tumor-suppressive activity¹⁰ against many kinds of carcinomas such as prostate, oral, skin¹¹, colon, breast, lung, pancreatic, colorectal⁹ and hepatic cancer *in-vitro*.¹² Many reports suggest that apigenin induces apoptosis in liver cancer cells and may play a vital role in the treatment of HCC.^{13–15} Apigenin, after the oral administration, is cleaved, absorbed and gets distributed inside the gastrointestinal lumen, and thus, bioavailability of apigenin is much less when administered orally.¹⁶ Further, free apigenin has a very high level of protein binding (10,000 times more than the

Funding Source: This work was supported by Department of Science and Technology (Government of India), Grant no. DST/Inspire Fellowship/2012/691.

Disclosure: The authors of this article have no conflicts of interest to declare.

*Corresponding author at: Department of Pharmaceutical Technology, Jadavpur University, Kolkata 700032, India.

E-mail addresses: biswajit.mukherjee@jadavpuruniversity.in, biswajit55@yahoo.com. (B. Mukherjee).

<https://doi.org/10.1016/j.nano.2018.05.011>

1549-9634/© 2018 Elsevier Inc. All rights reserved.



Comparison of Enhanced Solubility Profile Analysis of Thermodynamic Parameters and Pharmacokinetic Profile Related to Tamoxifen Citrate Solubilisation



Laboni Mondal, Biswajit Mukherjee*, Shreyasi Chakraborty, Sanchari Bhattacharya, Iman Ehsan, Soma Sengupta and Murari M Pal

Department of Pharmaceutical Technology, Jadavpur University, India

Received Date: June 14, 2018; Published Date: July 09, 2018

*Corresponding author: Biswajit Mukherjee, Department of Pharmaceutical Technology, Jadavpur University, Kolkata, West Bengal, India, Email:biswajit55@yahoo.com

Abstract

The aim of this study was to investigate the improvement of solubility of a poorly water soluble drug tamoxifen citrate (TC) by various methods such as cosolvency, micellisation, and complexation. Cosolvents (ethanol, polyethylene glycol-400), surfactants [polyoxyethylene sorbitan monooleate (Tween-80), poloxamer-407 and poloxamer-188], and cyclodextrins [β -cyclodextrin (BCD) and hydroxypropyl- β -cyclodextrin (HPBCD)] were used as solubilizing agents in this study. Solubility improvement approaches showed variable degrees of solubility improvement of TC. Among the solubilizing agents used, the modified β -cyclodextrin was found to be the most effective. The solubility of TC was enhanced to 6.31 mmolL⁻¹ in water (about 7.1 fold solubility improvement) using 0.05% m/v hydroxy propyl- β -cyclodextrin. Different thermodynamic parameters, enthalpy and entropy, were analyzed for solubility enhancement of TC with different cyclodextrins which showed enthalpy not the entropy was the driving force for TC solubilisation. The less positive enthalpy of BCD complexation than HPBCD complexation signifies the higher solubilising efficacy of HPBCD. Pharmacokinetic study was performed using HPBCD as solubility enhancer at its optimized concentration which also resulted in improved bioavailability when compared to the bioavailability obtained with free tamoxifen.

Keywords: Tamoxifen citrate; Solubility; Cosolvent; Surfactant; Cyclodextrin; Pharmacokinetic

Introduction

Tamoxifen citrate (TC) is an antiestrogenic drug and is first choice treatment of breast cancer in both pre- and post-menopausal women. The antiestrogenic effects may be related to its ability to compete with estrogen for binding sites in target tissues such as breast [1]. Chemically, TC is the isomer of a triphenylethylene derivative. The chemical name is (Z) 2-[4-(1,2-diphenyl-1-butenyl) phenoxy]-N,N-dimethylethanamine-2-hydroxy-1,2,3-propane tricarboxylate. Following a single oral dose of 20 mg tamoxifen, an average peak plasma concentration of 40 μ g L⁻¹ (range 35 to 45 ng ml⁻¹) occurred in 4-7 h after dosing [2,3] and this indicates poor bioavailability of the drug. Poorly water-soluble drugs often provide limited bioavailability if dissolution is the rate-limiting step in overall oral absorption process [4]. Since TC is poorly soluble in water (equilibrium solubility in water at 37 °C is 0.5 mg ml⁻¹) [5], it is, therefore, important to improve its solubility to ameliorate its bioavailability [6].

Although there has been enormous amount of research works performed using different techniques of solubilisation,

yet a comparative profile is very scarce. In this study, the effect of different solubilisation approaches such as micellar solubilisation, complexation by cyclodextrins and cosolvency on the aqueous solubility of TC has been presented in a comparative approach. An attempt has been made to provide an insight into the mechanism of solubilisation of TC particularly by complexation based on analysing thermodynamic parameters, since complexation was found to be the most successful approach among the methods tried.

Experimental

Materials

Poly (ethylene glycol) 400 (SRL Pvt. Ltd., Mumbai, India), β -cyclodextrin (Hi Media Laboratories Pvt. Ltd., Mumbai, India), tween-80 (S.d. Fine Chemical Limited, Mumbai, India), absolute ethanol (Merck Ltd., Mumbai, India) were obtained commercially. Hydroxypropyl- β -cyclodextrin, poloxamer-407, poloxamer-188 were purchased from Sigma-Aldrich, Bengaluru, India. TC (Khandelwal Laboratories Pvt. Ltd., Mumbai, India) was a gift sample.

CHAPTER 1

Hepatocellular Carcinoma: Diagnosis, Molecular Pathogenesis, Biomarkers, and Conventional Therapy

Biswajit Mukherjee^{*},¹, Manasadeepa Rajagopalan², Samrat Chakraborty¹, Prasanta Ghosh¹, Manisheetta Ray¹, Ramkrishna Sen¹ and Iman Ehsan¹

¹ Department of Pharmaceutical Technology, Jadavpur University, Kolkata 700032, India

² East West College of Pharmacy, Bangalore, Karnataka 560091, India

Abstract: Hepatocellular carcinoma (HCC), the most common liver malignancy, has been a significant cause of cancer-related deaths worldwide. Cirrhosis, hepatic viral infections, fatty liver, and alcohol consumption are notable risk factors associated with HCC. Furthermore, a crucial challenge in the therapeutic management of HCC patients is the late-stage diagnosis, primarily due to the asymptomatic early stage. Despite the availability of various preventive techniques, diagnoses, and several treatment options, the mortality rate persists. Ongoing investigation on exploring molecular pathogenesis of HCC and identifying different prognostic and diagnostic markers may intervene in the conventional mode of treatment option for better therapeutic management of the disease. Subsequently, tumor site and its size, extrahepatic spread, and liver function are the underlying fundamental factors in treating treatment modality. The development in both surgical and non-surgical methods has resulted in admirable benefits in the survival rates. Understanding the mechanism(s) of tumor progression and the ability of the tumor cells to develop resistance against drugs is extremely important for designing future therapy concerning HCC. This chapter has accumulated the current literature and provided a vivid description of HCC based on its classification, risk factors, stage-based diagnosis systems, molecular pathogenesis, prognostic/diagnostic markers, and the existing conventional treatment approaches.

Keywords: Cellular signaling pathway, Cirrhosis, HCC molecular pathogenesis, HCC- prognostic/diagnostic markers, HCC risk factors, Hepatocellular carcinoma (HCC), cell signaling during HCC development, Ongoing therapy against HCC, Stage-based diagnosis, Tumor microenvironment.

^{*} **Corresponding author Biswajit Mukherjee:** Department of Pharmaceutical Technology, Jadavpur University, Kolkata 700032, India; Tel/Fax: +913324146677; Emails: biswajit55@yahoo.com, biswajit.mukherjee@jadavpuruniversity.in



Chapter 6 - Guar gum-based nanomaterials in drug delivery and biomedical applications

Biswajit Mukherjee, Leena Kumari, Iman Ehsan, Prasanta Ghosh, Soumyabrata Banerjee, Samrat Chakraborty, Manisheeta Ray, Ashique Al Hoque, Ratan Sahoo

Show more 

+ Add to Mendeley  Share  Cite

<https://doi.org/10.1016/B978-0-12-820874-8.00016-6>


[Get rights and content](#)

Abstract

Guar gum is a natural polymer possessing various unique features such as biodegradability, biocompatibility, biosafety, etc. and it is widely used in various biomedical industries. However, the native form of guar gum exhibits difficulties in formulating biomedical devices due to its excessive swelling ability, instability, and likelihood of microbial contamination. These drawbacks could be overcome by tailoring the functional groups of guar gum to accomplish its derivatives with improved physicochemical properties. The various derivatizations of guar gum include cross-linking, carboxymethylation, amination, and grafting with other natural, synthetic, or semisynthetic polymers. Recently, various modified forms of guar gum are exploited to develop an array of nanomaterials for biomedical applications. In this book chapter, we have summarized the source and physicochemical properties of guar gum, its modification approaches, and its utilization in nanomaterial fabrication for drug delivery and biomedical applications. The limitations and future scopes of such nanomaterials are also discussed.



Conventional and Nonconventional Approaches to Site-Specific Targeting of Nanotherapeutics in Some Infectious Diseases and Metabolic Disorders

[Biswajit Mukherjee](#) , [Samrat Chakraborty](#), [Iman Ehsan](#), [Apala Chakraborty](#), [Leena Kumari](#), [Alankar Mukherjee](#) & [Shounak Sarkhel](#)

Chapter | [First Online: 31 July 2020](#)

241 Accesses

Abstract

Systemic fungal infection in pulmonary tissue and viral infections affecting peripheral nerve claim millions of lives every year. The inability of therapeutics to reach the diseased sites at an optimum concentration, lack of patient-friendly delivery strategies, and inability of delivery strategies to penetrate and/or release the therapeutic payload at the diseased sites, keeping the normal cells unaffected, are some of the reasons which demand alternative or other methods to successfully deliver drug to affected sites. Since the end of the last century, a novel drug delivery system (drug-nanocarrier system) has reached a new benchmark with the application of nanomedicine in the treatment of fatal metabolic disorders and infectious diseases. Despite its ability to increase permeability and penetrability to cells/tissues/organs, its uncontrolled biodistribution may cause cytotoxicity to nontargeted cells, resulting in improper therapeutic management. Therefore, ligand-based active targeting strategies are most popularly exploited by researchers around the world to develop site-specific targeting of diseased sites. A plethora of site-specific nanomedicines has been developed on the laboratory scale based on conventional active targeting strategies with ligands. Even after a lot of sincere efforts, the translation of laboratory to clinic is very limited due to toxicity, stability, and the nonspecific nature of ligands. Therefore, certain nonconventional approaches of targeting therapeutics, such as gene-silencing technology, management of glioma by incorporation of brain-mimicking lipid in nanoliposomal formulations, chemical-mediated nanoliposomal formulations specifically targeted to peripheral nervous systems (PNS), and innovation of novel delivery devices, offer significant promise for effective therapeutic management. This chapter focuses on the pros and cons and future prospects of various conventional and nonconventional approaches of drug targeting with an insight to develop powerful therapeutic weapons for effective therapeutic management of deadly diseases.



Transdermal Nanomedicines for Reduction of Dose and Site-Specific Drug Delivery

8

Biswajit Mukherjee, Soma Sengupta, Soumyabrata Banerjee, Moumita Dhara, Ashique Al Hoque, Leena Kumari, Manisheetta Ray, Iman Ehsan, and Alankar Mukherjee

Abstract

The emergence of new technologies provides unique opportunities to exploit novel approaches in drug delivery. Transdermal drug delivery systems (TDDS) are one of the imperative technologies of increasing interest with the benefits of sustained/controlled drug delivery leading to patient convenience and compliance. By definition, TDDS are topically administered medications, for example, patches or semisolids, which permeate the active ingredient through the intact skin for systemic effects in a sustained manner. Transdermal drug deliveries, therefore, are the noninvasive administration of active ingredients from the skin surface across its layers, to the systemic circulation. Nanomedicinal approaches through TDDS can be utilized for site-specific delivery of drugs which can lead to the reduction of dose, too. We have reported here TDDS providing nanomedicinal strategies to deliver drug(s) to the target tissues.

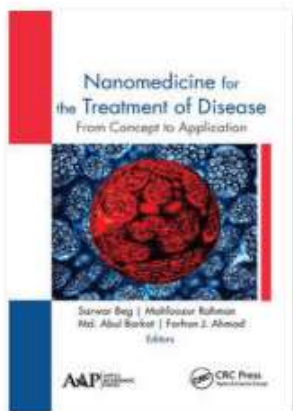
Keywords

Skin · Transdermal delivery · Nanomedicine · Dose · Site-specific delivery

8.1 Introduction

Skin, being the largest organ of our body, protects us as a physiological barrier from different infections, environmental stress, such as heat or cold, and permeates the sensation with the help of nerve endings residing beneath the skin. Certain active ingredients having the potency to cross this physiological barrier can even reach the

B. Mukherjee (✉) · S. Sengupta · S. Banerjee · M. Dhara · A. Al Hoque · L. Kumari · M. Ray · I. Ehsan · A. Mukherjee
Department of Pharmaceutical Technology, Jadavpur University, Kolkata, India



Chapter

Nanomedicinal Genetic Manipulation: Promising Strategy to Treat Some Genetic Diseases

By Biswajit Mukherjee, Iman Ehsan, Debasmita Dutta, Moumita Dhara, Lopamudra Dutta, Soma Sengupta

Book [Nanomedicine for the Treatment of Disease](#)

Edition	1st Edition
First Published	2019
Imprint	Apple Academic Press
Pages	38
eBook ISBN	9780429425714



Share

ABSTRACT

Genetic disease is characterized as an ailment due to a defect in an individual's genome, chromosomal abnormalities, and gene mutations. A successful therapeutic and diagnostic intervention on genetic diseases has been unrevealed predominately, and it demands technological development. Nanomedicine is a boon in various fields of medical applications from the development of diagnostic devices, contrast agents, in vivo imaging, analytical tools to drug delivery vehicles. Versatilities of nanomedicines owing to the dimension, biocompatibility, and manipulating capability to achieve successful delivery at the targeted site of action and their lower toxicity have made this field a technological revolution to combat different unmet needs in health. This is a possible alternative for combating chronic genetic disorders by targeting a particular gene(s) or tissue or cell, which creates a pathological state. Thus, nanomedicine could be a potential therapeutic tool to treat different genetic pathological conditions, such as diabetes, heart diseases, lysosomal storage disorders, Alzheimer's disease, cystic fibrosis, etc. In this chapter, we will discuss several strategies to manipulate or knock down the expression of the lethal gene(s) specifically responsible for some of such diseases. Here we mainly focus on diseases 104such as cancer and its fate while manipulating genetic alteration by the nanomedicinal strike.

CIRE

CENTRE FOR INTERDISCIPLINARY RESEARCH AND EDUCATION

404B, Jodhpur Park, Kolkata – 700068

25th March, 2017

CERTIFICATE OF PARTICIPATION

This is to certify that

Iman Ehsan

*has contributed through Lecture / Oral Presentation / Poster Presentation / Participation to the success
of the One Day National Symposium on Nanotechnology:
From Materials to Medicine and their Social Impact field on 25th March, 2017
at Birla Industrial and Technological Museum, Kolkata.*


Prof Sanjib Sarkar
President, CIRE

**National Seminar on
CLINICAL RESEARCH: PRESENT SCENARIO IN PHARMACOVIGILANCE
AND CLINICAL TRIALS**

on 17th February, 2018 at Dr. K. P. Basu Memorial Hall, Jadavpur University

This is to certify that Prof./ Dr./ Smt./ Shri..... *Amra. Ehsan*..... has participated in the National seminar on
of *Jadavpur University*.....

“Clinical Research: Present Scenario in Pharmacovigilance and Clinical Trials” held in Department
of Pharmaceutical Technology, Jadavpur University, on 17th February, 2018 as a *Delegate/ Speaker/*
Poster Presenter/ Participant.

POSITION: *1st/ 2nd/ 3rd*

Amra Ehsan

Organizing Secretary
Prof. (Dr.) Amallesh Samanta
Department of Pharmaceutical Technology
Jadavpur University

Organized by



Department of Pharmaceutical Technology
Jadavpur University, Kolkata-700 032

In association with



AMRI Hospitals, Dhakuria
Kolkata - 700029



Centurion
UNIVERSITY

*Shaping Lives...
Empowering Communities...*



Certificate

Awarded to

Iman Ehsan

For Attending/ Poster Presenting/ Delivering lecture in the

Indian Council of Medical Research (ICMR)

Sponsored National Seminar on

"Quality Control and Standardization of Ethnopharmaceuticals in the Present Era"

Held on 4th - 5th March 2018

at Centurion University of Technology and Management
Bhubaneswar, Odisha

Prof. Haribandhu Panda
Vice Chancellor, CUTM

Prof. Gurudutta Pattnaik
Convener

Mr. Mahesh Patnaik
Director, SPLS

NATIONAL SEMINAR
on
**Pharmacy & Healthcare:
Traditional Knowledge to Modern Techniques**

14th September, 2018



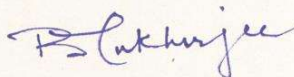
Certificate

This certificate is awarded to Prof. / Dr. / ~~Mr.~~ / Mrs. / Ms.

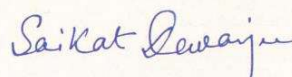
Iman Ehsan

for participation as Delegate/ ~~Resource Person~~ / ~~Chairing a session~~ /

Presenting a paper (~~Oral~~ / Poster).



Prof. Biswajit Mukherjee
Co-Chairman



Dr. Saikat Dewanjee
Organizing Secretary



Sponsored by:



Science and Engineering Research Board
Department of Science and Technology
Government of India, New Delhi

Organized by:



Advanced Pharmacognosy Research Laboratory
Department of Pharmaceutical Technology
Jadavpur University, Kolkata 700032



CERTIFICATE OF PARTICIPATION



Presented To

MS. IMAN EHSAN

for attending the

6TH INTERNATIONAL POSTGRADUATE CONFERENCE ON PHARMACEUTICAL SCIENCES 2018

International Medical University, Kuala Lumpur, Malaysia
15 - 16 August 2018

Ms. Kit-Kay Mak
Chairperson
6th IPOPS Organising Committee



Assoc. Prof. (Dr.) Mohd Zulkefeli bin Mat Jusoh
Dean, School of Pharmacy
International Medical University



PULSUS
WWW.PULSUSCONFERENCE.COM

Cancer Research 2019
Young Scientists Forum

Prof/Dr/Mr/Ms. **Iman Ehsan**

Jadavpur University, India

for presenting the oral entitled

Enhanced targeting of chemotherapeutic drug

to prostate cancer cells by antibody conjugated

polymeric nanoparticles

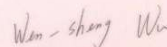
at the 24th International Conference on Cancer Research and Pharmacology
held during August 5-6, 2019 in Singapore

The award has been attributed in recognition of research paper quality, novelty and significance.



Raghu Pandurangi

Sci-Engi-Medco Solutions Inc. and Amplexi-LLC
USA



Wen-Sheng Wu

Tzu Chi University
Taiwan